Alma Mater Studiorum – Università di Bologna

# DOTTORATO DI RICERCA IN ASTRONOMIA

Ciclo XXII

Settore scientifico di afferenza: Area 02 - Scienze Fisiche

FIS/05 Astronomia e Astrofisica

## The Enhanced Single-dish Control System

## and wide surveys of compact sources

Presentata da: **SIMONA RIGHINI**

Coordinatore Dottorato
**Ch.mo Prof. Lauro Moscardini**

Relatore
**Ch.mo Prof. Daniele Dallacasa**
**Dott. Ettore Carretti**
**Ing. Alessandro Orfei**

**Esame finale anno 2010**

*In loving memory*
*of Anna, my mother.*

# SUMMARY

# INTRODUCTION

*This thesis work was carried out using the Medicina 32-m dish (Bologna, Italy), which is managed by INAF-IRA (Istituto Nazionale di Astrofisica – Istituto di Radioastronomia).*

The Italian radio telescopes currently undergo a major upgrade period in response to the growing demand for deep radio observations, such as surveys on large sky areas or observations of vast samples of compact radio sources.

The optimised employment of the Italian antennas, at first constructed mainly for VLBI activities and provided with a control system (FS – Field System) not tailored to single-dish observations, required important modifications in particular of the guiding software and data acquisition system.

The production of a completely new control system called ESCS (Enhanced Single-dish Control System) for the Medicina dish started in 2007, in synergy with the software development for the forthcoming Sardinia Radio Telescope (SRT). The aim is to produce a system optimised for single-dish observations in continuum, spectrometry and polarimetry. ESCS is also planned to be installed at the Noto site.

A substantial part of this thesis work consisted in designing and developing subsystems within ESCS, in order to provide this software with tools to carry out large maps, spanning from the implementation of On-The-Fly fast scans (following both conventional and innovative observing strategies) to the production of single-dish standard output files and the realisation of tools for the quick-look of the acquired data.

The test period coincided with the commissioning phase for two devices temporarily installed – while waiting for the SRT to be completed – on the Medicina antenna: a 18-26 GHz 7-feed receiver and the 14-channel analogue backend developed for its use. It is worth stressing that it is the only K-band multi-feed receiver at present available worldwide.

The commissioning of the overall hardware/software system constituted a considerable section of the thesis work. Tests were led in order to verify the system stability and its capabilities, down to sensitivity levels which had never been reached in Medicina using the previous observing techniques and hardware devices.

The aim was also to assess the scientific potential of the multi-feed receiver for the production of wide maps, exploiting its temporary availability on a mid-sized antenna. Dishes like the 32-m antennas at Medicina and Noto, in fact, offer the best conditions for large-area surveys, especially at high frequencies, as they provide a suited compromise between sufficiently large beam sizes to cover quickly large areas of the sky (typical of small-sized telescopes) and sensitivity (typical of large-sized telescopes).

The KNoWS (K-band Northern Wide Survey) project is aimed at the realisation of a full-northern-sky survey at 21 GHz; its pilot observations, performed using the new ESCS tools and a peculiar observing strategy, constituted an ideal test-bed for ESCS itself and for the multi-feed/backend system. The KNoWS group, which I am part of, supported the commissioning activities also providing map-making and source-extraction tools, in order to complete the necessary data reduction pipeline and assess the general system scientific capabilities.

The K-band observations, which were carried out in several sessions along the December 2008-March 2010 period, were accompanied by the realisation of a 5 GHz test survey during the summertime, which is not suitable for high-frequency observations. This activity was conceived in order to check the new analogue backend separately from the multi-feed receiver, and to simultaneously produce original scientific data (the 6-cm Medicina Survey, 6MS, a polar cap survey to complete PMN-GB6 and provide an all-sky coverage at 5 GHz).

## THESIS OUTLINE

**Chapter 1 – Hardware**

The main features of the Medicina dish are presented. Details follow to illustrate the K-band multi-feed receiver and the new analogue backend.

**Chapter 2 – ESCS**

The Enhanced Single-dish Control System is described. The initial section is devoted to its requirements, then the software tools chosen for its realisation are presented. The last section illustrates the general structure of ESCS as it was actually implemented.

**Chapter 3 – Software development**

This chapter focuses on the software tools I developed, both internally and externally to ESCS, describing their functions and illustrating how they were tested. Particular attention is devoted to the On-The-Fly scan implementation.

**Chapter 4 – Commissioning of the MF system**

The results obtained along the various commissioning sessions are presented. Explanations are given on the observing strategy adopted, and examples of the interesting features detected in the acquired data are shown. The encountered problems – and their solutions – are commented in detail. The actual system response is compared to the expected performance.

**Chapter 5 – The 6MS Catalogue: the Polar Cap at 5 GHz**

This chapter illustrates the 5 GHz observations, describes the observational setup and presents the preliminary results.

**Appendix A – 6MS**

Here the pilot version of the 6MS catalogue is listed.

# CHAPTER 1

# HARDWARE

*Those parts of the system that you can hit with a hammer (not advised) are called hardware; those program instructions that you can only curse at are called software.*
Unknown author

## 1. OVERVIEW

The Medicina dish, whose first light dates back to 1983, is a 32-m parabolic antenna located 35 Km south-east of Bologna (Italy). It is managed by the Istituto di Radioastronomia (IRA), which is part of the Istituto Nazionale di Astrofisica (INAF). This chapter provides a brief overview of its features, focusing more specifically on the description of the two main devices which have been exploited during this thesis: the K-band MF receiver and the analogue total power backend developed for its use, both of which, while waiting for the new Italian radio telescope – the Sardinia Radio Telescope (SRT) – to be completed, have undergone the commissioning phase on board of the Medicina dish (see Chapter 4).

## 2. THE MEDICINA DISH

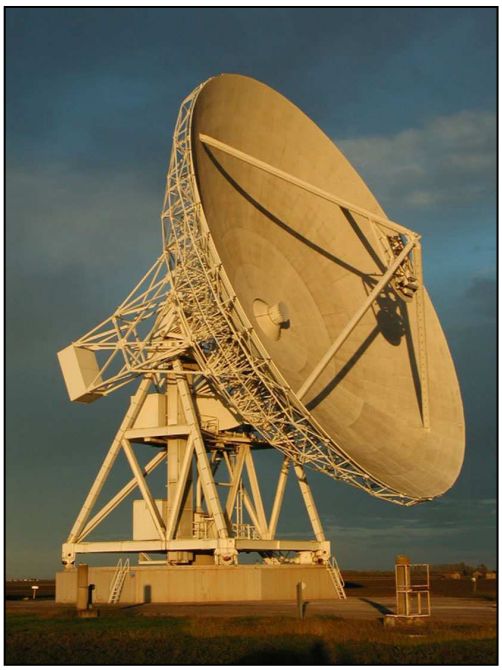

Figure 1.1 – Picture of the Medicina dish.

The Medicina antenna is a 32-m parabolic dish with Cassegrain optical configuration, installed on an altazimuthal mount.

Its two foci, the primary focus and the secondary (or Cassegrain) focus, host a total number of 7 single-feed receivers, which can be selected in frequency agility mode: the subreflector is remotely commanded to slide to the retracted position, and it takes less than four minutes to complete the primary to secondary focus switching (or vice versa).

Table 1.1 lists the main features of the overall antenna, while Table 1.2 provides details about its permanent receivers. They are adapted, Table 1.3, from the official Medicina dish user manual[1].

| | |
|---|---|
| **Location** | Medicina (BO), Italy |
| **Coordinates** | Latitude N 44° 31' 13.8"<br>Longitude E 11° 38' 48.9"<br>Altitude 25 m f.s.l. |
| **Frequency coverage** | 1.4 – 23 GHz |
| **Primary reflector diametre** | 32 m |
| **Secondary reflector diametre** | 3.2 m |
| **Available foci** | Primary F/D 0.32<br>Cassegrain F/D 3.04 |
| **Elevation range** | 3° – 90° |
| **Azimuth range** | ± 270° |
| **Slew rates (wind speed < 60 km/h)** | 48 °/min azimuth, 30 °/min elevation |
| **Surface accuracy (rms specified)** | 0.6 mm (at 60° of elevation) |
| **Active surface** | No |
| **Pointing accuracy (rms specified)** | 8 arcsec |
| **Half Power Beam Width (HPBW)** | 38.7 arcmin/ν(GHz) |
| **Gain** | 0.10 ÷ 0.16 K/Jy |
| **First secondary lobes** | ≈ 20 dB under the main lobe |
| **Receiver mounts** | Primary focus: movable positioner, 3 receiver bays<br>Cassegrain focus: fixed, 9 receiver bays |

Table 1.1 – Main features of the Medicina 32-m dish.

| **Band (Name)** | **$\nu_0$ (GHz)** | **$\lambda$ (cm)** | **Beam (arcmin)** | | **$\nu_{Lsky}$ (GHz)** | **$\nu_{Hsky}$ (GHz)** | **Receiver band (MHz)** | **Receiver noise temp. (K)** |
|---|---|---|---|---|---|---|---|---|
| | | | N/S | E/W | | | | |
| L | 1.4 | 21 | 31.0 | 31.3 | 1.35 | 1.45 | 2x80 | 50 |
| L | 1.6 | 18 | 27.5 | 27.6 | 1.595 | 1.715 | 2x80 | 60 |
| S | 2.3 | 13 | 18.6 | 17.3 | 2.20 | 2.36 | 2x160 | 40 |
| C | 5 | 6 | 7.50 | 7.40 | 4.30 | 5.80 | 2x400<br>2x800 | 12-14 |
| C | 6 | 5 | 7.00 | 6.50 | 5.90 | 7.10 | 2x400 | 57 |
| X | 8.3 | 3.6 | 4.80 | 5.00 | 8.18 | 8.98 | 2x800 | 25 |
| K | 22 | 1.3 | 2.00 | 2.00 | 21.86 | 24.14 | 2x800 | 80 |

Table 1.2 – List of the permanent receivers mounted on the Medicina antenna.
The C-band receivers are located in the Cassegrain focus, all the others are in the primary focus cabin.

[1] http://www.med.ira.inaf.it/parabola_page_EN.htm

Table 1.3 illustrates the efficiency and sensitivity for the various receivers. The last column gives the rms sensitivity for one second of integration in dual polarisation mode, using the theoretical radiometre formula.

| $\nu_0$ (GHz) | $T_{sys}$ (K) | $\eta_A$ (%) | G (K/Jy) | $\Delta S$ (mJy/s$^{-1/2}$) |
|---|---|---|---|---|
| 1.4 | 58 | 41 | 0.120 | 38.2 |
| 1.6 | 64 | 36 | 0.106 | 47.8 |
| 2.3 | 58 | 43 | 0.125 | 26.0 |
| 5 | 26 | 58 | 0.160 | 4.1 |
| 6 | 65 | 50 | 0.145 | 23.9 |
| 8.3 | 40 | 48 | 0.141 | 7.1 |
| 22 | 145 | 38 | 0.110 | 33.0 |

Table 1.3 – System temperature, efficiency, gain and sensitivity for the various frequencies.

The antenna, prior to the development of the Enhanced Single-dish Control System (Chapter 2), was operated only using the Field System (FS), the control software provided by the VLBI Network. This software, though reliable and constantly updated, was conceived for interferometric observations – substantially based on the position switching mode – and was not optimised for single-dish activities requiring different observing strategies.

## 3. THE K-BAND MULTI-FEED RECEIVER

While waiting for the Sardinia Radio Telescope to be completed, the 18-26 GHz multi-feed receiver realised for it was installed on the Medicina dish to undergo the commissioning phase.

It is the first multi-feed receiver available worldwide in the K-band.

It consists of seven corrugated horns in hexagonal arrangement, each providing Left Circular Polarisation (LCP) and Right Circular Polarisation (RCP) output channels, for a total of 14 channels. The instant bandwidth for every channel is 2 GHz, which is more than twice the maximum bandwidth that was previously available for K-band observations at the Medicina site.

The horns have an inner diameter of 68.8 mm, an outer diameter of 98.0 mm, and the distance between the centres of two adjacent feeds is 100 mm.

The feeds are installed inside a dewar (Figure 1.2 shows two phases of the installation), whose interior is cooled by means of a cold head – brought to 20 K using liquid nitrogen – and kept in vacuum conditions.

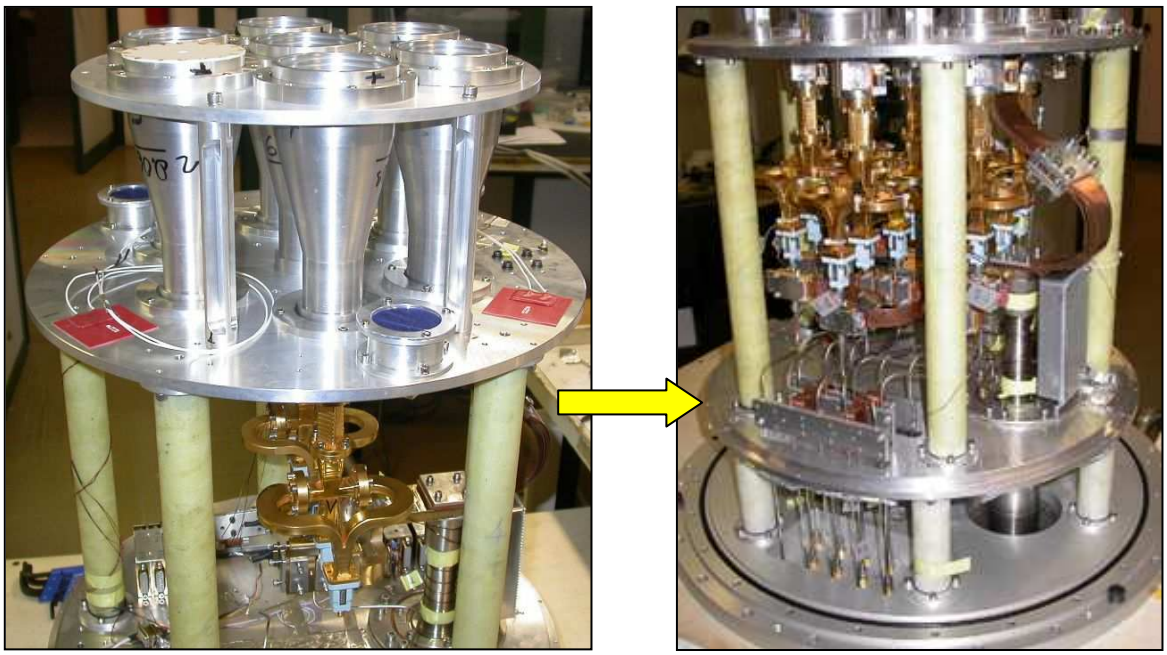

Figure 1.2 – The horns and all the cooled parts of the MF receiver during their installation inside the laboratories.

The dewar is equipped with a derotator, which is fundamental for the majority of the observing techniques to prevent the rotation of the observed field during long acquisitions.

| | **Medicina** | **SRT** |
|---|---|---|
| Rotation range ($^o$) | ±130 | ±120 |
| Max rotation speed ($^o$/sec) | 4.37 | 4.37 |
| Positioning Accuracy (arcsec, on sky) | 0.055 | 0.036 |
| Positioning Resolution (arcsec, on sky) | 0.020 | 0.013 |

Table 1.4 – Parameters relative to the derotator, for its installation on the Medicina antenna and on SRT.

On the Medicina antenna, the MF system has been installed in the central bay of the Cassegrain focus cabin (Figure 1.3).

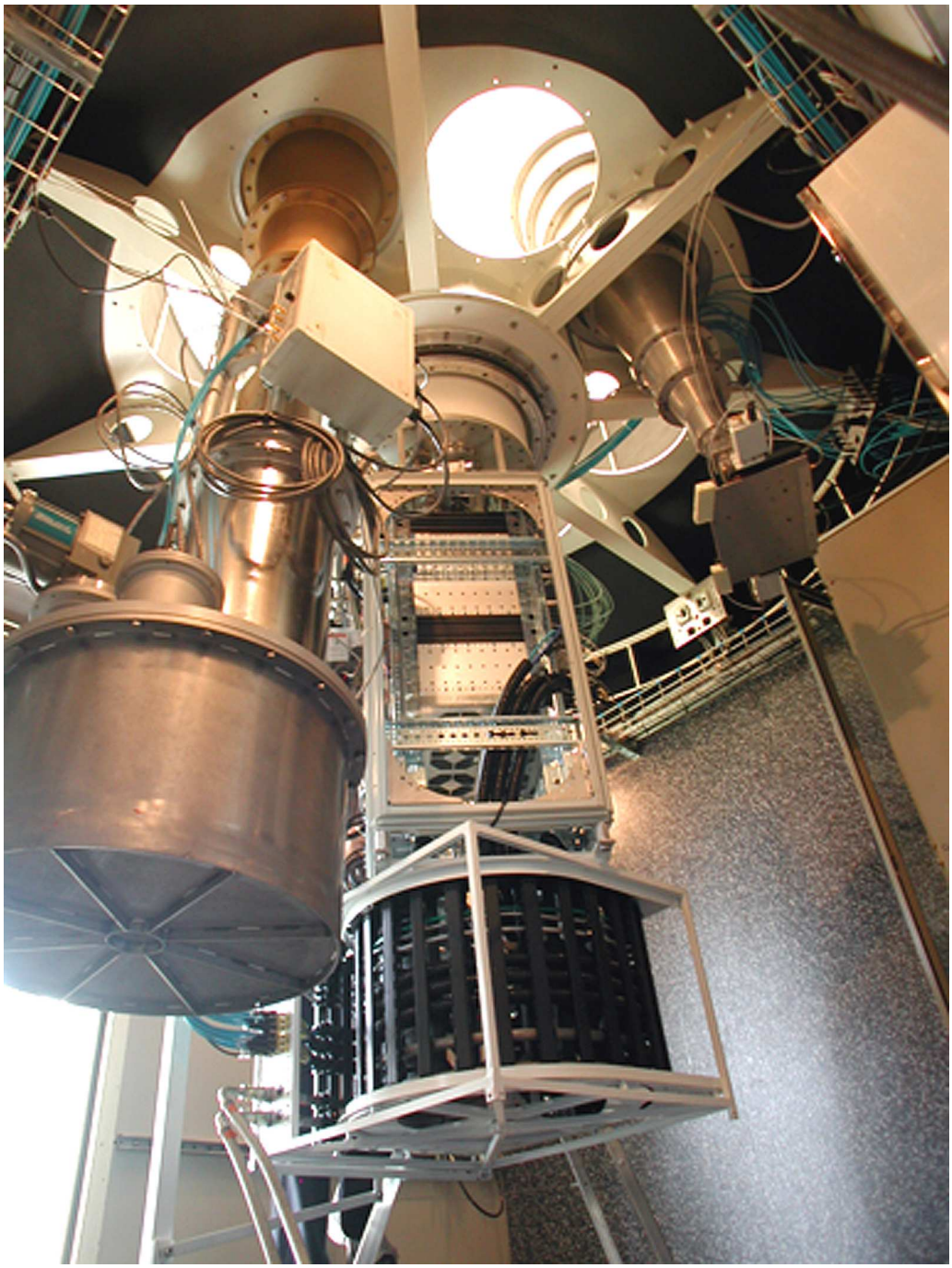

Figure 1.3 – The final installation of the MF receiver in the Cassegrain focus cabin in Medicina.

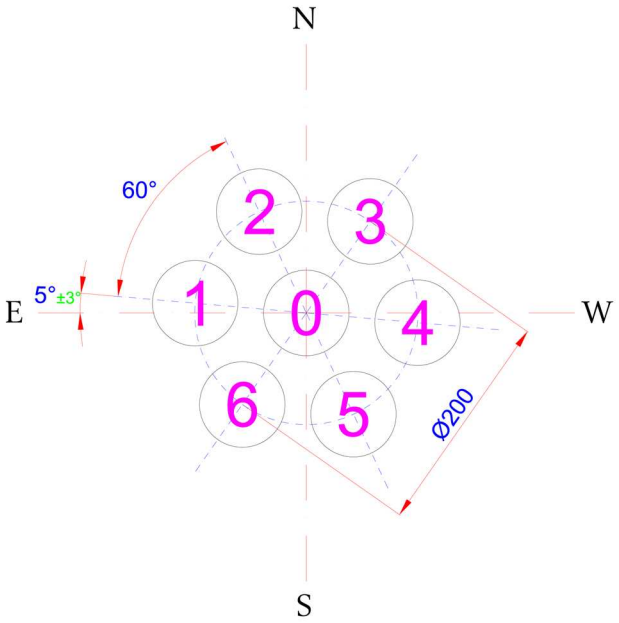


Figure 1.5 – The displacement of the seven feeds as they are installed on the Medicina dish.

Looking at the sky from inside the focus cabin, the displacement of the seven feeds is the one illustrated in Figure 1.5.

The slight offset (~ 5°) with respect to the ideal alignment is automatically taken into account when commanding and reading the derotator position by part of the user.

The beamsize relative to each feed can be estimated by means of the following formula:

$$\Delta\theta_{FWHM}\,(radians) = \left[1.02 + 0.0135\,|T_E\,(dB)|\right]\frac{\lambda}{D}$$

where $T_E$ is the taper value, $\lambda$ is the wavelength of the observed radiation, D is the antenna diameter.

@ 18 GHz $T_E$ = -3.5 dB → FWHM = 115” = 1.92’

@ 22 GHz $T_E$ = -5.3 dB → FWHM = 96” = 1.60’

@ 26 GHz $T_E$ = -8.0 dB → FWHM = 84” = 1.40’

Measurements performed during the first phase of the commissioning (Verma et al., 2009) give an actual FWHM = 92” @ 22 GHz, and a distance of 212” between the centres of two adjacent beams on the sky. As concerns the system performance, the reported reference values are the measured system temperature and antenna gain, given in Table 1.5 for the 22 GHz frequency.

| | |
|---|---|
| $T_{sys}$ (Elev.=45°, $\tau$ = 0.1) | 75 K |
| Gain | 0.105 K/Jy |

Table 1.5 – System temperature and antenna gain measured at 22 GHz

## 4. THE TOTAL POWER BACKEND

The wide bandwidth delivered by the multi-feed outputs (28 GHz) is detected by a total power backend. Due to time constraints it was decided to provide a traditional analogue backend, instead of developing a digital version using the modern FPGA (Field Programmable Gate Array) devices, which would have taken more time to design and develop.

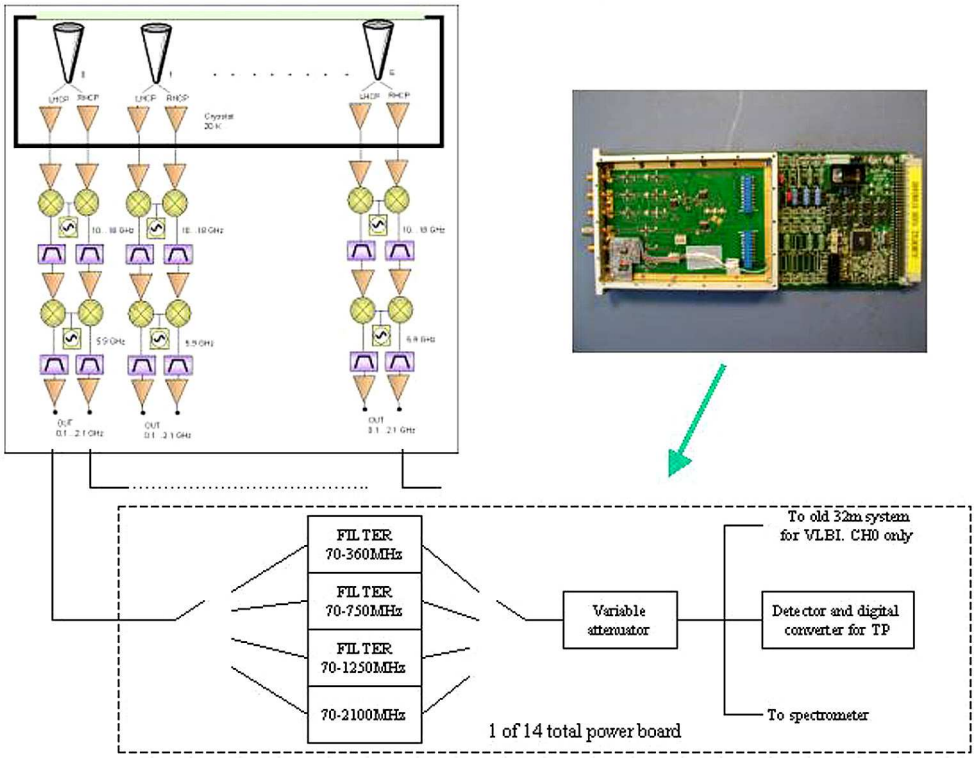


Figure 1. – Block diagram of the MF acquisition system.

The backend is formed by fourteen printed circuit boards, also including a digital part for board control and setup, and fourteen voltage-to-frequency converters to digitise the detected signals. The digitised samples are sent to the acquisition computer by means of a LAN (Local Area Network). Each board is designed to have three inputs, so that it can be connected to any receiver located on the three antenna foci of the SRT. The backend architecture is such that each input, before detection, is available at two backend outputs. This allows the system to simultaneously send every receiver output

to another backend, for instance a FPGA backend (e.g. for spectroscopy or VLBI observations), or to a remote detector (this last chain is specifically optimised in dynamics for a fibre optic link).
Prior to the detection, the signal goes through:

- an equalizer, to compensate the different attenuations – which vary with frequency – of the coaxial cables coming from each antenna focus;
- a variable attenuator, to set the signal power level in a suitable range;
- a filter bank, to reduce the bandwidth if necessary.

All these characteristics make this system both a data acquisition machine and a signal distributor.
The control stage of the acquisition system, realised by a small Linux computer with an embedded FPGA board, allows the control system to remotely set up the equaliser, the attenuation values, the filter bandwidth and the sample rate of the acquisition.
The sampling signal can also control the switching of a noise source of known temperature, which is injected through the receiver chains, so that the gain variation of the receivers can be tracked and compensated during the post processing phase (see Chapter 2 §2.4).
The main specifications of this backend can be summarised as follows:

- 14 x 3 IF inputs in the range 0.1 - 2.1 GHz;
- 2 IF outputs in the range 0.1 - 2.1 GHz;
- bandwidths: 230, 725, 1200, 2000 MHz;
- cable equalisation up to 12 dB;
- 0 - 15 dB variable attenuators, configurable with 1 dB step;
- sampling rate: 0.001 - 1 sec;
- up to 21 bit resolution;
- automatic cancellation of output offset;
- noise source chopping frequency: 0.5 - 500 Hz.

# CHAPTER 2

# ESCS (ENHANCED SINGLE-DISH CONTROL SYSTEM) [1]

*There are two ways of constructing a software design.*
*One way is to make it so simple that there are obviously no deficiencies.*
*And the other way is to make it so complicated that there are no obvious deficiencies.*
Sir Charles A. R. Hoare

## 1. OVERVIEW

INAF-IRA is leading the development of the control system for the Sardinia Radio Telescope (SRT), the 64-m dish at present under construction in S. Basilio (Cagliari). The plan is to fully exploit the antenna single-dish capabilities and the new-generation microwave receivers which are going to be installed on SRT – with multi-feed configurations, instantaneous bandwidth up to 2 GHz wide and a few tens of simultaneous channels. This forced the complete re-design of the observation management system with respect to that in use at the other Italian antennas, as they were not provided with such devices.

The necessity to produce a new control system for SRT timely matched the need to update the Medicina and Noto systems as well. For two decades these observatories have been mainly devoted to interferometry and were managed using the Field System (FS) – the control software developed and distributed by the VLBI consortium. In recent times the requests to exploit the 32-m antennas for single-dish activities have become more numerous, and keep increasing. To allow the execution of single-dish observations, various users have been developing customised scripts under the FS along the years, but no comprehensive and shared tools were released to specifically take care of single-dish activities in an organic and optimised way.

This inspired the decision to provide the Medicina and Noto antennas with a specific single-dish control system, which also constitutes the core for the development of *Nuraghe*, the system under construction for the SRT. This way, all the Italian radio astronomical antennas will essentially share the same control system, allowing for the

[1] Based on INAF-IRA Technical Report 409/07, Righini S. et al, 2007.

constitution of a national network and giving the opportunity to operate all the telescopes remotely, from a single control centre.

The Medicina-Noto system is called Enhanced Single-dish Control System (ESCS).

Its goal is to enable the antennas to perform optimised, user-friendly single-dish observations, including high-sensitivity deep surveys in continuum, spectrometry, and polarimetry. This requires innovation in the execution of the observations, providing the user with comprehensive tools to setup and control the antenna, the receivers and the backends. It is also compelling to generate output data in conventional file formats, in order to allow the use of the most widespread processing software.

## 2. ESCS SYSTEM REQUIREMENTS

At the beginning of 2008 the group involved in the development of ESCS (which I'm part of) agreed on the main requirements for this system. The primary goal is to provide the antennas with tools to carry out observations in the most common modes, performing them in any coordinate frame and allowing the control of all the devices – antenna, frontend, backend, etc… – in a comprehensive and user-friendly way, by means of on-line commands or using proper schedules. Another key point is the coexistence of ESCS with the FS, as the VLBI observations are still going to be carried out using the latter.

The following sections give details on the various aspects which were discussed, illustrating the choices made for the development of ESCS.

### 2.1. Observing modes and antenna management

Several observing techniques were considered, taking into account the ones usually available in other observatories. The complete list follows, however *Tracking* and *OTF-scan* modes were identified as those to be implemented with the highest priority, as they are the modes required by most of the observers.

Modes list

- *Tracking*: observations in sidereal tracking, along with more complex modes – by means of constant and variable rates applied to the coordinates; an internal

ephemeris calculator could be implemented to track Solar System objects starting from their orbital parameters;

- *Position switching*: alternate on-source and off-source acquisitions;
- *Raster scan*: sequence of discrete tracking acquisitions to map a given area of the sky;
- *Beam switching*: this method requires a multi-beam receiver. Two beams are employed, one is kept on-source, the other off-source. Periodical inversion of the beams, achieved with a different pointing, is allowed to take into account the different gains;
- *On-The-Fly (OTF) scan*: the antenna performs a scan at constant speed centred on a specified sky target - identified by user-defined parameters, such as start and stop positions. Usually the scan is along the great circle connecting the two points, unless differently specified (e.g. pure R.A. scan at a constant Dec.). Sequences of scans can be appropriately set to map a defined area of the sky (usually by scripts generating a schedule of the scan sequence once centre coordinates, area size, and grid step are provided). Users can select the beams to be employed: using two or three aligned beams only, the source is scanned and a proper ON-OFF operation can be performed off-line to remove the atmospheric contribution. The single acquisition is very fast – e.g. the rate should allow to scan a beam in down to 0.1 seconds. According to the receiver gain calibration procedure the acquisition rate should be as fast as 100 Hz. The user should be able to set scan coordinates in the Celestial, Galactic and Horizontal systems, at least;
- *Cross-scan*: two orthogonal scans centred on the source;
- *Beam switching OTF*: two non-aligned beams respectively scan the source and an adjacent sky area. Periodical inversion of the beams is allowed to take into account the different gains;
- *Wobbling*: on-source and off-source acquisitions are achieved tilting the subreflector. The possible movements vary accordingly to the receiver position and the beam width. Mechanical constraints allow a maximum wobbling frequency of about 1Hz;

- *Frequency switching*: the spectral observations are performed always tracking on-source and varying the local oscillator frequency, in order to alternate the line position in different portions of the sampled band;
- *Artificial satellite tracking*: similarly to the Solar System bodies tracking, this mode requires the implementation of a specific tool to compute the position of artificial satellites or space debris fragments on the basis of TLEs (Two-Line Element).

As concerns the antenna pointing, the privileged operating mode was identified in the "time-tagged program track". It consists in commanding in advance a sequence of positions, each labelled with a UT timestamp corresponding to the instant the antenna must point to the given position. It minimises the load for the station computer and offers the best tracking quality. It is widely independent of the latency fluctuations in the computers and in the communication line. The pointing model rms is required to stay within the threshold of 0.1*HPBW.

Coordinate systems

For any observing mode, users must be allowed to insert the source coordinates in the system they prefer, such as Equatorial, Horizontal, Galactic, Ecliptic. The system is in charge of converting them to the Horizontal (Az-El) commands needed to point the antenna. The highest priority was given to the Equatorial (any epoch), Horizontal and Galactic systems.

Subreflector

The mirror must be completely retracted along the y axis when the primary focus is used (this fulfils the frequency agility requirements).

The system must take care of the secondary mirror movements. Mechanical actuators are installed and allow the mirror to tilt around the x and y axes. In addition the whole system can translate along the x and y axis. These adjustments are aimed at conveying the incoming radio waves to the selected secondary focus feed, and can be exploited to perform wobbling observations and focus tuning. For high frequency observations, such as the ones performed in K-band, the pointing model must command proper

adjustments to the subreflector position – varying with elevation – in order to compensate for gravitational deformations.

Derotator

A tool to use a derotator, which is required in case of multi-feed receivers, must be included in the system. It is to be noticed that not all the observation modes require the field to be derotated, so the derotator activation must be optional. Table 2.1 lists the specifications for the derotator of the 18-26 GHz multi-feed receiver. Values for the installation on the Medicina dish and on SRT are given.

| | **Medicina** | **SRT** |
|---|---|---|
| Rotation range ($^o$) | ±130 | ±120 |
| Max rotation speed ($^o$/sec) | 4.37 | 4.37 |
| Positioning Accuracy (arcsec, on sky) | 0.055 | 0.036 |
| Positioning Resolution (arcsec, on sky) | 0.020 | 0.013 |

Table 2.1 – Parameters relative to the derotator of the 18-26 GHz MF

Weather sensors

The weather station measurements must be read by ESCS, in order to be displayed in the antenna monitors and to be written in the data files. Recording temperature, relative humidity and atmospheric pressure is of critical importance, especially for high-frequency observations, as they are employed in the estimation of the atmospheric opacity, which in turn is a key value for data calibration.

Measuring the wind speed, instead, is vital to minimise damage risks: an automatic antenna-parking system must activate in extreme weather conditions, in particular in case of wind speed exceeding 80 km/h.

Dynamical antenna time allocation

It must be noticed that the constant updates on the antenna status and on the site conditions allowed by ESCS will make a dynamical allocation of the antenna time possible. High-priority projects – e.g. requiring low atmospheric opacity, as in the case of high-frequency observations – are to be carried out only if weather conditions are sufficiently good, otherwise starting the "normal" observations. This kind of management requires the definition of parameter thresholds and the presence of operators who take care of the observation switch in real-time.

## 2.2. Calibrations

To ensure all the archived data can be correctly calibrated it is important to include a "calibration start-up" at the beginning of every observing run.

Measurements useful to calibrate the observations and track the antenna performance must be obtained periodically (at least daily, depending on weather conditions and observing frequency). Non-invasive procedures – such as the measurement of meteorological parameters – can be frequently performed during the observation and stored in the station log and/or within the output files. All the setup and calibration procedures are meant to be stored in local files and are available to the local staff to obtain statistics and useful data for the antenna monitoring.

Pointing

The procedure consists in performing cross-scans on point-source calibrators to obtain updated information on pointing accuracy. A similar procedure already exists in the Field System (FIVEPT command), and inspired the development of such a tool for ESCS. The FS pointing model seems to be accurate enough up to 22 GHz and is used in the ESCS system as well.

To obtain a higher precision pointing, the use of metrological facilities is foreseen. Several devices will be activated and monitored on-line – e.g. inclinometers (already available) or temperature sensors (already available on the *alidade* and to be installed on the *quadrupod*). The metrology group of SRT has been extensively working on this task.

Antenna Gain

Periodic calibration campaigns produce a model of the antenna gravitational deformations, which allows to calibrate the data for the gain variations due to the loss of efficiency.

Additional details must be taken into account in case of multi-feed receivers, requiring specific calibration procedures to be carried out during the observation sessions, since:

- different beams are expected to show different gains (requiring flat-field acquisitions);
- multi-beam gravitational deformations must be taken into account.

The calibration procedures must be easily available to the users, along with the resulting updated model.

Focus

Moving the antenna during daytime, the different exposure to solar heat produces temperature variations and, as a consequence, focus migration. Focus calibration is thus required. The focus position is determined performing a cross-scan on a strong source and finding the subreflector placement which maximises the received power. A strategy to perform focusing for a multi-beam receiver is being studied. Various radio telescopes (such as the GBT and Effelsberg antennas) provide the user with an auto-focus tool, which will be usefully implemented in ESCS as well.

Atmospheric attenuation

Since no independent radiometer is available, the opacity measures are to be carried out with the 32-m dish during the observation sessions. The opacity is estimated by means of sky dips, which are OTF or raster scans performed moving the antenna in elevation only: measures of the system temperature are taken at different elevations, in order to estimate the opacity value. $T_{sys}$ is, in fact, the only observable needed to solve for the opacity ($\tau$) the following equation:

$$T_{sys} = T_{sky} + T_{rec} + T_c + T_{sp} + T_{CMB}$$

where: $T_{rec}$ (temperature of receiver), $T_c$ (temperature of the receiver cover), $T_{sp}$ (spillover temperature) and $T_{CMB}$ (temperature of the Cosmic Microwave Background) are all known – measured or estimated – values[2], while:

$$T_{sky} = T_{atm} \left[1 - e^{-\tau X_{air}}\right]$$

in which the parameters are: $T_{atm}$, the temperature of the atmosphere and $X_{air}$, the secant of the zenith angle – i.e. 1/cos(90°-elevation). With several measurements for $T_{sys}$ vs. elevation, algorithms such as the Levenberg–Marquardt (LMA) are applied to fit the data and estimate $T_{atm}$ and $\tau$.

Flux

A proper standard flux calibration procedure must be set and made available to users (observers/operators). It is intended to find the Count-to-Jy calibration factors for all channels (up to 14: two polarizations and 7 receivers) and all frequency channels. The standard procedure will likely consist of one scan (or sequence of scans) on sky flux calibrators. A list of possible calibrators well spread throughout RA must be made available, for all the observed frequencies.

Polarisation

A proper standard polarisation calibration procedure shall be set and made available to users (observers/operators). It is intended to find the Count-to-Jy calibration factors for both Q and U, polarisation angle and polarisation leakages (instrumental polarisation fraction), both in combination with the total flux calibration and polarisation only calibration (e.g. background diffuse emission cannot use total flux data, because of the missing large scale flux). The polarisation calibration is more complex than the total flux one, since it depends on the backend actually in use (e.g. analogue or digital backends). Each backend operated by ESCS needs a specific procedure.

[2] INAF-IRA Technical Report 430/09, Verma R. et al, 2009.

Multi-beam geometry

The position of the beams w.r.t. the pointing reference point must be measured and included in the output data, in order to correctly recover the sky pointing of each beam during the post-processing.

## 2.3. RFI monitoring

In order to provide the observers with all the useful information, it is important to monitor the RFI presence in the various radio bands. This is even more critical using ESCS, as the new high data-rate observing techniques permit to reach a sensitivity which is two order of magnitude better than before, such exposing the observations to more numerous RFI.

It is impossible to daily monitor the RFI, since this procedure would subtract antenna time, but meaningful statistics can be extracted mixing several inputs, such as:

- archived information about stable and known RFI;
- “listening campaigns” carried out by the on-site RFI Group;
- dedicated observations performed with the 32-m dish, especially within the bands which cannot be covered by the RFI Group instruments;
- detections reported in feedback forms that users are asked to fill in after their observing sessions.

As concerns ESCS, a spectral quick-look of the data under acquisition is a useful tool to be included in the system, allowing the user to preview the status. The incoming data shall be displayed both in a “refresh mode” and a “cascade mode”, to follow their evolution with time.

The actual removal of RFI-affected data is then performed off-line. The Westerbork and Effelsberg antennas are provided with a RFI mitigation system which should be investigated to evaluate whether it can be successfully implemented at the Italian radio telescopes as well.

## 2.4. Data acquisition

Common GUI

The ESCS system, even if composed of several units, is planned to be accessible from a unique Graphic User Interface: starting from a single panel, the users will be able to configure their observations completing all the phases of the antenna setup.

The programs must be differentiated because different types of observation require specific setups and commands, however the interface should be common. In practice, simply selecting the observing mode from the main window, the system will display all the sections necessary to perform the frontend and backend setup for that specific mode, while the general system takes care of the antenna pointing and other tasks. Simplifications and grouping can be imagined, e.g. continuum observations can be thought as spectral acquisitions taking place with a single, or very few, channel and a very large bandwidth. Every specific window of the interface, hiding a program dedicated to the specific system component, should contain the default setup relative to standard observations. The various user-defined parameters can then be saved in a configuration file. The parameters can also be set by schedule files which can be loaded through the GUI.

Also antenna monitors, calibration and quick-look panels will be accessed in this framework.

Every GUI section should have textual and graphic interfaces (“expert” and “novice” modes respectively), so that expert users can exploit the textual shells to perform a more sophisticated setup and use custom pipelines.

Scheduling

The system must produce human readable and editable schedules. This can be obtained applying some macros to initial input parameters: in case the antenna is to produce a map, for instance, the user can indicate the map centre coordinates and the map extension – or the start and end point coordinates – so that the system produces a list of scan schedules. The map will be realised by performing the whole scan sequence.

Of course, users can write their own schedules, according to a standard form, or edit the existing ones. If system failures cause the observations to stop, then the acquisition is to

be automatically restored starting from the schedule line which was in execution before the interruption.

In the future, a software tool able to consider a given source list and produce an optimised schedule should be developed – for example to observe a sequence of targets in time intervals around their transit.

Data rate and synchronisation

To evaluate the data rate produced during observations, a "worst – yet realistic – case scenario" is taken into account. The most complex receiver available is the 18-26 GHz multi-feed, with 14 output lines, each having a 2 GHz bandwidth. For every line, it is possible to activate a noise mark of known temperature oscillating at the desired rate, in order to calibrate for the receiver gain drifts. An optimal value for the mark switching frequency has been initially identified in 42 Hz, which allows to acquire data without suffering from the interference of the 50Hz signal and its harmonics. This implies the acquisition of a value every 12 milliseconds.

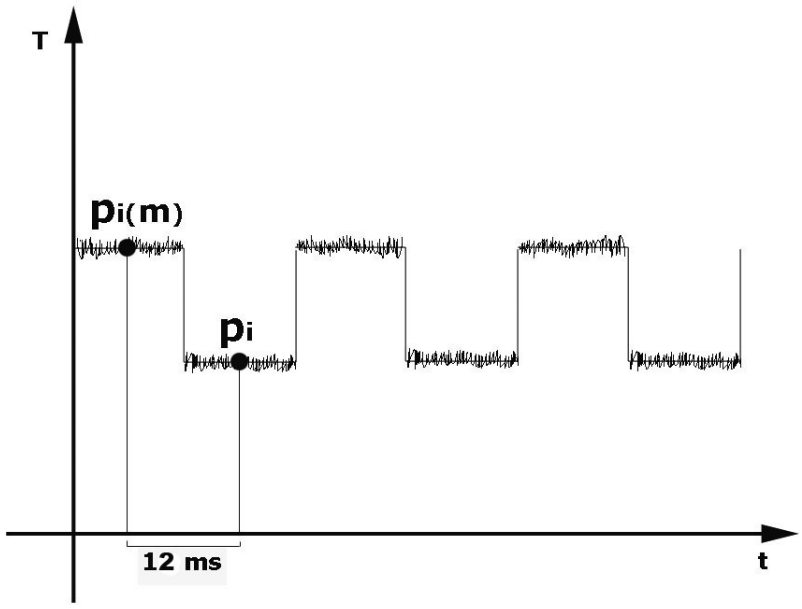


Figure 2.1 – Antenna Temperature vs time in a switching-mark observation

The sky measurement and the relative calibration - obtained using a mark of known temperature - are given by:

$$\left( p_i \; ; \frac{p_i}{p_i(m) - p_i} T_{cal} \right)$$

where $p_i$ is the antenna temperature measured on the sky, $p_i(m)$ is the value taken when the calibration mark is on, as schematised in Figure 2.1, and $T_{cal}$ is the mark temperature. Following the above mentioned setup, a $p_i$-$p_i(m)$ pair is acquired every 24ms. For example, if the observed band is split into 4 sub-

band boards (which is a possible setup for the multi-feed), the acquired data – taking into account also the polarisation parameters – will be:

14 x 4 x 2 samples every 12 ms → 9334 sample/s

The needed dynamics is 20 bit, which is translated inside the computer in 32 bit.
As a consequence, the recorded data, including all the system data such as the time mark, will reach an amount of about 37 KByte/s.
This corresponds to the production of 3 GByte every 24 hours, which is compatible with the available hardware, both in terms of network transmission rate and hard-disks storing capacity.
Much higher data rates will be required by digital backends.
The synchronisation of the different computers/devices will be performed via software: this allows synchronisations down to 1-ms, which seems to be sufficient, unless specific constraints require hardware solutions, that should be investigated together with the backend developers. It must be evaluated whether and when real-time is needed.
The backends are usually installed next to the frontends, thus reducing the needed cables and the possibility of problems arising from them.

Housekeeping data collection and management

A lot of parameters coming from different antenna instruments and tools will be recorded more slowly than the scientific data. In the following a non-comprehensive list:

- Antenna data: inclinometers, temperature sensors,…
- Receiver data: vacuum value, cryogenic temperature, power supplies status, LNA currents, indoor temperature, other device temperatures,...
- Weather data: outdoor temperature, atmospheric pressure, humidity, wind speed

Multiple backend usage

The possibility to use different backends simultaneously (e.g. to acquire continuum and spectrometric data together) should be included.

Guest backends/software

ESCS is aimed at managing all the devices now present on the antenna, becoming a standard also for the instruments which are going to be developed and installed in the future. However a "back door" should be left open in order to welcome external users who need to use different hardware and software systems .

In the initial "transition phase" the main goal is to gather as many backends and users as possible, providing solutions to those who are already developing custom devices. In the future the Institute of Radioastronomy should give clear guidelines for developers in order to produce compatible hardware and software.

Field System

The FS is a system conceived for VLBI observations, and represents a standard for all the antennas involved in these interferometric activities. As a consequence, it must still be available in the future. It is planned to be run on a separate computer: the Field System will work as a client of ESCS

### 2.5. Data output: MBFITS

The ESCS group chose the MBFITS (Multi-Beam FITS) format as a standard for every observation. This hierarchical format is being developed by several groups around the world (§ APEX MBFITS manual[3]). MBFITS permits to store a large amount of data, including detailed information on the various system devices setup, thus consenting a wide range of post-processing approaches. Its structure is conceived to record data taken from a multi-beam receiver, including all the parameters which define the status of such a device – e.g. the derotator position, the geometry of the beams, etc… Also for archival purposes and other users' use (after the proprietary time expires), any observation should be stored in MBFITS format. If guest backends do not have a native MBFITS output, a converter to an at least minimal MBFITS format should be provided.

[3] http://www.apex-telescope.org/observing/APEX-MPI-ICD-0002.pdf

MBFITS is to be considered as a standard output, required to anybody accessing the Institute antennas.

### 2.6. Other tools

Users must be provided with useful tools to plan and perform observations, and to check the quality of the acquired data in real-time. Moreover, the user must have access to data reduction tools for the various types of observations, although they are likely to be external to ESCS – chosen among the most widespread programs in use.

Quick look

A constant update of the data quick-look must take place during the observations. The user must be able not only to monitor the antenna status, but to evaluate the results of the calibration operations and have a preview of the acquired data. Various panels must be displayed to accomplish to these requests, providing also the possibility to interact with this quick-look facilities and execute basic commands and pipelines.

Data reduction tools

The observatory must be provided with a series of data reduction tools, in order to perform an accurate off-line analysis for any given kind of single-dish observation. It must be determined which software is available off-the-shelf – preferably choosing among the most widespread programs in use – or if custom solutions are needed, to perform data reduction for:

- Total power
- Polarimetry
- Spectroscopy
- Multiple backends
- Exotic (space probes tracking, space debris monitoring, ...)

Beam map

It is desirable to produce, for every receiver, maps of the beam(s) up to the secondary lobes – or even farther – to be employed in the “clean” phase of the post-processing.

Since the 32-m dishes are quite small antennas, their relatively low sensitivity could make it difficult to reveal lobes beyond the secondary ones, which are 18-20dB under the main lobe. Even operating a cross-scan on a strong source, farther lobes might not be mapped. However, it is important to try to obtain accurate beam maps as they would be extremely helpful, especially in deep surveys.

Catalogues

Catalogues of specific sets of sources are functional to various phases of the observation. In particular, updated lists of calibrators must be available to the observer, consisting of:

- pointing calibrators
- antenna gain calibrators
- polarimetry calibrators
- raw calibrators (Sun, Moon, planets)

The information relative to the listed sources – e.g. coordinates, flux, etc… – is to be frequently revised. It is possible to retrieve updates from observatories, such as the VLA, which monitor these calibrators and periodically dispatch accurate measures.
The calibrator flux is often expressed as a function of frequency, in the form of a polynomial curve. In analogy to a present FS tool, the expected flux of the needed calibrator should be computed on-line considering the running observation setup and depending on the relative dimension of the source with respect to the antenna beamsize.
Along with calibrator catalogues, source catalogues must be available to the observers.
Source catalogues are widely available on the Internet querying on-line databases (such as SIMBAD). However, at least the most important ones must be included in the local system, for the observers to consult.
In principle it should be possible to keep track of all the observed sources, automatically building a database of all the entries received by the antenna pointing system, but this approach was not believed to be effective. In fact, such a database would end up containing also mistaken inputs; moreover the proprietary time constraints have to be taken into account.

"Static antenna" mode

The system must include the possibility to check the antenna setup without commanding the source pointing. It is equivalent to a normal observation, but the source tracking and antenna motion are disabled. This can be obtained simply including a check-box in the main setup panel to enable/disable the actual pointing commands. This way, the user performs the complete antenna setup and checks the correct functioning of the selected receiver and backend, but does not lose time with dish slewing.

### 2.7. Service-Mode observations

In perspective, all the antennas operated by the Institute of Radioastronomy might be planned to mainly provide service-mode observations: the Institute staff carries out the observations – using the various antennas – on behalf of the observers. This can be more easily accomplished as all the antennas are provided with the same control system; under this circumstance, all the antennas can be managed from a single centre. This policy is aimed at optimising the antenna usage (e.g. exploiting the best weather conditions or the most suitable instrument/device for the contingent needs of a project).
Particularly expert and frequent users could then be authorised to have direct remote access. Anyway a "standard visitor mode" will be available to the astronomers wishing to attend their observations.

### 2.8. Archiving

The increased usage of the Medicina and Noto antennas as single-dish facilities, not to mention the additional employment of SRT, asks for an efficient and user-friendly archive to host the large amount of raw data.
A first solution is to list the MBFITS files – including: observations, tests, calibrations, etc… – with some basic parameters like target, backend, date/time, gain, focus, etc…, so that queries can be performed. The initial idea was to develop this database in MSQL but, since ACS provides an archive structure, this architecture is more likely to

be exploited, keeping in mind that the archive is planned to be common to all the IRA telescopes.

A comprehensive archive of the acquired data and the related information must include all the following items:

- Weather data
- Opacity data
- Antenna gain data
- Focus position data
- Pointing error data
- RFI data
- Housekeeping data
- Observations data

The database must be queried by several parameters. Ideally, by any of the parameters included in the file headers, in order to perform specific queries for a number of scientific, statistic and maintenance purposes. The antenna performance can be monitored and evaluated. Also the weather conditions and RFI situation at the site can be traced, producing meaningful statistics.

General users will access observation/calibration files only, while local staff will be granted access to files flagged as “private”.

## 3. ESCS DESIGN AND DEVELOPMENT INSTRUMENTS

The choice of the development tools was a logical consequence of the project constraints:

- employment of free software;
- system scalability – new functions and sections must be added without affecting the previously developed ones;
- system durability – i.e. ease of maintenance;
- client-server architecture – the system is divided into servers, providing services, and clients such as GUIs and user applications which can run on a different machine (or even platform).

In addition, since ESCS is planned to manage all the Italian radio telescopes, the system design must take into account the needs of the different telescopes.

The main software/hardware instruments to develop the ESCS system have been identified in:

- Unix-Linux platform;
- ACS (ALMA Common Software) framework;
- PCs - other machines;
- TCP/IP and CORBA communication protocols;
- C++ as programming language, Python for scripting;
- QT libraries and JAVA for GUI;
- Doxygen as automatic documentation tool;
- UML (Unified Modelling Language) to schematise the system architecture.

The choice of the software tools was suggested by their reliability and widespread use, allowing the ESCS developers to exploit the many shared resources available and assuring an easier maintenance of the system.

The preference for the C++ programming language was motivated by three main reasons:

- the main developers of ESCS already had expertise in C++ programming;
- among the choices allowed by ACS (C++, Java, Phyton, see §3.1) it offers the best performance and greatest flexibility;
- C++ permits to operate at low level with hardware devices in a more straightforward way.

### 3.1. ACS (ALMA Common Software)

ALMA is a huge millimetre and sub-millimetre interferometer at present under construction in the Atacama Desert (Chile) within a cooperation among Europe, North America and Japan. Once completed, this complex instrument – designed employing state of the art technologies – will count more than 50 12-m antennas.

ACS (ALMA Common Software) is the framework in which the ALMA control software is being developed, providing infrastructures, common patterns, services, libraries and documentation to all the people creating the system. Originally conceived

for ALMA, ACS has spread among many other teams thanks to the extensible concepts and tested standards it is based on. The number of non-ALMA customers of ACS has increased during the years, including groups which are not even related to Radioastronomy. Because of this, the new acronym of Advanced Control Software was proposed.

Overview

ESCS – or any other control system developed in the ACS framework – runs over ACS, which provides a general and common interface between the high level software, hardware and other software parts on the top of the operating system (see Figure 2.2). ACS is based on CORBA[4] middleware which takes care of exchanging messages between platform independent DOs (Distributed Objects). Distributed Objects are software modules that collaborate to perform some tasks though being located on different computers – but they can also be different processes running on the same machine.

The advantages of DOs are:

- parallelism: Objects can run contemporarily;
- failure containment: if a single Object fails, it does not cause the general system failure;
- multi-platform, multi-language support: Objects can cooperate even if they are running on top of different operating systems.

A further simplification is given by the fact that the tough details of the underlining CORBA mechanisms are hidden by many APIs (Application Programming Interface) provided by ACS, so that ACS programmers don't have to deal with the complexity of CORBA.

[4] http://www.corba.org/

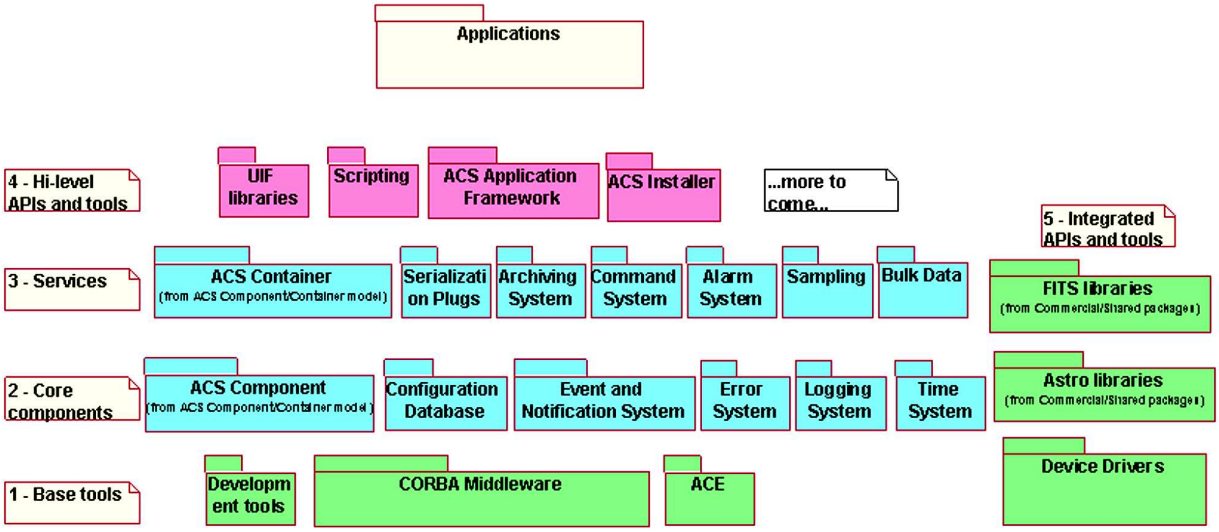


Figure 2.2 – UML general scheme for ACS

Reasons behind the choice of ACS

As already mentioned, ACS offers many advantages to the developer, even if at the cost of a very steep learning curve due to the complexity of this system. The main reasons why ACS has been chosen for the NURAGHE/ESCS development are:

- ACS offers several ready-to-use services (logging, alarms, monitoring, archiving, etc...) that are mandatory for the production of any control software;
- ACS is built on the knowledge of other control softwares based on CORBA;
- the Distributed Object model allows to design a reliable, optimally load-balanced system;
- a vast community of ACS customers is contributing to the software repository; sharing codes and ad-hoc solutions is extremely useful to reduce the development time, avoiding the necessity to “reinvent the wheel”;
- all ACS code is under the GNU Lesser General Public License (LGPL), allowing the complete and free reuse of the code;
- ACS is built and distributed with off-the-shelf, freeware tools and components (like CORBA). This means achieving reliability at no cost;
- ACS customers (mainly ALMA) are all contemporary major projects; this is a guarantee that the software will be improved and maintained for many years.

More on the architecture of ACS

The ACS Architecture is based on the "Component-Container model" (§ ALMA Common Software Architecture[5]), whose aim is to allow software organization and development separating functional concerns from technical concerns.

A Component is defined in as a software element that exposes its services through a published interface and explicitly declares its dependencies on other components and services. Containers provide an environment where Components run, with support for basic services like logging system, configuration database, persistency and security.

ACS provides a simple implementation of the Component-Container model in C++, Java and Python.

As Figure 2.2 shows, the packages constituting ACS are grouped in 5 layers.

Each package is allowed to use services provided by other packages standing on lower layers and on the same layer, but not on higher layers.

1. *Base Tools* - the bottom layer contains base tools that are distributed as part of ACS to provide a uniform development and runtime environment on top of the operating system, for all higher layers and applications. These are essentially off-the-shelf tools. ACS just provides packaging, installation and distribution support. This ensures that any installation of ACS has the same basic set of tools, whose versions are described in the documentation coming with each ACS release. Three main packages are present in this layer:
    - Development tools – compilers, configuration controls tools, languages, debuggers, documentation tools;
    - CORBA Middleware – packaging of off-the-shelf CORBA implementations to cover the languages and operating systems supported by ACS;
    - ACE – distribution of the Adaptive Communication Environment.

[5] http://www.eso.org/~gchiozzi/AlmaAcs/OnlineDocs/ACSArchitecture.pdf

2. *Core components* - this layer provides essential components for the development of any application, such as:
    - ACS Component – base interfaces and classes for the Component part of the "ACS Component Model". In particular C++ Distributed Objects, Properties and Characteristics are implemented in this package;
    - Configuration Database – interfaces and basic implementation for the Configuration Database from where the system retrieves its configuration, initialisation and deployment parameters;
    - Event and Notification System – it provides a generic mechanism to asynchronously pass information between data publishers and data subscribers, in a many-to-many relation scheme;
    - Error System – API to handle and log runtime errors, tools for defining error conditions, tools to browse and analyse runtime errors;
    - Logging System – API for logging of data, actions and events. Transport of logs from the producer to the central archive. Tools for browsing logs;
    - Time System – time and synchronization services.

3. *Services* - the third layer implements services that are not strictly necessary for the development of applications but are meant to allow the optimisation of the system performances:
    - ACS Container – design patterns, protocols and high level services for the Component/Container lifecycle management;
    - Archiving System – API and services for archiving monitored data and events from the runtime system. Tools to browse, monitor and administer the flow of data toward the archive;
    - Command System – tools for the definition of commands, API for runtime command syntax checking, API and tools for dynamic command invocation;
    - Alarm System – API and tools for the configuration of hierarchical alarm conditions, API for requesting notification of alarms at the application level, tools for displaying and handling the list of active alarms;
    - Sampling – low level engine and high level tools for fast data sampling;

- Bulk Data – API and services for the transport of bulk science data (images or big data files) and continuous data streaming.

4. *Hi-level APIs and tools* - the fourth layer provides higher-level APIs and tools to offer a path for the implementation of applications, in order to implicitly obtain conformity to design standards. Among these, there are:
   - UIF Libraries – development tools and widget libraries for User InterFace development;
   - ACS C++, Java, and Python Application Frameworks – implementation of design patterns for the development of standard applications.

5. *Integrated APIs and tools* - the 5th group of packages contains software that is used by many ALMA Subsystems, but that is not used by other ACS packages. These packages are for convenience integrated and distributed together with ACS but are not integral parts of ACS. They include tools which are useful for Radioastronomy:
   - Device Drivers – low-level drivers for commonly used devices;
   - Astronomical libraries – libraries for astronomical calculations and data reduction;
   - External libraries – support for the handling of standard output files is just an example of other high-level components that is to be integrated and/or distributed as part of ACS.

# 4. ESCS STRUCTURE

In this chapter we will analyze the core of ESCS which is the server part of the client/server, application/component architecture as defined before. Of course the system consists also of a large section dedicated to higher level application, scripts and user interfaces that will not be described in detail.

The system is package-based: each package – or subsystem – is a group of components that stay logically or functionally together. This choice facilitates the system design, as it is divided in virtually independent working units, and also the implementation, as each programmer can focus on the development of a single section.

ESCS essentially consists of 5 packages (Figure 2.3), which work together in order to reach the goal: perform the observation.

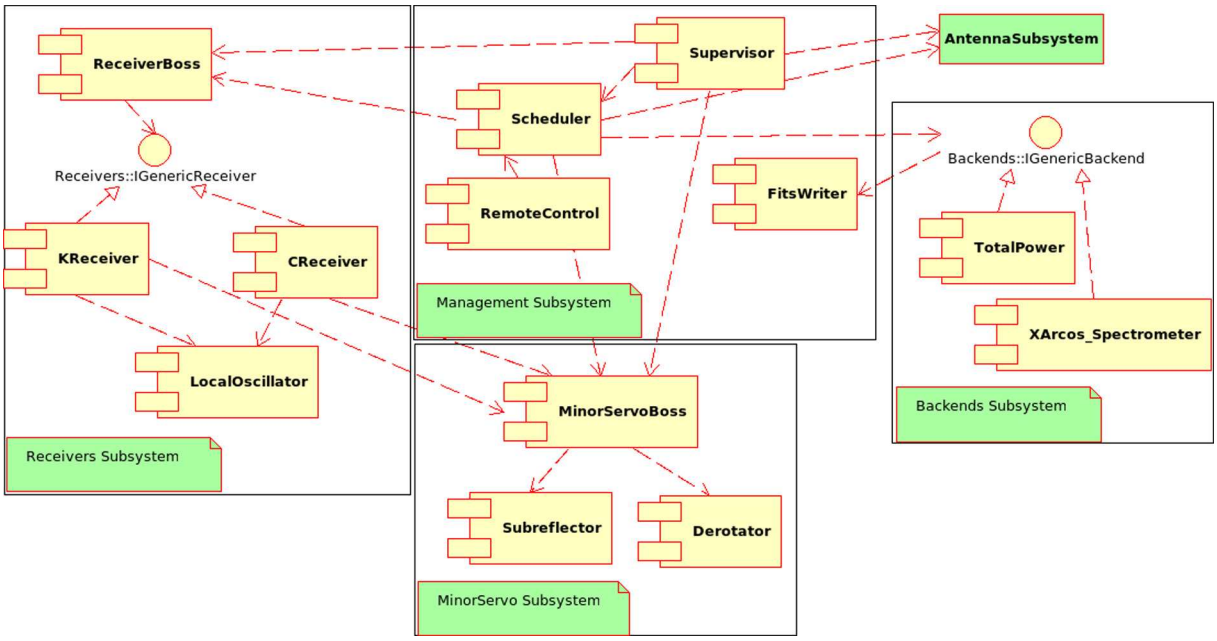


Figure 2.3 – UML scheme of the overall ESCS system. The five packages - or subsystems - are named Receivers, Management, MinorServo, Backends and Antenna.

The cooperation becomes possible thanks to a communication interface that is mainly realised by means of the “Boss” components. Almost all packages have a “Boss” component which leads them, being updated on their status and being in charge of issuing all high level operations that involve directly their package. Any functionality of a package is called for through the “Boss”. This kind of isolation allows the change of a subsystem architecture without affecting all the other subsystems.

Short descriptions of each subsystem are provided in the following sections. More information is given on the Antenna package, as it is in advanced progress status – close to the release that will be installed at the SRT – and because it is the package I was mostly involved in.

### 4.1. Management subsystem

This subsystem is the entry point for the user allowing the control of the telescope with the purpose of performing any kind of observation.

The package contains a standalone component for the production of the output FITS file (FitsWriter, see Chapter 3 §3). In case, it is possible to add other components devoted to store the data in different file formats – binary, ASCII, standard astronomical formats, etc.

The package leader is called “Scheduler”. It accesses all the subsystems and is able to perform high-level operations simultaneously involving one or more subsystems; for example the computation of the system temperature requires to command a receiver and interrogate a backend. The Scheduler reads and interprets observing schedules (see Chapter 3 §4), commanding the resulting operations to the telescope mount, the receiver and the backend. It also works thanks to an interpreter of “human-readable” commands, so that it associates any operation to a text command. This way the user can also write macros and configuration procedures to be executed manually or by means of schedules. Command lines can also be exploited to remotely access the system, without performing any login on the machine where the system runs. This is possible because of the RemoteControl component, which accepts a connection on a TCP port and forwards the human-readable commands to the Scheduler.

The package is provided with a supervisor, whose aim is to check the status of the whole system. For example, this component collects status information from the Boss of every subsystem, then decides if everything is working correctly. In case of problems, it raises a warning, which is a pre-alarm condition which may not interfere with the ongoing observation, or an error, which is a fatal condition that does not allow the observation to go on. The supervisor has higher priority on all the other subsystems and can stop the observations without notice – e.g. in case of high-speed wind thrusts.

### 4.2. Receiver subsystem

Every receiver, with all the parts it is composed by, is controlled by a component as if it was a unique hardware device. Every implementation is specific and hardware-dependant, however the Boss is isolated from any technical detail since all the components are seen through a common interface.

At present the receivers partially included in the ESCS system are the K-band MF (Chapter 1 §3) and the 5 GHz single feed, both installed in the secondary focus cabin of the Medicina dish. These components are kept active even when the receivers are not in use, because their duty is also to monitor the "vital parameters" of those devices, as the power supply, the cryogenic temperature, etc…

When the Boss subsystem is asked to configure a given receiver, it points to the relative component forwarding the configuration command to it. It is the component to execute the needed operations, as the Local Oscillator frequency setting – which, in turn, is managed by a separate component as the LO is common to all the receivers.

The Boss is always able to operate on the configured receiver:

- switching on and off the calibration mark;
- specifying the temperature of the calibration mark, given the feed number, the polarisation and the frequency band;
- checking the receiver status;
- indicating the array geometry in case of multi-feed receivers.

### 4.3. Backend subsystem

This package can be defined as a hybrid, as it lacks a true Boss: every backend component is directly managed by the Scheduler of the Management subsystem. It also constantly deals with the FitsWriter component within Management, so the Backend subsystem can be regarded as a sort of "extension" of the Management one.

The Scheduler needs to directly administer the currently active backend to improve the efficiency. It deals with the generic backend via a unique interface, without knowing whether the backend in use is a total power device, a spectrometer or a polarimeter.

The interface can be adjusted to take into account the different hardware solutions, but this can be handled without compromising the above mentioned level of abstraction.

The data acquired by the backend are sent to the FitsWriter – and in the future to other data formatter and recorder – using a proper protocol based on the CORBA Audio/Video streaming service.

Every Backend component exposes the methods which allow the Scheduler to start, suspend and stop the data acquisition, exploiting a time mark provided by the Scheduler itself.

### 4.4. MinorServo subsystem

In the Medicina release of ESCS, this package controls:

- the positioning of the primary focus receivers;
- the positioning of the six axes of the subreflector;
- the positioning of a multi-feed derotator.

At present the only implemented function is the management of the derotator. Once completed, the MinorServo subsystem will take care of positioning the receivers and perform their "tracking" – i.e. adjust their positions according to an optimised curve for the compensation of the gravitational deformations, which is fundamental for high-frequency (narrow beam) observations.

The Boss of this subsystem will also be provided with advanced tools to perform the wobbling of the subreflector and focusing procedures.

### 4.5. Antenna subsystem[6]

This subsystem is in charge of controlling the telescope main drives. The Antenna package is not only able to drive the azimuth and elevation axes, but it also includes all the required high-level functionalities to perform a radio observation, such as the OTF component - whose development was one of my tasks - which is described in Chapter 3, §2.

Some preliminary notes are necessary in order to introduce the terminology used hereafter. In particular, brief definitions about coordinate frames and coordinate

[6] further details in INAF-IRA Technical Report 424/08, Orlati, A. and Righini S., 2008.

conversions are due, since the coordinates handling within the system takes place along a series of passages.

The system works in equatorial coordinates (Right Ascension, Declination). All other coordinates types are converted to that frame before being used.

At any time, the following categories of coordinates are present inside the system:

- *Input Equatorial Coordinates*: the coordinates of the source as given in input by the user or supplied by a catalogue. If coordinates are provided exploiting other frames (see below), the system will convert them into the equatorial one;
- *Input Galactic Coordinates*: the coordinates of the source as given in input by the user in the galactic frame. In this case the input coordinates are transformed into the equatorial frame;
- *J2000 Equatorial Coordinates*: the equatorial coordinates at J2000.0. They can coincide with the Input Equatorial Coordinates;
- *Apparent Equatorial Coordinates*: these coordinates are computed taking into account effects like precession, nutation and annual aberration;
- *Apparent Horizontal Coordinates*: horizontal coordinates (Azimuth, Elevation) depend on the site of the observer. They are directly converted from the apparent equatorial ones. The apparent coordinates, both equatorial and horizontal, are comprehensive of user-defined offsets, if any;
- *Raw Horizontal Coordinates*: raw coordinates are the coordinates where the system believes the antenna can find the source. Atmospheric and instrumental effects (e.g. refraction and pointing model) are taken into account;
- *Commanded Horizontal Coordinates*: These are the coordinates actually commanded to the antenna mount. They can differ from the raw ones if "instant" effects are taken into account by means of metrology systems, etc...;
- *Encoders Coordinates*: these coordinates are read directly from the mount encoders. They measure the current horizontal coordinates the antenna is pointing to;
- *Observed Horizontal Coordinates*: they are derived from the encoder coordinates, removing all the effects related to the mount. In case of an ideal mount, apparent and observed must be equal;

- *Observed Equatorial Coordinates*: these are directly converted from the Observed Horizontal given the site and the time of the observation. They are referred to the standard epoch J2000.0;
- *Observed Galactic Coordinates*: they are directly converted from the observed equatorial ones.

Applying these conventions, the pointing error measured within the Antenna Control Unit (ACU) corresponds to the difference between the commanded horizontal coordinates and the encoders ones.

Here follow the descriptions of the Antenna subsystem components.

Observatory

The deployment of this component takes into account the specific site geodetic coordinates. It implements all the operations related to the site, e.g. time computations. Since the required tracking and pointing precision for SRT is 2 arcseconds, the difference between UT and UT1 (DUT1) must be taken into account. This is to be updated on a regular basis collecting the information from the web.

Mount

The component takes care of the ACU and, inside the subsystem, is the one to directly deal with the telescope hardware. Since the SRT ACU will be significantly dissimilar from the one installed in Medicina, the ESCS implementation of the Mount component is forcibly specific. Nonetheless, from the subsystem point of view they are functionally identical. To manage this, a common interface has been added: this way the rest of the Antenna subsystem “sees” the Mount component though that interface and does not care about the particular mount implementation it is dealing with. In other words, the Mount component behaves like a plug-in, installed in the system only during the deployment phase.

One of the common features enlisted in the Mount interface that it is worth to highlight is that the ACU can work with various modes. Among them there are:

- *Rate* - the telescope is driven commanding speeds for the two axes;

- *Preset* - the telescope is commanded to go to fixed Az,El positions;
- *Programtrack* - the telescope is ordered to point to a given position at a certain time; if a sequence of points is loaded in advance, the ACU interpolates the correct tracking curve.

The interface lists several methods to retrieve information from the mount, to set the mount working mode and to command the antenna pointing. It also includes a monitor of the current status of the mount, useful to quickly recognise if the mount is facing problems.

Pointingmodel

It gives the Azimuth and Elevation corrections resulting from the pointing model. The pointing model parameters are read directly from the proper tables stored in the Configuration Database (CDB). It provides a method to specify the receiver in use, and a method to read-back the offsets to be applied to the horizontal coordinates.

Refraction

It returns the corrections due to the atmospheric refraction. It needs site information and measurements from meteorological sensors: temperature (°C), relative humidity (fraction from 0 to 1) and pressure (mbar).

EphemGenerator

The subsystem must take care of all the possible observation strategies that directly involve the telescope main drives. Typically they consist in the classical sidereal tracking or in On The Fly scans, but satellites or planets/minor bodies tracking could be requested as well. For every strategy, a different generator of coordinates is necessary.
At the same time, the Antenna Boss (see below) needs to command the telescope without caring about which particular observation is going on at the moment. For that reason it has been defined the EphemGenerator interface, that exposes all the features required for a coordinate calculator. Thus, changing the observation mode consists in changing the implementation of this interface, in other words loading a different component that inherits from the same interface. The Observatory component is

employed for coordinates conversions and time computations. The ephemeris generators planned to be available are:

- *Skysource* - this component has been the first to be implemented, as its task is the most basic one: it generates a tracking curve to perform sidereal tracking. Several “applications” might need this kind of generator contemporarily, so it has been implemented as a dynamic component: it can have an undefined number of instances in the system;
- *OTF* - it is already available. Its aim is to perform On-The-Fly scans (see Chapter 3, §2);
- *Solarsystembody* - this component, at present not implemented, is planned to generate a tracking curve for any Solar System body. The final goal is to perform the computation of the tracking curve for planets and minor bodies starting from their orbital parameters. A faster solution could be to interrogate on-line the JPL-Horizons Ephemeris Generator and automatically download the coordinates;
- *Satellite* - an additional special tool to compute tracking curves for artificial satellites or space debris orbiting around the Earth can be developed exploiting the TLE (“Two Line Elements”, orbital parameters) available on-line. Further investigations about this topic still needs to be carried out;
- *Moon* – this is an already implemented simple generator that allows the tracking of the Moon. In the future it could be expanded with other features to calculate the lunar phase, the apparent dimension of the disk and the positions of specific sections – e.g. the limbs.

AntennaBoss

This component is the supervisor of the Antenna subsystem, it is in charge of starting the observation, setting up the telescope mount and checking the system status and health.

In order to use the antenna it is necessary to call the setup() method; it unstows the telescope, then synchronizes the ACU with the host computer system time and finally commands the “programtrack” operational mode.

Since the observed and raw coordinates reported as attributes of this component are referred to the present time (coming from the last readings of the encoders coordinates) and since the network latencies and the programtrack mode can cause the readings to be late, the component allows to query for coordinate pairs at a given time; if the requested time is not available the Boss will answer with the linear interpolation between the nearest time marks.

More specifically when a request to perform an observation is issued, the component performs the following steps:

- first of all it determines which generator has to be used and, in case, it takes charge of loading it;
- then the component gets the tracking information from the ephemeris generator (apparent coordinates); the correction offsets are collected from the refraction and pointing model (raw coordinates). The raw coordinates are then passed to the mount. This cycle is repeated until a tracking curve is uploaded in advance for an adequate amount of time;
- at the same time it collects from the mount the “encoders” coordinates and the offsets, so that a "trace back" in the computation of coordinates can be used to calculate the observed ones (both horizontal and equatorial);
- raw and observed coordinates are accessed using a time stamp, TCP latency and delays force to interpolate linearly between two "real" samples in order to avoid to flood the network when readings of these values are required frequently.

Boss is also in charge of publishing to a common notification channel the information about the tracking and the status.

# CHAPTER 3

## SOFTWARE DEVELOPMENT [1]

*Always code as if the guy who ends up maintaining your code*
*will be a violent psychopath who knows where you live.*
Martin Golding

## 1. OVERVIEW

During the first part of the project I was in charge of the design and development of ACS components to carry out specific task within Nuraghe/ESCS. The main ones were:

- **OTF**, to perform On-The-Fly scans;
- **FitsWriter**, to collect the output data streams of the backend and write them into a standard FITS file;
- **Schedule reader**, to interpret user-defined schedules and command sequences of scans to OTF.

Related to these components and to specific requirements for the system commissioning, more software modules were identified and developed in C++:

- Automatic production of schedules for a peculiar observing strategy (see Chapter 4 §2.2);
- Conversion of each FITS file achieved with the MF receiver into SDFITS files – one file for each feed, containing projected and flux-calibrated data.

Finally, a set of IDL programs was realised to plot the FITS and SDFITS content, and to perform basic operations on data. These programs currently constitute the core of the data quick-look tools available at the Medicina station.

This chapter illustrates details on the main software tools, with examples taken from real applications. It also shows examples of the tests carried out to check their performance. All the information here reported are relative to the software version in use until March 2010; the software is planned to be updated in late March 2010 to include new features.

[1] Based on INAF-IRA Technical Report 425/08, Righini S., 2008.

## 2. OTF COMPONENT

Prior to ESCS, the Medicina dish control system was not provided with tools to perform on-the-fly scans. Single observers who needed to use the antenna in OTF mode had to develop custom solutions, not integrated in the main system. A procedure to conduct such scans was thus required within ACS.

OTF is the ACS component I have developed and is aimed at computing the sequence of pointings which constitute a single line of a scan. For example: given two positions in the sky, specified by equatorial (J2000.0), horizontal, or galactic coordinates, plus other parameters such as the scanning duration, geometry and start UT time, the OTF component produces the list of UT-based coordinates to be commanded to the antenna in order to perform a smooth scan. The first release of this component executes scans in the desired coordinate frame, along three possible geometries: constant latitude, constant longitude, or great circle. An additional option is available, mainly meant for pointing calibration scans: horizontal scans across a sidereal position.

The route computation also rules - following user-defined parameters - the execution of the pre-scan acceleration ramp and the post-scan deceleration ramp, so that the whole antenna path is deterministically known in advance.

In the initial phases, off-line simulations have shown that the scan computation was performed correctly, then antenna tests demonstrated that very fast scans up to 20°/min could be conducted keeping a proper pointing accuracy (0.1 HPBW) even with the narrowest beam available on the Medicina dish (1.6 arcmin @ 22 GHz) – see section 2.2.

### 2.1. On-the-fly scans: concept

On-the-fly scanning is an observational method (Mangum et al., 2007) which dramatically reduces “dead times” with respect to modes like beam switching and raster scans. It increases the antenna throughput, allowing fast spanning of large sky areas. Data acquisition, in fact, takes place while the antenna is moving along a precisely computed path across the sky. The faster the scan, the greater the stability of the system

hardware and of the environmental conditions (such as weather parameters) during the acquisition.

The maximum speed at which the scan can be executed depends on the mechanical limits of the telescope mount and on the antenna sensitivity: the observer must compute how much integration per beam is needed to reach the desired flux limit for the single scan, and consequently determine the proper scan speed and the data sampling rate – which, in turn, must meet the requirements of the data acquisition system.

For consistency with the MBFITS consortium definitions, in the ESCS system we define “subscan” the elementary acquisition, a sequence of which constitutes the “scan”, i.e. the total observation. In a classic OTF mapping, a subscan corresponds to a single “line” of the map, whose points correspond to the samples acquired at a constant rate. During the observation design and planning, the subscan inter-spacing must be fixed considering that the final map must at least fulfil the Nyquist critical sampling criterion.

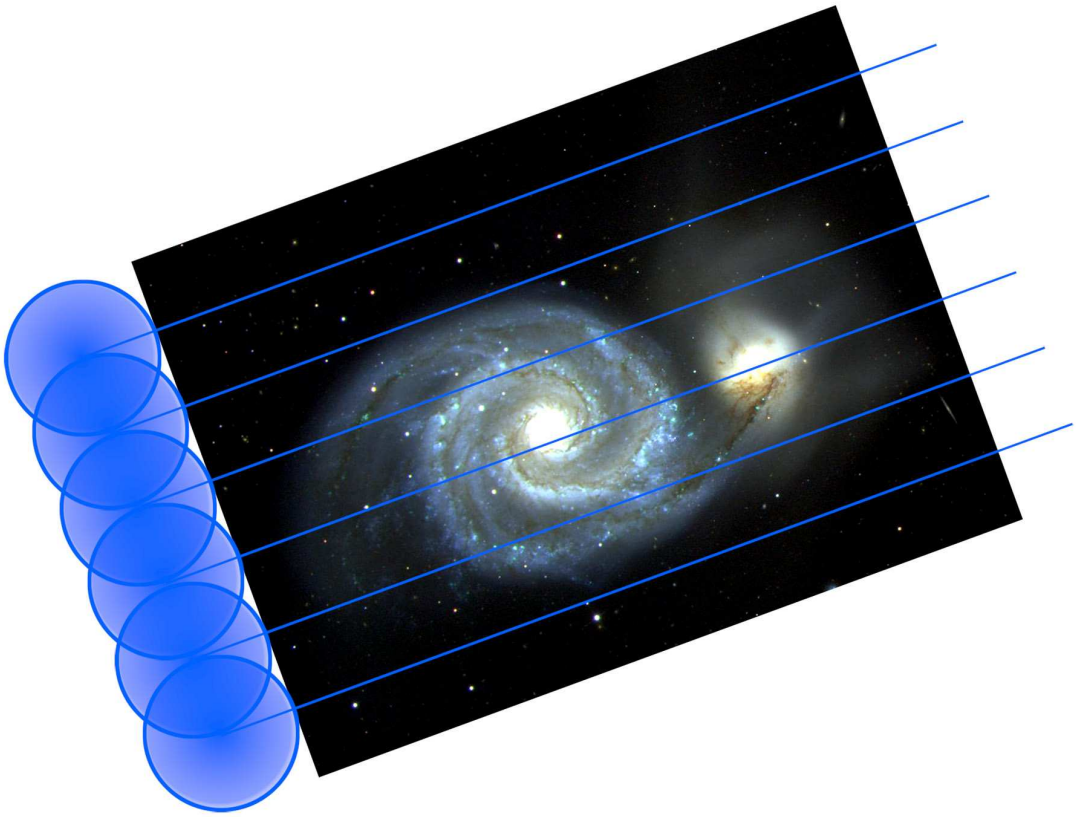

Figure 3.1 – Representation of an on-the-fly scan over the M51 galaxies. Each blue line shows the path of the beam centre across the sky. Adjacent lines (i.e. subscans) are spaced by HPBW/2 so that the final map is correctly sampled. Subscans can be performed in the same direction - rewinding the beam each time - or following a back-forth path in order to cut-off the slewing time.

## 2.2. The Nuraghe/ESCS OTF component

As explained in Chapter 2 §3.1, in ACS we call “component” each system element which is in charge of a specific task. The component named OTF is responsible of computing the sequence of pointings realising a single on-the-fly subscan. It gets the input values from an external scheduler, which reads a schedule either written by the user or generated by another program. The schedule-writing code, elaborating the general map parameters and determining the boundaries of each subscan, is currently available for horizontal scans only.

In addition to the configuration constraints, OTF obtains other parameters from AntennaBoss, the component which manages the antenna pointing and calls OTF. Table 3.1 lists the input parameters needed to set a single subscan and passed as arguments of the method called *setSubScan()*.

The component also reads the following values, specific for the telescope in use, from the Configuration Data Base (CDB):

- Maximum azimuth slewing rate allowed by mechanical constraints (°/s);
- Maximum elevation slewing rate allowed by mechanical constraints (°/s);
- Maximum azimuth scan rate allowing correct pointing (°/s);
- Maximum elevation scan rate allowing correct pointing (°/s);
- Maximum azimuth acceleration (°/s$^2$);
- Maximum elevation acceleration (°/s$^2$);
- Acceleration “Scale Factor” – scaling the maximum Az-El acceleration in order to perform smooth acceleration/deceleration ramps before/after the constant speed scan;
- Site information (longitude, latitude, elevation, etc…);
- Observation-related information (HPBW, DUT1, etc...).

Some of these parameters were determined for the Medicina dish with on-field tests.

| | |
|---|---|
| **initAz** | Azimuth (radians) where the antenna is located when OTF is called. This is automatically obtained from AntennaBoss. |
| **initSector** | CW or CCW relative to the initAz value.<br>This is automatically obtained from AntennaBoss. |
| **initEl** | Elevation (radians) where the antenna is located when OTF is called. This is automatically obtained from AntennaBoss. |
| **initTime** | UT instant (100 ns since 1582-10-15 00:00:00) when the OTF is called. This is automatically obtained from AntennaBoss.ss |
| **lon1** | If the description (see below) is start-stop, longitude (radians) of the constant speed scan starting point. Otherwise it corresponds to the longitude (radians) of the subscan central point. Value is obtained from user input data. |
| **lat1** | If the description is start-stop, latitude (radians) of the constant speed scan starting point. Otherwise it corresponds to the latitude (radians) of the subscan central point. Value is obtained from user input data. |
| **lon2** | If the description is start-stop, longitude (radians) of the constant speed scan stopping point. Otherwise it corresponds to the full span in longitude (radians) of the subscan. Value is obtained from user input data. |
| **lat2** | If the description is start-stop, latitude (radians) of the constant speed scan stopping point. Otherwise it corresponds to the full span in latitude (radians) of the subscan. Value is obtained from user input data. |
| **coordFrame** | Reference frame for the input coordinates. It can be equatorial J2000.0 (EQ), galactic (GAL) or horizontal (HOR). Value is user-defined. |
| **geometry** | Subscan geometry, it can be constant longitude (LON), constant latitude (LAT) or great circle (GC). Value is user-defined. |
| **subScanFrame** | Reference frame for the execution of the subscan. It can an be equatorial J2000.0, galactic or horizontal. Value is user-defined. |
| **description** | Subscan definition. It can be start/stop or centre/span. Value is user-defined. Centre/span description does not apply to great circle scans. |
| **direction** | Increase or decrease, relative to the varying coordinate. Does not apply to great circle subscans. |
| **startUT** | UT instant (100 ns since 1582-10-15 00:00:00) at which the data acquisition is commanded to start. It coincides with the instant when the constant speed scanning starts. Value is user-defined. |
| **subScanDuration** | Duration of the constant speed scanning (s). Value is obtained from user input data. |

Table 3.1 – Attributes of the *setSubScan* method inside the OTF component

Once the initialisation and setup are complete, OTF controls if the user-defined parameters are correct. In particular it checks that:

- values match with the available options (e.g. the coordFrame value cannot be “ecliptic” because this coordinate frame is not implemented) and that they are correct;

- values are consistent with each other. For example, a great circle geometry is not compatible with the centre/span description;
- the azimuth and elevation rates stay below the allowed limits during the whole subscan. This is particularly critical for great circle scans, since they can imply very high values for the rates in restricted sections of their curved paths along the sky – for this reason, the whole path is simulated in advance. In case the Az-El speeds exceed the instrumental limits the program raises an error and ends. A warning only is raised, instead, if the speed is below the maximum values but exceeds the limits tested to be reliable for a correct pointing.

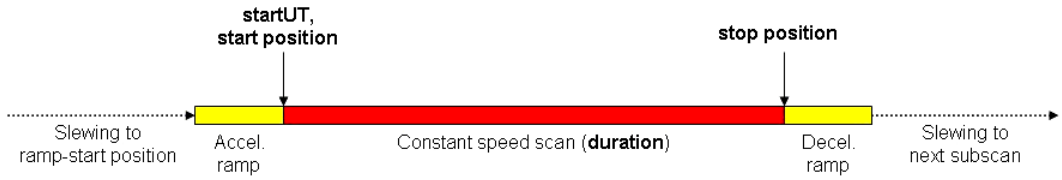


Figure 3.2 – Schematisation of the timeline/path of a subscan. The antenna system defines, elaborating the user-input information ore reading the schedule, the subscan boundaries and duration (bold parameters), referring to the constant speed scan (red line), which are passed to the OTF component. This adds the acceleration/deceleration ramps (yellow lines), computing their start and stop positions and the relative timings. The initial ramp start position is commanded to the antenna, which slews to those coordinates, waits for the ramp start UT time, runs the accelerated path and begins the "constant speed path" at the correct time and position.

The next step is the computation of the acceleration/deceleration ramps to be appended to the constant speed scan (Figure 3.2). The user-defined start coordinates and UT time are, in fact, relative to the beginning of the cruise speed path and OTF automatically computes the ramps to match them. Acceleration and scale factor values written in the CDB are used to compute a uniformly accelerated route. The coordinates and UT time relative to the first point of the acceleration ramp are commanded to start the antenna motion.

OTF then checks if this ramp-start position can be reached in time: when called, it is passed the current UT instant and antenna position and computes if the necessary antenna slewing time is short enough to reach the ramp start coordinates within the commanded UT time. If the target is too far, a warning is raised and the general system (ESCS) cross-checks the impossibility to reach the commanded position; if the problem

is confirmed, the subscan aborts and the system skips to the next one in the schedule (if any). At this point, everything is set and the OTF component is asked to compute the sequence of pointings realising the subscan, and also to check whether the actual motion correctly follows the predicted positions.

This happens by means of two methods, which are recursively called by AntennaBoss:

- *getHorizontalCoordinates* – given a certain UT instant, it gets the corresponding azimuth and elevation positions the antenna is going to be commanded to, as a function of the subscan setup. This method is called in advance, i.e. passing a UT instant which is some seconds ahead;
- *checkTracking* – given a UT instant, it checks that the corresponding true position of the antenna coincides with the previously predicted one, within 0.1*HPBW. This method is called in realtime, i.e. passing the current UT instant.

The overall scheme of the OTF component is illustrated in Figure 3.3.

Figure 3.4 shows an example of OTF output: the sequence of positions to be commanded to the antenna mount to perform the subscan.

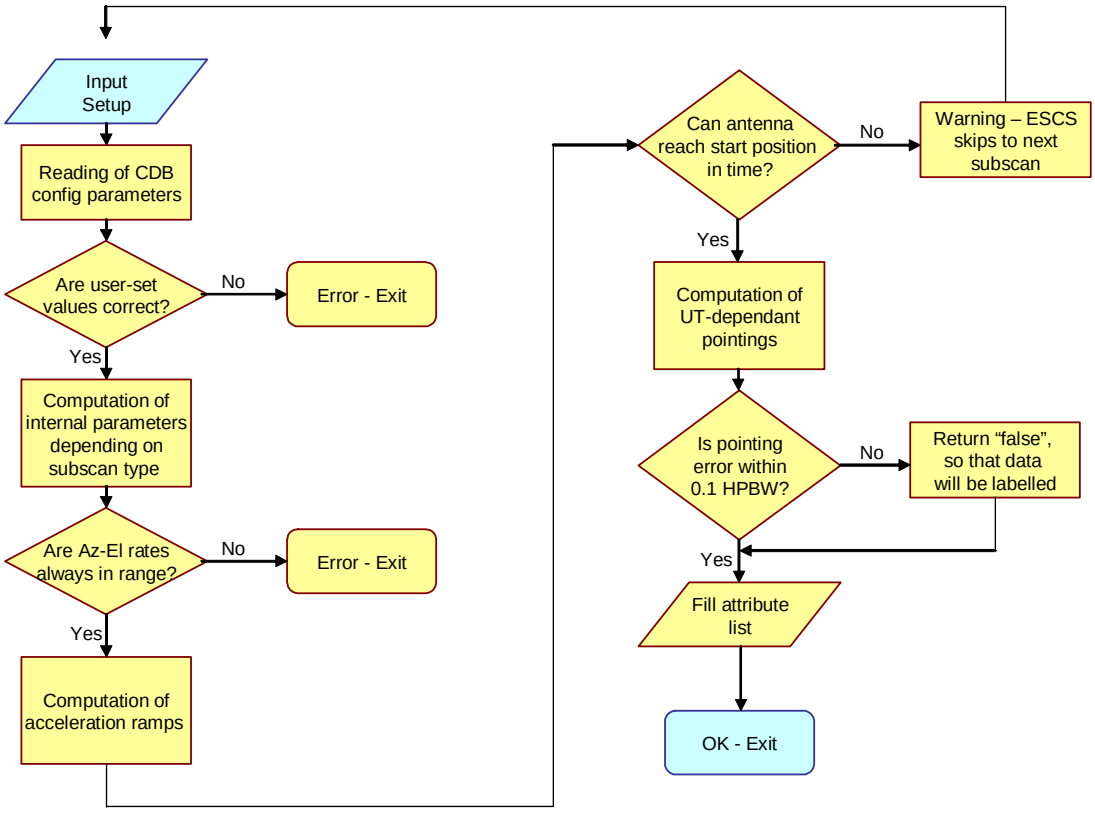




Figure 3.3 – Flowchart illustrating the main features of the OTF component.

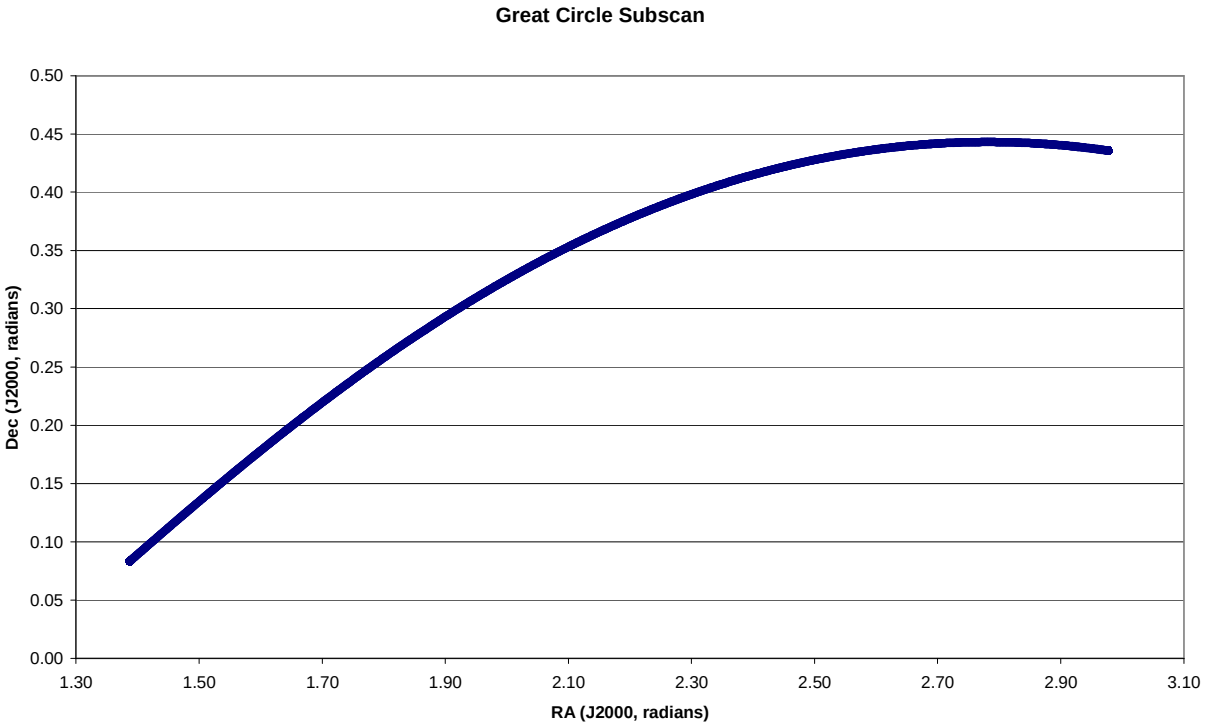


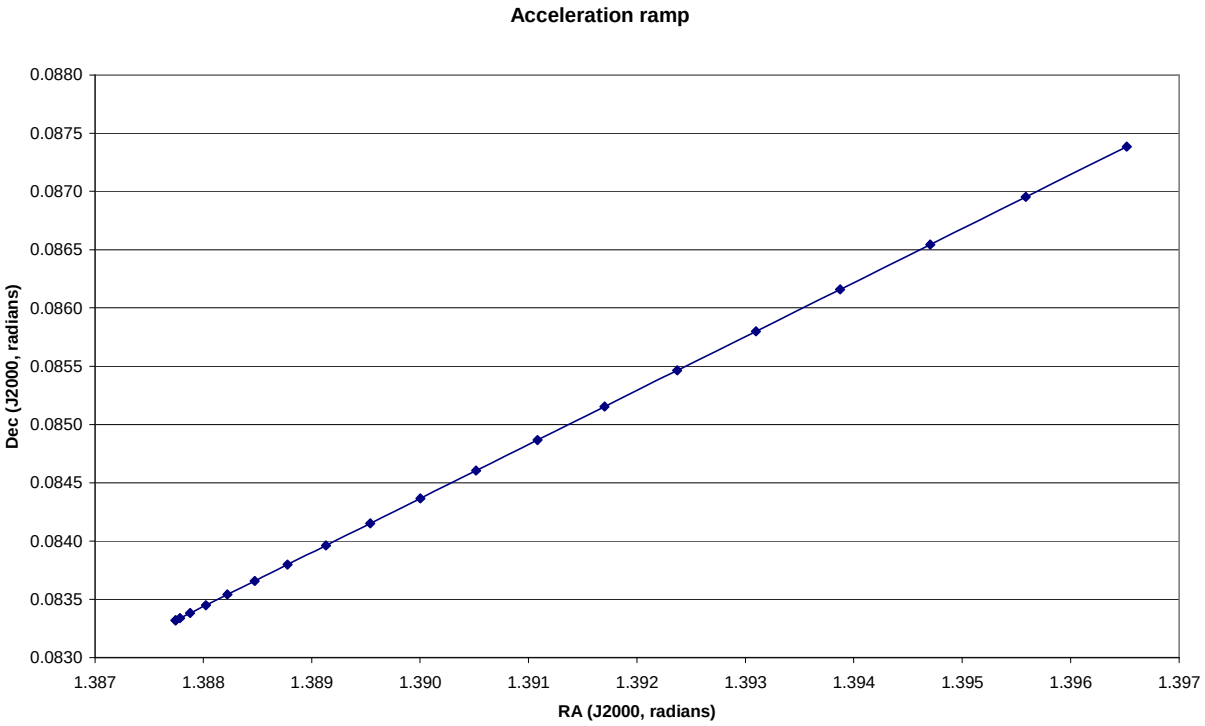


Figure 3.4 – Example of a great circle subscan computed by the OTF component. The top figure shows the overall sky path. The bottom plot zooms on the initial acceleration ramp path: samples are equally spaced in time, and the uniformly accelerated motion is evident. Setup parameters: startLon 80.0°, startLat 5.0°, stopLon 170.0°, stopLat 25.0°, coordFrame=subScanFrame Equatorial, description StartStop, duration 600 s.

## 2.3. OTF tests with the Medicina dish

Several scans were performed to test the OTF component, varying the azimuth/elevation speed and acceleration scale factor to estimate the maximum values generating acceptable pointing errors.

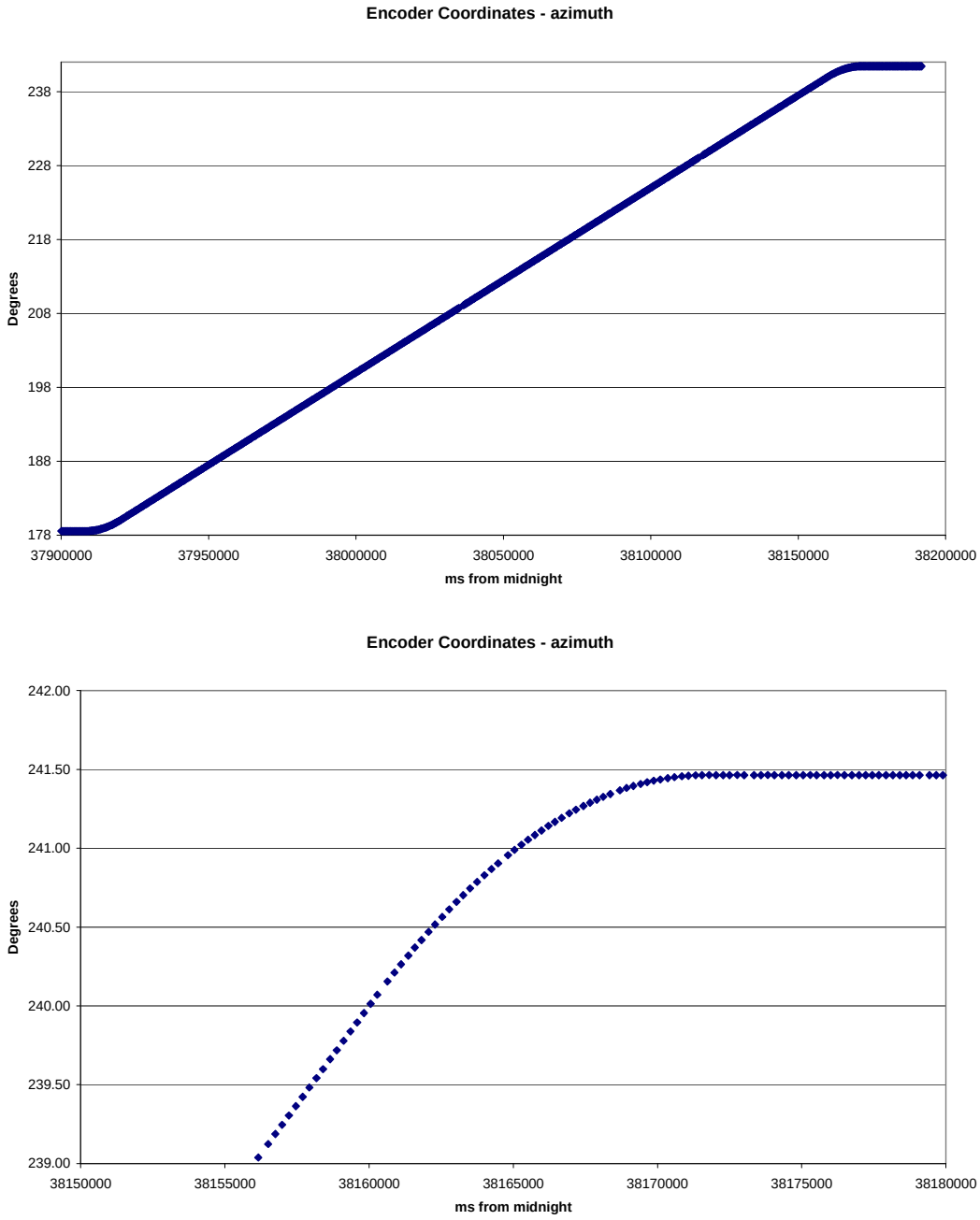


Figure 3.5 – Example of a real constant elevation subscan performed using the OTF component. The top figure shows azimuth vs. time for the whole path. The bottom plot zooms on the final deceleration ramp: samples are taken every 200 ms. Setup parameters: startLon 180.0°, startLat 45.0°, stopLon 240.0°, stopLat 45.0°, coordFrame=subScanFrame Horizontal, description StartStop, duration 240 s.

Since the ESCS system was initially not provided with a tool to get the commanded and encoder coordinates concurrently (i.e. at the same UT), the chosen solution was to download the encoder coordinates and the associated pointing error, which was calculated internally to the ACU (Antenna Control Unit) as the difference between the commanded and the encoder values.

This turned out to produce occasional and isolated incorrect values of the pointing error measure: as figure 3.6 shows, there were outliers appearing with a sort of regular "arrangement", highlighted by the red lines. These values (as high as 0.03 degrees = 1.0*HPBW) could not have any physical meaning, since they would imply that the antenna was going one beamsize off-pointing and returning to the correct position in less than 200 milliseconds (the data sampling interval of the test), which is clearly not possible. The reason is not fully certain yet, but the very likely explanation is a time delay happening inside the ACU resulting in commanded and encoder coordinates not always relative to the same UT time. Because of the fast antenna speed, their difference yielded extremely high values. In fact, travelling at 10 °/min the antenna was spanning 0.03° in a sampling interval; this way, confronting coordinates relative to different instants meant measuring an excess (and false) error up to about one HPBW.

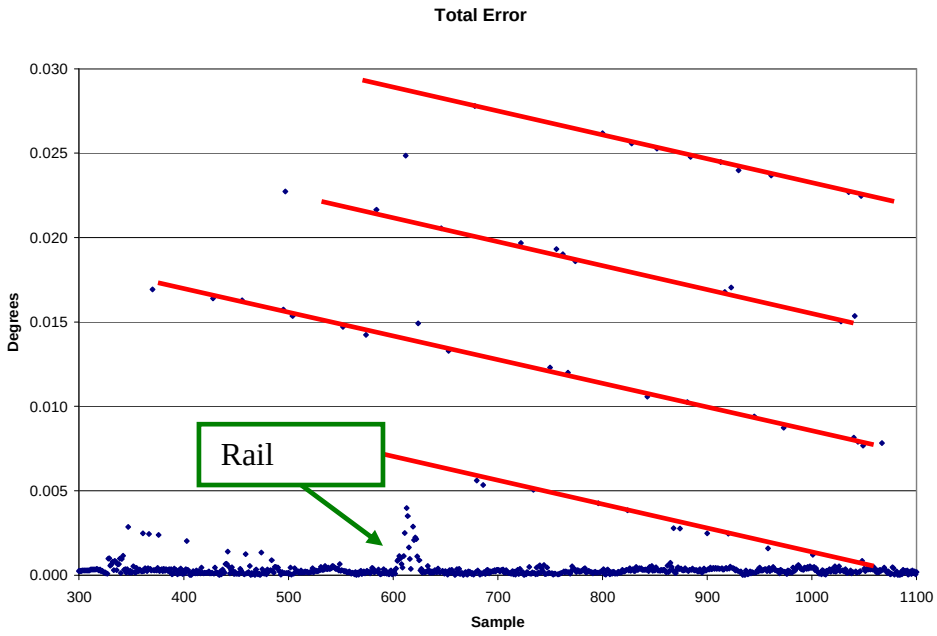


Figure 3.6 – Total pointing error (difference between commanded-encoder coordinates, computed by the ACU) as a function of time. This is a single subscan performed at constant elevation (45°), moving the antenna along azimuth only, from 180° to 220°, with a data sampling interval of 200 ms. The "bump" appearing after sample #600 is due to the antenna mount wheels passing on the rail junctions. Red lines highlight the recurrent presence of outlier values.

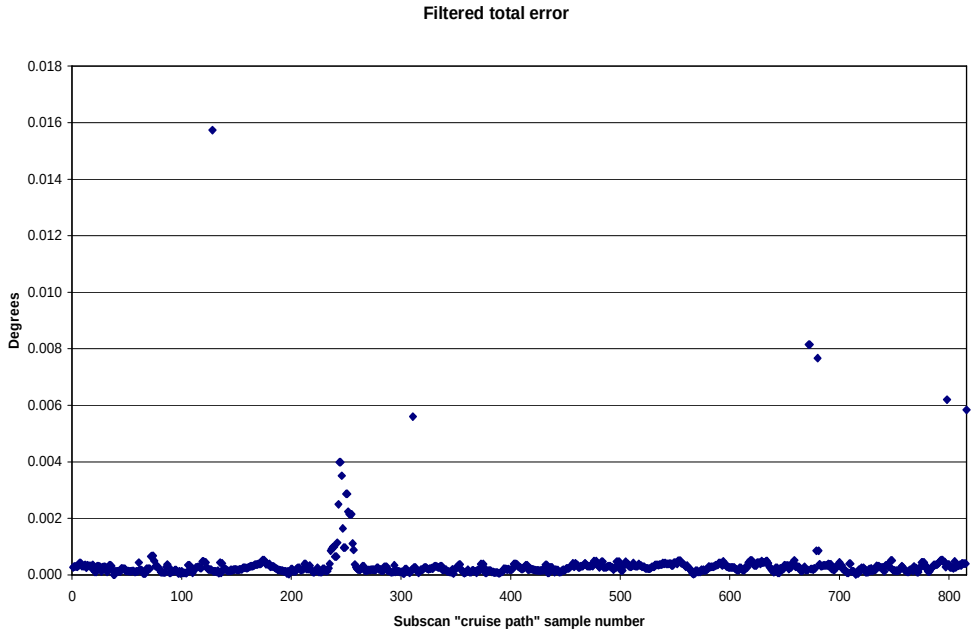


Figure 3.7 – Values after the application of a 3-point median filter. Data were cropped: the graph shows the constant speed path only. Notice the change in the y-axis scale; the few outlier values which were not removed are lower than 0.5*HPBW.

To deal with a sensible statistics data were cleaned from the outlier values using a 3-point median filter. This led to the almost complete removal of the inconsistent measures, while preserving true features like the “bump” appearing around sample #250 of Figure 3.7, produced by the antenna mount wheels revolving on the base rail junctions.

Table 3.2 illustrates some examples of the final statistics on the measured pointing error, given as a fraction of the HPBW. Many of these tests focused on azimuth scans, since the observations to be carried out for my PhD project were based on fast azimuth scans (see Chapters 4 and 5).

| DOY | Coord. Frame | Start Lon-Lat | Stop Lon-at | Geom | Durat | Scale Factor | Cruise Speed | Cruise Speed | P.Error Mean | P.Error 3σ |
|---|---|---|---|---|---|---|---|---|---|---|
| | | ° | ° | | s | | °/m Az | °/m sky | %HPBW | %HPBW |
| **199** | **EQ** | **170 - 0** | **190 - 40** | **GC** | **480** | **30** | **-** | **~ 5.5** | **1.64** | **5.11** |
| 217 | HOR | 180-45 | 220-45 | LAT | 240 | 30 | 10 | 7.0 | 1.06 | 8.86 |
| **217** | **HOR** | **180-45** | **220-45** | **LAT** | **192** | **30** | **12.5** | **~ 8.8** | **1.25** | **11.25** |
| 217 | HOR | 180-45 | 220-45 | LAT | 100 | 30 | 24 | ~ 16.8 | 1.95 | 23.65 |
| **217** | **HOR** | **180-45** | **220-45** | **LAT** | **240** | **50** | **10** | **7.0** | **1.07** | **10.03** |
| 217 | HOR | 180-45 | 220-45 | LAT | 192 | 50 | 12.5 | ~ 8.8 | 1.01 | 7.41 |
| **217** | **HOR** | **180-45** | **220-45** | **LAT** | **100** | **50** | **24** | **~ 16.8** | **1.73** | **11.34** |
| 217 | HOR | 180-45 | 220-45 | LAT | 240 | 10 | 10 | 7.0 | 1.08 | 8.86 |
| **217** | **HOR** | **180-45** | **220-45** | **LAT** | **192** | **10** | **12.5** | **~ 8.8** | **1.21** | **8.55** |
| 217 | HOR | 180-45 | 220-45 | LAT | 100 | 10 | 24 | ~ 16.8 | 2.10 | 25.01 |
| **248** | **HOR** | **180-45** | **240-45** | **LAT** | **240** | **10** | **15** | **~ 10.4** | **1.90** | **11.79** |
| 248 | HOR | 180-45 | 240-45 | LAT | 240 | 15 | 15 | ~ 10.4 | 2.60 | 10.38 |
| **248** | **HOR** | **180-45** | **240-45** | **LAT** | **240** | **30** | **15** | **~ 10.4** | **1.94** | **5.88** |

Table 3.2 – Statistics relative to some test OTF scans. DOY is Day Of Year, the following columns refer to the subscan parameters listed in Table 3.1. The columns highlighted in blue show the measured pointing error as a percent fraction of the beamsize.

Results demonstrated that an azimuth scan cruise speed of 24 °/min produces a stable antenna pointing only performing very slow and long acceleration ramps (i.e. for high "scale factor" values, see Tables 3.3 and 3.4).

Ideal values to combine quite short ramps with fast scanning are:

- scale factor = 15 (yielding ramps less than 10 seconds long)
- constant cruise azimuth speed = 15 °/min

| **Scale Factor** | **Azimuth Acceleration** °/s$^2$ | **Resulting Az Ramp Duration (s)** *Cruise speed (°/min)* | | | |
|---|---|---|---|---|---|
| | | ***5*** | ***10*** | ***15*** | ***24*** |
| 10 | 0.040 | 2.08 | 4.17 | 6.25 | 10.00 |
| **15** | **0.027** | **3.13** | **6.25** | **9.38** | **15.00** |
| 20 | 0.020 | 4.17 | 8.33 | 12.50 | 20.00 |
| **30** | **0.013** | **6.25** | **12.50** | **18.75** | **30.00** |
| 50 | 0.008 | 10.42 | 20.83 | 31.25 | 50.00 |
| **100** | **0.004** | **20.83** | **41.67** | **62.50** | **100.00** |

Table 3.3 Nominal duration of each acceleration/deceleration ramp for the different scale factors and cruise speeds (azimuth scans)

| **Scale Factor** | **Azimuth Acceleration** °/s$^2$ | **Resulting Az Ramp Extension (°)** *Cruise speed (°/min)* | | | |
|---|---|---|---|---|---|
| | | ***5*** | ***10*** | ***15*** | ***24*** |
| 10 | 0.040 | 0.09 | 0.35 | 0.78 | 2.00 |
| **15** | **0.027** | **0.13** | **0.52** | **1.17** | **3.00** |
| 20 | 0.020 | 0.17 | 0.69 | 1.56 | 4.00 |
| **30** | **0.013** | **0.26** | **1.04** | **2.34** | **6.00** |
| 50 | 0.008 | 0.43 | 1.74 | 3.91 | 10.00 |
| **100** | **0.004** | **0.87** | **3.47** | **7.81** | **20.00** |

Table 3.4 – Sky extension of each acceleration/deceleration ramp for the different scale factors and cruise speeds (azimuth scans)

## 3. FITSWRITER

The final output data format of the ESCS system is MBFITS (MBFITS manual[2]), tailored to handle multi-feed data. Its definition was still underway when the MF and backend commissioning started. Moreover, the complexity of this file format, containing a large amount of details, did not allow for a fast implementation within ESCS.

For these reasons, it was decided to use an intermediate step on the way to MBFITS: ESCS was provided with a component in charge of receiving data from a generic backend and store them into standard FITS files.

On the backend side the output data streams, called channels, were organised as follows.

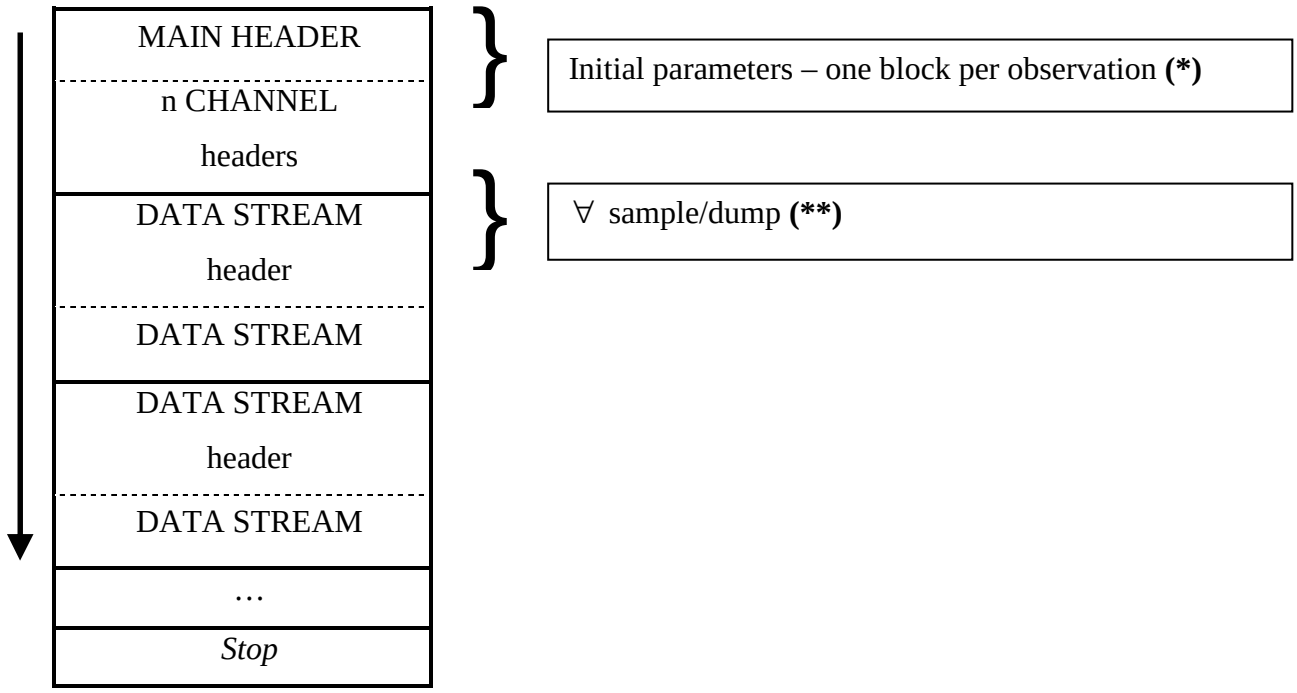


Figure 3.8 – Scheme of the output data stream of the backend

[2] http://www.apex-telescope.org/observing/APEX-MPI-ICD-0002.pdf

**(*)**

Main Header: "***TMainHeader***"

Attributes

*channels* – number of channels in the data stream (using the MF it is 14)

*beams* – number of beams in use (for the complete MF it is 7)

*integration* – integration time relative to the single sample (milliseconds)

*sampleSize* – size of the single sample (expressed in bytes)

Header for each channel: "***TChannelHeader***"

Attributes

*id* – identity code for the channel

*bins* – number of spectral bins (total power = 1)

*polarisation* – polarisation type (3 possibilies: LHCP, RHCP, Full_Stokes)

*bandWidth* – total bandwidth of the channel (MHz)

*frequency* – IF at the beginning of the band (MHz)

*attenuation* – attenuation value applied to the channel

*sample rate* – sampling rate (MHz)

*feedNumber* – number of the feed to which the channel is relative to

**(**)**

Header for each sample: "***TDumpHeader***"

Attributes

*time* – mean UT of the sample (absolute: 100ns from 00:00 of October, 15 - 1582)

*dumpSize* – size of the dump (bytes)

*calOn* – boolean value indicating if the calibration mark is on

Additional information is extracted from the observation setup in order to fill in the various headers and tables forming the final FITS file (see the following paragraphs).

***Data stream***

It's organised so that the quantities vary in the following order: spectral bins first, then polarisations and channels. Figures 3.9, 3.10 and 3.11 schematise some of the possible configurations.

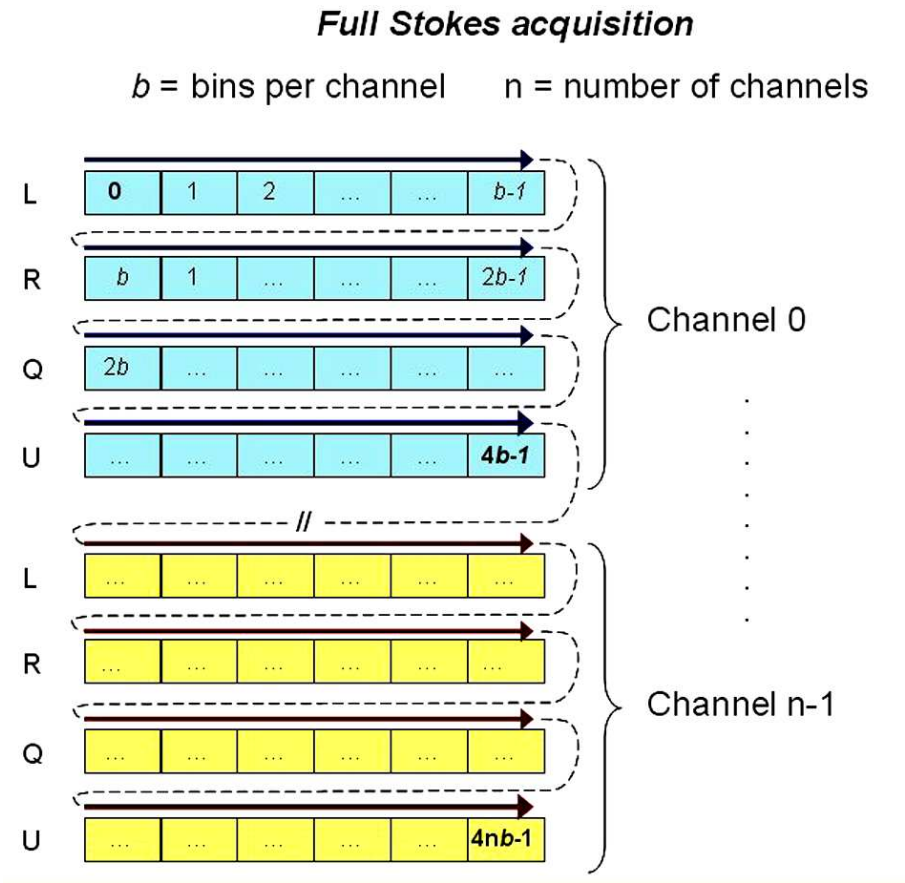


Figure 3.9 – Data stream structure for full Stokes spectral acquisitions

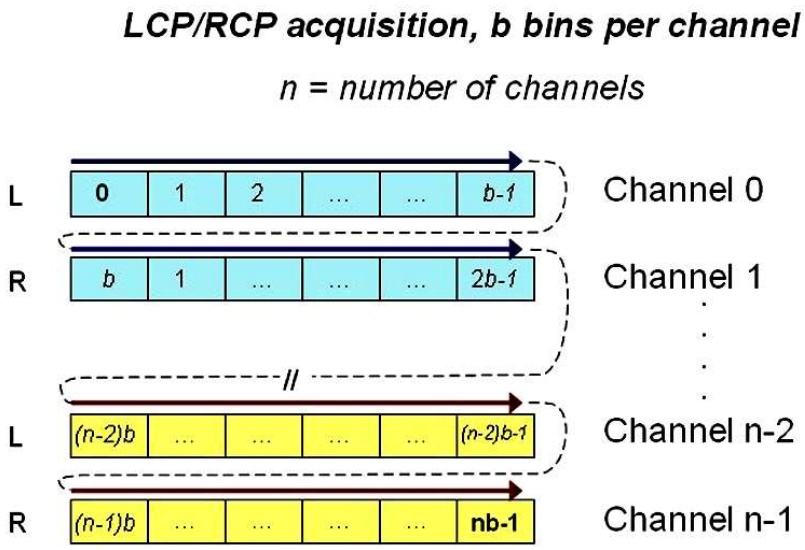


Figure 3.10 – Data stream structure for LCP/RCP only spectral acquisitions

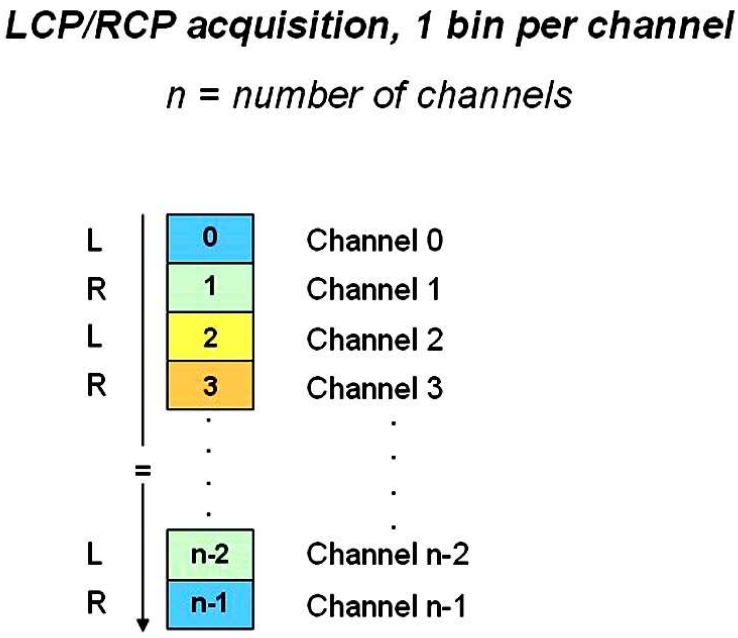


Figure 3.11 – Data stream structure for LCP/RCP total power acquisitions

This last example represents the data stream setup which was employed during the commissioning of the MF receiver and the new analogue backend: 14 channels in total power (1 frequency bin per channel, LHCP/RHCP polarisations). In any case, the

FitsWriter component is general-purpose, as long as the generic backend output complies with the previously described organisation of the data flow.
My contribution for the production of the component FitsWriter has initially been its design and definition. The C++ class called CFitsWriter, - based on the cfitsio libraries and fully integrated in the ESCS system - was then provided by Marco Bartolini, one of the programmers working at the Medicina radiotelescope station. I finally took part to the overall development and implementation of the component, which was carried out in cooperation with Andrea Orlati, the main developer of the whole ESCS system.

FitsWriter composes the filename on the basis of the date and time at the first data writing into the file – which is as the scan at constant speed starts – adding some keywords specified in the schedule as follows:
YYYYMMDD-HHMMSS-HHMMSS-ProjectName-Label.fits
(Date) (UT) (LST) (From the schedule)
This way the filename is always unique; the identification of the project to which it belongs and of the date of its acquisition is straightforward, allowing for easier archiving and querying.

The structure of the FITS file produced by this component consists in:
- a standard FITS primary header;
- three tables: CHANNEL TABLE, FEED TABLE, DATA TABLE, each of which is accompanied by its header.

The figures given in the following pages show examples of the different headers and tables, relative to a file obtained using the MF reveiver. They consist in screen captures of the various file sections as diplayed by “HEASARC-FV FitsViewer”.

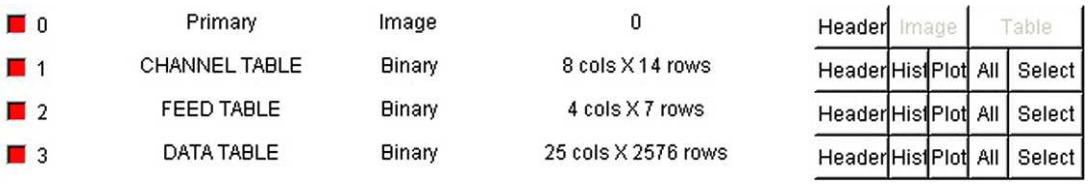


Figure 3.12 – Overall structure of the FITS file, as the HEASARC-FV FitsViewer shows it

```
SIMPLE  =                    T / file does conform to FITS standard
BITPIX  =                    8 / number of bits per data pixel
NAXIS   =                    0 / number of data axes
EXTEND  =                    T / FITS dataset may contain extensions
COMMENT   FITS (Flexible Image Transport System) format is defined in 'Astronomy
COMMENT   and Astrophysics', volume 376, page 359; bibcode: 2001A&A...376..359H
COMMENT V. 0.8 Created by  S. Righini, M. Bartolini  & A. Orlati
DATE    = '2009-02-18T00:12:21' / file creation date (YYYY-MM-DDThh:mm:ss UT)
BEAMS   =                    7 / number of beams of antenna
HIERARCH integration =       0 / integration time in milli
CHANNELS=                   14 / number of channels
HIERARCH sample size =       4 / number of bytes of a single sample
HIERARCH Project_Name = 'KNoWS   ' / description
OBSERVER= '        '           / description
HIERARCH Receiver_code = 'KKC     ' / description
END
```

Figure 3.13 – Main Header

```
XTENSION= 'BINTABLE'           / binary table extension
BITPIX  =                    8 / 8-bit bytes
NAXIS   =                    2 / 2-dimensional binary table
NAXIS1  =                   48 / width of table in bytes
NAXIS2  =                   14 / number of rows in table
PCOUNT  =                    0 / size of special data area
GCOUNT  =                    1 / one data group (required keyword)
TFIELDS =                    8 / number of fields in each row
TTYPE1  = 'id      '           / label for field   1
TFORM1  = 'J       '           / data format of field: 4-byte INTEGER
TTYPE2  = 'bins    '           / label for field   2
TFORM2  = 'J       '           / data format of field: 4-byte INTEGER
TTYPE3  = 'polarization'       / label for field   3
TFORM3  = 'J       '           / data format of field: 4-byte INTEGER
TTYPE4  = 'bandWidth'          / label for field   4
TFORM4  = 'D       '           / data format of field: 8-byte DOUBLE
TUNIT4  = 'MHz     '           / physical unit of field
TTYPE5  = 'frequency'          / label for field   5
TFORM5  = 'D       '           / data format of field: 8-byte DOUBLE
TUNIT5  = 'MHz     '           / physical unit of field
TTYPE6  = 'attenuation'        / label for field   6
TFORM6  = 'D       '           / data format of field: 8-byte DOUBLE
TUNIT6  = 'db      '           / physical unit of field
TTYPE7  = 'sample rate'        / label for field   7
TFORM7  = 'D       '           / data format of field: 8-byte DOUBLE
TUNIT7  = 'MHz     '           / physical unit of field
TTYPE8  = 'feedNumber'         / label for field   8
TFORM8  = 'J       '           / data format of field: 4-byte INTEGER
EXTNAME = 'CHANNEL TABLE'      / name of this binary table extension
COMMENT parameters for each single channel
HIERARCH Local_Oscillator = 17900. / Local oscillator in MHz
END
```

Figure 3.14 – Channel Table Header

| | id | bins | polarization | bandWidth | frequency | attenuation |
|---|---|---|---|---|---|---|
| Select | J | J | J | D | D | D |
| All | | | | MHz | MHz | db |
| Invert | Modify | Modify | Modify | Modify | Modify | Modify |
| 1 | 0 | 1 | 0 | 2.000000000000E+003 | 1.000000000000E+002 | 9.000000000000E+000 |
| 2 | 1 | 1 | 1 | 2.000000000000E+003 | 1.000000000000E+002 | 9.000000000000E+000 |
| 3 | 2 | 1 | 0 | 2.000000000000E+003 | 1.000000000000E+002 | 9.000000000000E+000 |
| 4 | 3 | 1 | 1 | 2.000000000000E+003 | 1.000000000000E+002 | 9.000000000000E+000 |
| 5 | 4 | 1 | 0 | 2.000000000000E+003 | 1.000000000000E+002 | 9.000000000000E+000 |
| 6 | 5 | 1 | 1 | 2.000000000000E+003 | 1.000000000000E+002 | 9.000000000000E+000 |
| 7 | 6 | 1 | 0 | 2.000000000000E+003 | 1.000000000000E+002 | 9.000000000000E+000 |
| 8 | 7 | 1 | 1 | 2.000000000000E+003 | 1.000000000000E+002 | 9.000000000000E+000 |
| 9 | 8 | 1 | 0 | 2.000000000000E+003 | 1.000000000000E+002 | 9.000000000000E+000 |
| 10 | 9 | 1 | 1 | 2.000000000000E+003 | 1.000000000000E+002 | 9.000000000000E+000 |
| 11 | 10 | 1 | 0 | 2.000000000000E+003 | 1.000000000000E+002 | 9.000000000000E+000 |
| 12 | 11 | 1 | 1 | 2.000000000000E+003 | 1.000000000000E+002 | 9.000000000000E+000 |
| 13 | 12 | 1 | 0 | 2.000000000000E+003 | 1.000000000000E+002 | 9.000000000000E+000 |
| 14 | 13 | 1 | 1 | 2.000000000000E+003 | 1.000000000000E+002 | 9.000000000000E+000 |

Figure 3.15 – Part of the Channel Table

```
XTENSION= 'BINTABLE'           / binary table extension
BITPIX  =                    8 / 8-bit bytes
NAXIS   =                    2 / 2-dimensional binary table
NAXIS1  =                   28 / width of table in bytes
NAXIS2  =                    7 / number of rows in table
PCOUNT  =                    0 / size of special data area
GCOUNT  =                    1 / one data group (required keyword)
TFIELDS =                    4 / number of fields in each row
TTYPE1  = 'id      '           / label for field   1
TFORM1  = 'J       '           / data format of field: 4-byte INTEGER
TTYPE2  = 'xOffset '           / label for field   2
TFORM2  = 'D       '           / data format of field: 8-byte DOUBLE
TTYPE3  = 'yOffset '           / label for field   3
TFORM3  = 'D       '           / data format of field: 8-byte DOUBLE
TTYPE4  = 'relativePower'      / label for field   4
TFORM4  = 'D       '           / data format of field: 8-byte DOUBLE
EXTNAME = 'FEED TABLE'         / name of this binary table extension
END
```

Figure 3.16 – Feed Table Header

| | id | xOffset | yOffset | relativePower |
|---|---|---|---|---|
| Select | J | D | D | D |
| All / Invert | Modify | Modify | Modify | Modify |
| 1 | 0 | 0.000000000000E+000 | 0.000000000000E+000 | 1.000000000000E+000 |
| 2 | 1 | 1.027805000000E-003 | 0.000000000000E+000 | 9.700000000000E-001 |
| 3 | 2 | 5.139030000000E-004 | -8.901180000000E-00‹ | 9.900000000000E-001 |
| 4 | 3 | -5.139030000000E-00‹ | -8.901180000000E-00‹ | 9.700000000000E-001 |
| 5 | 4 | -1.027805000000E-00: | 0.000000000000E+000 | 9.500000000000E-001 |
| 6 | 5 | -5.139030000000E-00‹ | 8.901180000000E-004 | 9.700000000000E-001 |
| 7 | 6 | 5.139030000000E-004 | 8.901180000000E-004 | 9.700000000000E-001 |

Figure 3.17 – Feed Table; xOffset and yOffset are the distances of the lateral beams from the central one, expressed in radians

```
XTENSION= 'BINTABLE'           / binary table extension
BITPIX  =                    8 / 8-bit bytes
NAXIS   =                    2 / 2-dimensional binary table
NAXIS1  =                  152 / width of table in bytes
NAXIS2  =                 2576 / number of rows in table
PCOUNT  =                    0 / size of special data area
GCOUNT  =                    1 / one data group (required keyword)
TFIELDS =                   25 / number of fields in each row
TTYPE1  = 'time    '           / label for field   1
TFORM1  = 'D       '           / data format of field: 8-byte DOUBLE
TUNIT1  = 'MJD     '           / physical unit of field
TTYPE2  = 'raj2000 '           / label for field   2
TFORM2  = 'D       '           / data format of field: 8-byte DOUBLE
TUNIT2  = 'radians '           / physical unit of field
TTYPE3  = 'decj2000'           / label for field   3
TFORM3  = 'D       '           / data format of field: 8-byte DOUBLE
TUNIT3  = 'radians '           / physical unit of field
TTYPE4  = 'az      '           / label for field   4
TFORM4  = 'D       '           / data format of field: 8-byte DOUBLE
TUNIT4  = 'radians '           / physical unit of field
TTYPE5  = 'el      '           / label for field   5
TFORM5  = 'D       '           / data format of field: 8-byte DOUBLE
TUNIT5  = 'radians '           / physical unit of field
TTYPE6  = 'par_angle'          / label for field   6
TFORM6  = 'D       '           / data format of field: 8-byte DOUBLE
TUNIT6  = 'radians '           / physical unit of field
TTYPE7  = 'derot_angle'        / label for field   7
TFORM7  = 'D       '           / data format of field: 8-byte DOUBLE
TUNIT7  = 'radians '           / physical unit of field
TTYPE8  = 'tsys    '           / label for field   8
TFORM8  = 'D       '           / data format of field: 8-byte DOUBLE
TUNIT8  = 'K       '           / physical unit of field
TTYPE9  = 'flag_cal'           / label for field   9
TFORM9  = 'J       '           / data format of field: 4-byte INTEGER
TTYPE10 = 'flag_track'         / label for field  10
TFORM10 = 'J       '           / data format of field: 4-byte INTEGER
TTYPE11 = 'weather '           / label for field  11
TFORM11 = '3D      '           / data format of field: 8-byte DOUBLE
TTYPE12 = 'Ch0     '           / label for field  12
TFORM12 = '1E      '           / data format of field: 4-byte REAL
TTYPE13 = 'Ch1     '           / label for field  13
TFORM13 = '1E      '           / data format of field: 4-byte REAL
. . .
```

Figure 3.18 – Data table header (section for channels > Ch1 is not shown)

| Select / All / Invert | time<br>D<br>MJD<br>Modify | raj2000<br>D<br>radians<br>Modify | decj2000<br>D<br>radians<br>Modify | az<br>D<br>radians<br>Modify | el<br>D<br>radians<br>Modify | par_angle<br>D<br>radians<br>Modify |
|---|---|---|---|---|---|---|
| 1 | 5.488000857615E+004 | 4.302401674541E+000 | 1.344986964564E+000 | 3.180516989626E-001 | 7.770213752123E-001 | -1.458780571726E+00( |
| 2 | 5.488000857661E+004 | 4.302497532468E+000 | 1.345163464791E+000 | 3.178024338560E-001 | 7.770210948630E-001 | -1.458867848840E+00( |
| 3 | 5.488000857707E+004 | 4.302593390395E+000 | 1.345339965018E+000 | 3.175531687494E-001 | 7.770208145137E-001 | -1.458955122155E+00( |
| 4 | 5.488000857753E+004 | 4.302687396458E+000 | 1.345514128291E+000 | 3.173072331901E-001 | 7.770206791128E-001 | -1.459041836920E+00( |
| 5 | 5.488000857800E+004 | 4.302779550471E+000 | 1.345685954377E+000 | 3.170646275110E-001 | 7.770206886750E-001 | -1.459127994691E+00( |
| 6 | 5.488000857846E+004 | 4.302871704485E+000 | 1.345857780463E+000 | 3.168220218319E-001 | 7.770206982372E-001 | -1.459214150807E+00( |
| 7 | 5.488000857892E+004 | 4.302963858498E+000 | 1.346029606550E+000 | 3.165794161529E-001 | 7.770207077993E-001 | -1.459300305269E+00( |
| 8 | 5.488000857939E+004 | 4.303056012512E+000 | 1.346201432636E+000 | 3.163368104738E-001 | 7.770207173615E-001 | -1.459386458079E+00( |
| 9 | 5.488000857985E+004 | 4.303148015414E+000 | 1.346372961427E+000 | 3.160946287766E-001 | 7.770207268949E-001 | -1.459472458628E+00( |
| 10 | 5.488000858031E+004 | 4.303239704434E+000 | 1.346543872690E+000 | 3.158533277573E-001 | 7.770207363686E-001 | -1.459558144697E+00( |

| derot_angle<br>D<br>radians<br>Modify | tsys<br>D<br>K<br>Modify | flag_cal<br>J<br>Modify | flag_track<br>J<br>Modify | weather<br>3D<br>Modify | Ch0<br>1E<br>Modify | Ch1<br>1E<br>Modify |
|---|---|---|---|---|---|---|
| 3.333578870000E-001 | 1.000000000000E+000 | 0 | 1 | Plot | 5.381250E+002 | 7.628750E+002 |
| 3.333578870000E-001 | 1.000000000000E+000 | 0 | 1 | Plot | 5.378000E+002 | 7.632500E+002 |
| 3.333578870000E-001 | 1.000000000000E+000 | 0 | 1 | Plot | 5.378000E+002 | 7.634000E+002 |
| 3.333578870000E-001 | 1.000000000000E+000 | 0 | 1 | Plot | 5.380000E+002 | 7.627750E+002 |
| 3.333578870000E-001 | 1.000000000000E+000 | 0 | 1 | Plot | 5.382750E+002 | 7.618750E+002 |
| 3.333578870000E-001 | 1.000000000000E+000 | 0 | 1 | Plot | 5.385500E+002 | 7.611250E+002 |
| 3.333578870000E-001 | 1.000000000000E+000 | 0 | 1 | Plot | 5.386250E+002 | 7.612750E+002 |
| 3.333578870000E-001 | 1.000000000000E+000 | 0 | 1 | Plot | 5.383750E+002 | 7.615750E+002 |
| 3.333578870000E-001 | 1.000000000000E+000 | 0 | 1 | Plot | 5.382250E+002 | 7.621000E+002 |
| 3.333578870000E-001 | 1.000000000000E+000 | 0 | 1 | Plot | 5.380000E+002 | 7.627000E+002 |

Figure 3.19 – Data Table (columns for channels > Ch1 are not shown).
$T_{sys}$ column here shows a dummy value, since the initial release of ESCS did not allow to measure $T_{sys}$ during scans.
Column meaning:
time = Modified Julian Day
raj2000, decj2000 = J2000.0 observed Equatorial coordinates pointed by the central beam
az, el = observed Horizontal coordinates pointed by the central beam
par_angle = parallactic angle for the position pointed by the central beam
derot_angle = rotation angle of the MF dewar with respect to the rest position
tsys = system temperature
flag_cal = flag indicating if the calibration mark is on (1) or off (0)
flag_track = flag indicating if the pointing error is within 0.1 HPBW (1) or not (0)
weather = array of the ground-measured weather parameters
Ch*N* = output data stream coming from channel *N*, given in arbitrary counts

### 3.1. Channel-feed map

Inside the Channel Table, the correspondence between each channel and the number of the feed to which it is connected is specified. For reasons relative to the backend output lines, it is formalised as follows:

| | |
|---|---|
| CH 0 – Feed 2 LCP | CH 1 – Feed 2 RCP |
| CH 2 – Feed 3 LCP | CH 3 – Feed 3 RCP |
| CH 4 – Feed 4 LCP | CH 5 – Feed 4 RCP |
| CH 6 – Feed 5 LCP | CH 7 – Feed 5 RCP |
| CH 8 – Feed 6 LCP | CH 9 – Feed 6 RCP |
| CH 10 – Feed 0 LCP | CH 11 – Feed 0 RCP |
| CH 12 – Feed 1 LCP | CH 13 – Feed 1 RCP |

## 4. THE SCHEDULE READER

I also took part to the development of a "scheduler" for ESCS (see also Chapter 2 §4.1). This component reads a schedule file set to configure the hardware, and gives instructions to the other ESCS components to perform a sequence of LST-based (or UT-based) OTF subscans – or commands for other tracking modes, which were not implemented in the initial phase. The schedule file set consists of four files:

- ***BckFileName*.bck** → This file lists the configuration parameters for the backend. The content is organised as in the following examples:

```
STD:BACKENDS/MFTotalPower {
        integration = 40
        calSwitch = 0
        configure = *,-1,330.0,0.000025,10.0,-1,-1
        enable = 1,1,1,1,1,1,1,1,1,1,1,1,1,1
 }

HIGH:BACKENDS/MFTotalPower {
        integration = 25
        calSwitch = 2
        configure1 = 1,-1,2000.0,0.000025,9.0,-1,-1
        configure2 = 2,-1,2000.0,0.000025,9.0,-1,-1
        enable = 1,1,0,0,0,0,0,0,0,0,0,0,0,0
 }
```

The first field is the procedure name and must be unique in the file, then follows the name of the backend instance the procedure refers to. Between brackets the

configuration commands for the backend are given. They must comply with what the backend expects, so they may vary from case to case. The above examples refer to the new continuum backend. The meanings of the commands are:

**integration** = sampling interval, given in milliseconds;

**calSwitch** = flag indicating if acquisitions take place with a duty cycle involving the switching of the calibration mark;

**configure*N*** = configuration commands for the various data streams (-1 means default or not pertinent value, * means all channels): channel number, frequency (MHz), bandwidth (MHz), sampling rate (MHz), attenuation (dB), polarisation, bins.

- ***CfgFileName*.cfg** → This file lists the configuration parameters for the frontend (subreflector position, local oscillator frequency, receiver setup, etc…). In the present release it is not used as the frontend setup implementation is still underway, but it must exist in the working folder;

- ***LisFileName*.lis** → This is the list of the subscan configurations. It specifies the setup parameters for a series of subscans labelled with an ID number. Here is an example of how the file must be written (with TAB-separated values):

| #ID | type | lon1 | lat1 | lon2 | lat2 | frame | sFrame | geom | descr | dir | duration |
|---|---|---|---|---|---|---|---|---|---|---|---|
| 1 | OTF | 15.500 | 23.000 | 18.000 | 27.000 | EQ | EQ | GC | SS | INC | 240.000 |
| 2 | OTF | 0.000 | 0.000 | 30.000 | 0.000 | GAL | GAL | LAT | SS | INC | 120.000 |
| 3 | OTF | 45.000 | 45.000 | 20.000 | 0.000 | HOR | HOR | LAT | CEN | DEC | 90.000 |
| 4 | OTF | 45.000 | 45.000 | 20.000 | 0.000 | HOR | HOR | LAT | CEN | INC | 90.000 |

The first line, introduced by a "#" symbol, is a comment line and is ignored by the system; it contains the column labels, which correspond to the keywords listed in Table 3.1. In particular:

**lon1, lat1, lon2, lat2** = same as the identically named keywords (see Table 3.1), but here the values are in degrees;

**frame** = coordinate Frame (EQ, HOR or GAL);

**sFrame** = subscan coordinate Frame (EQ, HOR or GAL);

**geom** = scan geometry (LON=constant longitude, LAT=constant latitude, GC=great circle);

**descr** = description (SS=start-stop, CEN=center-span);
**dir** = direction (INC=increase, DEC=decrease);
**duration** = subScanDuration (seconds).

Then the subscan list follows.

*Subscan 1* is a great circle scan performed in equatorial J2000.0 coordinates, starting from the position $(RA_1,DEC_1)=(15.5°,23.0°)$ and ending at position $(RA_2,DEC_2)=(18.0°,27.0°)$, lasting 240 seconds. The indication of direction (here: INC) is necessary but, in the specific case of great circle scans, is not considered by the system, since it is meaningless for this scan geometry.

*Subscan 2* is a constant latitude scan in galactic coordinates. It is specified by means of the start and stop position – in increasing direction – which respectively are: $(l_1,b_1)=(0.0°,0.0°)$ and $(l_2,b_2)=(30.0°,0.0°)$. Subscan is performed in 120 s.

*Subscan 3* is a constant latitude scan in horizontal coordinates, i.e. an azimuth scan. It is described by means of a central position and a span: the central position is (Az,El)=(45.0°,45.0°), and the span is 20.0° in azimuth. Considering that the direction is specified as "decrease", this means that the scan start position will be (Az,El)=(55.0°,45.0°) while the scan stop position will be (Az,El)=(35.0°,45.0°).

*Subscan 4* is identical to subscan3, but is performed in the opposite direction.

- ***ScheduleName*.scd** → This is the schedule, i.e. the operating list of time-based subscans. This file must begin with a header written as follows (keywords and values are TAB-separated):

  PROJECT: *ProjectName*
  OBSERVER: *ObserverName*
  SCANLIST: *LisFileName*.lis
  MODE: UT *[n]*
  CONFIGLIST: *CfgFileName*.cfg
  BACKENDLIST: *BckFileName*.bck

  The "MODE" keyword refers to the user choice concerning the schedule timing. Its value can be LST or UT. If the LST timing is chosen, the user must specify, with a tab-separated integer *[n]*, the number of times the schedule is to be cyclically run.

After the header, there is a comment line indicating the column labels, followed by the schedule rows, filled with TAB-separated values:

| #ID | Label | startUT | duration | gap | scan# | config | backend |
|---|---|---|---|---|---|---|---|
| 1 | Source1 | 12:00:00.000 | 240.00 | 10.000 | 1 | -1 | NULL |
| 2 | Source2 | 12:05:00.000 | 240.00 | 10.000 | 1 | -1 | NULL |
| 3 | Source3 | 12:10:00.000 | 240.00 | 10.000 | 1 | -1 | STD:MANAGEMENT/Writer1 |
| 4 | Scan1 | 12:15:00.000 | 90.00 | 10.000 | 3 | -1 | HIGH:MANAGEMENT/Writer1 |
| 5 | Scan2 | 12:16:40.000 | 90.00 | 10.000 | 4 | -1 | NULL |
| 6 | Label | 12:19:30.000 | 120.00 | 10.000 | 2 | -1 | NULL |

After the line ID, the start time is given (hh:mm:ss.sss), preceded by a label, which is used in the composition of the FITS filename. Then the subscan duration (always in UT seconds) relative to the constant speed path follows. The “gap” value is the time interval – in UT seconds – that ESCS waits, after the completion of the constant speed scan, before commanding the antenna to the next subscan. In practice, it must be equal to the duration of the deceleration ramp plus a short “safety overhead”.
If a certain antenna slewing is necessary between two consecutive subscans, it is not to be included in the “gap” value. Instead, it must be taken into account when determining the startUT/startLST instant of the following subscan.

Column “scan#” indicates the ID number of the subscan to be executed, as listed in file FileName.lis.

The config column indicates where to find the configuration parameters for the receiver: -1 stands for the current implementation, which does not allow the use of the configuration file and relies on the setup performed externally. In the next ESCS release, this column will specify the procedure name – within the *CfgFileName*.cfg file – to be used for the frontend setup.

The last column is devoted to the backend setup, if the value is “NULL” the data recording will not take place, otherwise the string specifies the backend procedure and the target – i.e. the component actually writing the output, in the form:

PROCEDURE:TARGET

In the above example, the string STD:MANAGEMENT/Writer1 means we are calling the STD procedure given in the .bck file and using Writer1 (under the Management subsystem) as the data writer.

Focusing on lines 4 and 5: these are scans sweeping the same azimuth strip in opposite directions, which means that the first scan stops exactly where the second must begin. Therefore there is no slewing between the two, and the second scan begins right 100 seconds (duration+gap) after the first one.

# 5. SOFTWARE TOOLS FOR THE COMMISSIONING OF THE NEW MF OBSERVATIVE SETUP

Finally, in order to perform test observations during the MF/backend/ESCS commissioning phase I developed a suite of software tools for observation setup, data quick look, and data reduction. Even though some of them are very specialised for the observations I conducted, these tools are now available to all the observers using ESCS as basic instruments to prepare and perform observing sessions, and to inspect the acquired data. A brief summary of these tools is presented here; more information is given in Chapter 4, where their application is shown in detail.

## 5.1. RScanSched

A peculiar observing technique – consisting in recursive azimuth scans taken at constant elevation – was employed to map selected sky areas (Chapter 4 §2). Since this technique relies on the precision in starting each subscan at a given LST along 24-hours schedules, a specific C++ program called *RScanSched* was developed in order to produce such schedules, starting from a set of configuration parameters.

## 5.2. Fits2sd

The production of maps from azimuth scans is achieved by means of a FORTRAN program developed by Ettore Carretti and optimised to the specific needs of these tests by the author himself. To meet the requirements in terms of input file format, such minimising the necessity to modify the map-making code, the FITS files had to be converted in the SDFITS (Single Dish FITS) format, which is a standard FITS "flavour" specific for single-dish acquisitions (Garwood, 2000). This implied the production of an SDFITS file for every feed used in the observations – whose data

streams had been stored in two columns of the original FITS Data Table – taking care of assigning the properly projected coordinates to the lateral feeds. The projection algorithm is specific for the above mentioned observing technique, so this converter, which is another C++ program, is not general purpose, though it can be easily updated in order to serve a wider range of observing methods. The conversion also requires to specify a counts-to-Jy conversion factor for the flux calibration of the data.

### 5.3. IDL programs

Several programs were developed in the IDL environment in order to perform the quick-look and some basic operations on the FITS files. An incomplete list follows:

- procedures to plot in quasi-realtime the files saved while running a schedule, selecting which channel and which sample number range to plot, or to plot the subscan paths across the celestial sphere. To mention a few: *lastfits.pro, fitszoom.pro, scanplot.pro*
- *fitsplotter.pro* – it produces a Postscript file with the plots of all the channels (counts vs. sample number) for every FITS file in the specified folder;
- *fitsplotter_FFT.pro* – it couples the above simple plots of the raw data to the plot of the FFT magnitude, useful to check if some ripple is embedded in the continuum data;
- *fits2txt.pro* – it produces ASCII tables whose columns contain time, coordinates and data streams taken from the FITS file in the specified folder;
- *calibration21GHz.pro* and *calibration5GHz.pro* – these are to be used with OTF scans of flux calibrators – to be chosen within a source list which is written inside the procedures themselves. Their aim is to fit a Gaussian to the beam profile obtained by the "transit" of the calibrator across the beam, and to compute the Jy/count conversion factor, along with an estimate of the SNR (signal to noise ratio). As the names suggest, the two versions are respectively devoted to 21 GHz and 5 GHz observations, achieved with the new analogue backend.

# CHAPTER 4

# COMMISSIONING OF THE MF SYSTEM

*There are more things in heaven and earth, Horatio,*
*Than are dreamt of in your philosophy.*
W. Shakespeare - Hamlet Act 1, scene 5

## 1. OVERVIEW

The commissioning phase for the MF receiver/backend system started in December 2008. A significant part of this thesis consisted in conducting high sensitivity observations to test the system performances at its limits and find out possible residual effects, such as instabilities small enough not to be discovered in laboratory, but still significant to worsen the expected sensitivity, or issues related to the installation of the equipment on the telescope, like interfaces with other pieces of equipment or the contamination by RFI.

The observations mainly consisted in a survey of the Polar Cap to test the performances with compact sources. For such an aim several observing sessions took place and all the software tools described in Chapter 3 were used.

This chapter illustrates in detail the observing technique developed, and the results of the many tests carried out.

## 2. THE OBSERVING TECHNIQUE

### 2.1. Reasons and goals for OTF-survey tests

OTF scans allow the telescope to map wide areas of the sky in a short time interval. Fast and brief scans are particularly helpful as they are carried out under virtually constant atmospheric conditions (see Chapter 3 §2.1). In addition, in short time intervals also the hardware system can be considered stable.

Acquisitions are performed at high data-rate – values down to a sampling interval of 1 ms are possible – allowing accurate tests of the telescope performance, shedding light on subtle details of the behaviour of the whole chain, from the receiver to the data

acquisition and recording system, as the fast rate data are free from the effects of the 1/f noise .

The final maps also contain valuable scientific information, since no wide maps achieved above 15 GHz are at present available for the Northern celestial hemisphere. For this reason, several astronomers from the Institute of Radioastronomy joined the MF commissioning group for the benefit of the KNoWS (K-band Northern Wide Survey) project, which is described in §2.5.

### 2.2. Details on the observing strategy

The observing strategy chosen for this project is based on that conceived and developed by Ettore Carretti for the project S-PASS at the Parkes radiotelescope (Carretti et al. 2009, Carretti et al. 2010). The S-band Polarization All Sky Survey (S-PASS) aims at studying the CMB polarized foregrounds and the Galactic magnetism and consists of a survey of the diffuse polarized emission of the entire southern sky at 2.3 GHz.

The scanning strategy is based on fast azimuth scans at constant elevation. Fast scans are imperative to carry out such big surveys in a reasonable amount of time. At the Parkes telescope it was possible to achieve scan speed up to 15 °/min with full precision position information. Being the Parkes telescope a much bigger and more massive instrument than the Medicina dish, this gave us a good confidence that a similar performance could also be obtained with the Medicina telescope.

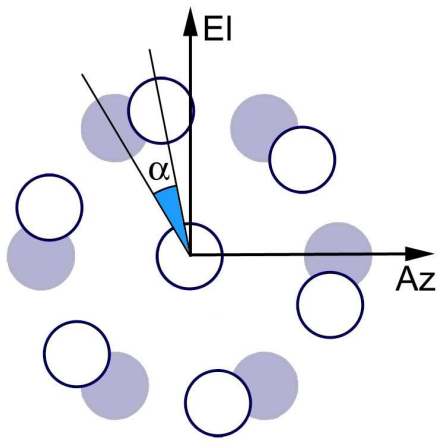


Figure 4.1 – The projected beams in the Az-El frame. Empty circles correspond to the rotated positions.

To optimise the area scanned by the 7 beams, the multi-feed array is rotated by an angle $\alpha = 19.1°$ with respect to its rest position. This way, the paths run by the individual beams are equally spaced in elevation realising a regular sampling of the sky.

Figure 4.1 shows the projected beams in their rest position (filled circles), and the rotated beams (empty circles), with respect to the Horizontal reference frame.

The apparent rotation of the celestial sphere is exploited to cover the sky area to be mapped, which is a "Declination belt" spanning 24 hours in Right Ascension. In a single sidereal day this technique allows to observe, in the Equatorial frame, "wavy" stripes within the belt, as shown in figure 4.2.

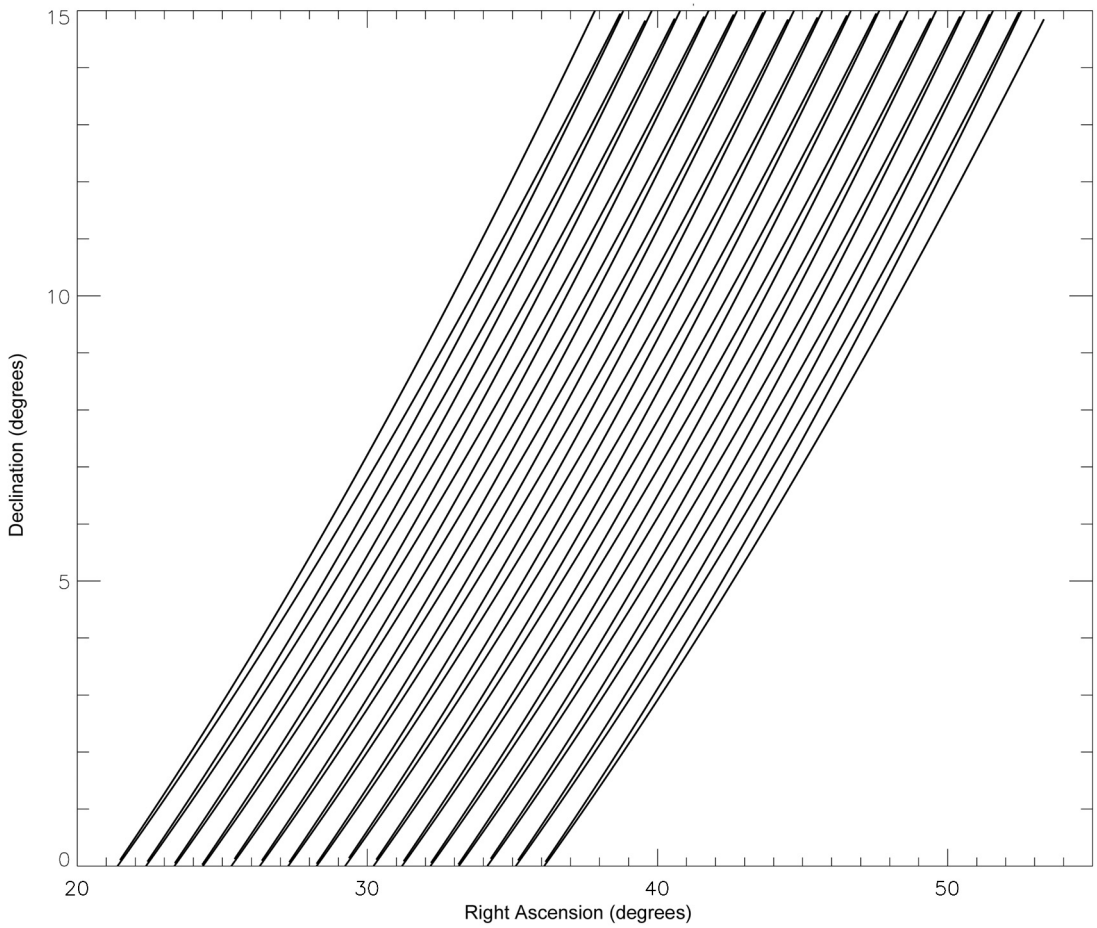


Figure 4.2 – RA-Dec plot of central beam positions during 32 subscans taken spanning in azimuth from 98.5° and 124.5° at a constant elevation of 30°, running at 15°/min. Those horizontal scans translate into a wavy pattern in the Equatorial frame, within the 0°-15° declination range.

To complete the map this scheme must be repeated in the following days, shifting the stripe pattern to fill in the missing areas until the Nyquist sampling is reached. In practice, this translates into starting the azimuth scans sequence at a different LST. The sidereal time interleave between two adjacent sequences is computed so that the stripes covered by the scans differ by half a beamsize or less.

The receiver has 7 feeds oriented as previously shown and spaced by about a beamwidth. As a consequence, sets of two scans spaced by half a beamsize are required

to cover the sky, so that each of these sets realises 14 tracks spaced at the Nyquist sampling. To perform a regular coverage of the sky it is then sufficient to space these sets of two scans by a full size of the MF (see Figure 4.3).

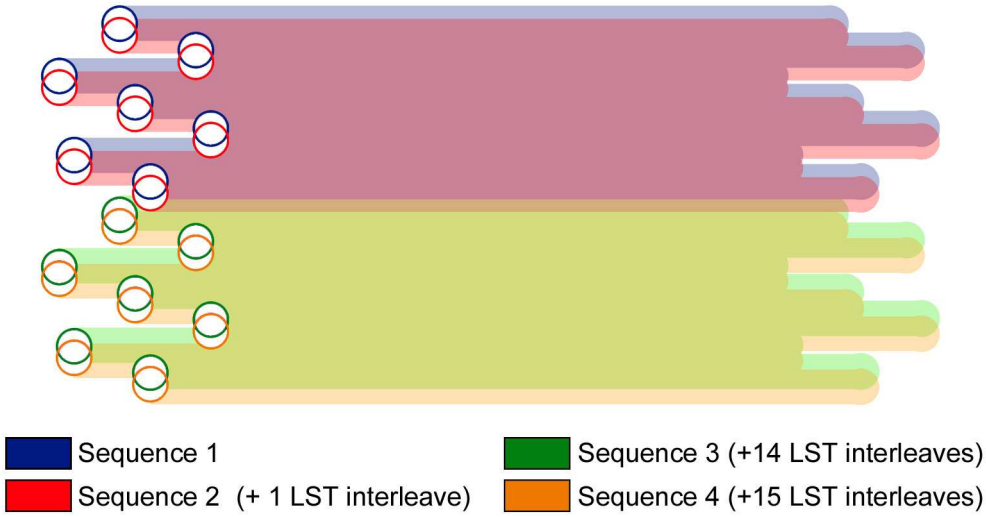


Figure 4.3 – Schematisation of the different sequences of horizontal scans and their interspace.

Observing at a constant elevation is extremely helpful for both data stability and calibration. The ground emission will not vary significantly, and the same will happen for the atmospheric opacity: when observing in steady, uniform weather conditions such as in a dry, clear day, the opacity is only a function of the airmass, which is proportional to the secant of the zenith angle (90°-elevation).

In these ideal conditions, the flux calibration of the maps is achieved observing flux calibrators when they transit at the same elevation of the horizontal scans, this way obtaining a direct conversion factor from the backend arbitrary unit to flux density. Further and more refined procedures are necessary in case the sky conditions are not uniform or vary significantly between the calibration observations, in particular involving the application of an atmospheric model to estimate the opacity value from ground-measured weather parameters. These are available in the FITS files, associated to every data sample.

The choice of constant-elevation OTF scans was also supported by a contingent requirement: the Medicina dish elevation rail should undergo maintenance and cannot

guarantee an accurate pointing if the elevation changes rapidly, so it is not advisable to perform scans implying a fast motion in elevation.

### 2.3. Expected sensitivity

A single OTF subscan performed in the 20-22 GHz band, with a sampling interval equal to 40 ms, has a theoretical instant noise which can be computed by means of the radiometer equation:

$$rms=\frac{kTsys}{\sqrt{Bt}}=7.8\text{mK}=70.9\text{mJy}$$

where k = 1 (for single polarisation), $T_{sys}$ = 70 K (for $\tau$ = 0.1, El=45°), B = 2 GHz (bandwidth), t = 0.040 s (integration time), antenna gain at 21 GHz = 0.11 K/Jy. The assumed $T_{sys}$ accounts for both receiver noise and signal contribution (sky, ground and atmospheric emission).

As a reference value to assess the performance of the system we use the one-second integration sensitivity, which reads $\sigma_{1s}$ = 1.56 mK $s^{1/2}$ = 14.2 mJy $s^{1/2}$.

Using these values we can achieve a first order estimate of the expected sensitivity of a map obtained exploiting the above mentioned scanning strategy. The following hypothesis refers to OTF scans at 15 °/min, in the 20-22 GHz band, performed at the constant elevation El=45°:

- the actual scan speed on sky is 15 °/min * cos(El) = 10.7 °/min;
- one beam-sized pixel (1.6 arcmin) is observed for 0.150 s in each individual subscan;
- the scanning strategy includes back-forth scans. Along with the proper spacing between next subscans (half a beamwidth), this leads to observe the beam-sized pixels for 4 times, for a total integration time $t_{px}$=0.600 s. Every feed observes two polarisations, which further improves the sensitivity by a factor of $\sqrt{2}$;
- considering $T_{sys}$ = 70 K, B = 2 GHz, t = 0.600 s (integration time), and k = $1/\sqrt{2}$ (dual polarisation total power) the radiometer equation yields:

$$rms=\frac{kTsys}{\sqrt{Bt}}=1.4\text{mK}=12.7\text{mJy}$$

This means that 50 mJy sources are observed at 4σ.

### 2.4. Required time

The actual amount of time needed to complete a map depends on the specific choice in terms of scanning strategy.

In the hypothesis of covering the whole Northern sky (Dec = [0°,+90°]) in a single map, it is necessary to perform scans in the azimuth range [0°,180°] at the elevation of the North Celestial Pole (EL=44.52° for Medicina). This solution requires 41 days of observations (overhead included), but it is not optimised as the highest Declinations are greatly oversampled.

A more optimised strategy requires to subdivide the sky in three-four "Declination belts", each performed with azimuth scans at optimal elevations. Numerical computations show that this allows a reduction down to about 33 days, with a more uniform sampling of the various Declination belts. This solution is also more suitable for test purposes as small belts can be completed in just a few days.

For example, for the largest part of the tests we chose to use the polar cap area ranging at Dec ~ [72°,+90°] (see section §3.5) which has an area of about 1000 square degrees and can be fully sampled in 4 days with 15 °/min scans between 0° and 25° of azimuth taken at EL 44.52°.

### 2.5. The science within: the KNoWS project

The observations performed for commissioning purposes were also accompanied by scientific goals. As illustrated in the previous sections, the chosen observing strategy allows the telescope to map large areas of the sky in a few days, reaching a sensitivity of nearly 10 mJy rms. This performance matches the needs of a proposed project named KNoWS (K-band Northern Wide Survey) led by E. Carretti whose aim is to carry out a blind survey of compact sources at 21 GHz on the entire Northern Celestial

Hemisphere, down to a detection limit of 50 mJy (5σ). The main goal is to extract a complete, unbiased sample of extragalactic sources, complementing the AT20G, an equivalent survey of the southern sky recently carried out at Narrabri (Australia) with the Australia Telescope Compact Array with the same detection limit (Ricci et al. 2004, Massardi et al. 2008). The KNoWS and the AT20G surveys together will provide an unprecedented, full all-sky coverage at such high frequencies. The main scientific aim is two-fold:

- extragalactic point sources are one of the major foreground contaminants for CMB experiments, both in total intensity and polarisation. A survey of the entire sky is required to identify and flag the sources from CMB experiments maps and estimate the residual contamination. KNoWS points at the realisation of the Northern section;
- at high radio frequency the synchrotron-dominated objects fade out, leaving space to the rare class of objects with flat/inverted spectrum. A very large, possibly all-sky, sample is necessary to conduct a statistically significant analysis of the various sub–classes of objects (BLLac, GPS/HFF, ADAF, etc.) and derive their average properties with sufficient precision.

The project is aimed at building an unbiased radio source sample, while subsequent follow-up observations will allow the full characterization of the sources in both total intensity and polarization.

## 3. TEST SESSION *I*: JANUARY-MAY 2009

Tests in survey mode began at the end of January, 2009.

The goals of the first session were:

- to check for hardware/software faults or instabilities;
- to identify the best 2GHz-wide sub-band within the 18-26 GHz frequency band, both in terms of response to the weather conditions and of absence of RFI;
- to select the most suitable Declination belt for the test survey, and decide whether to perform the azimuth scans – inside that belt – pointing towards East or West: every belt can be mapped exploiting two azimuth ranges which are symmetrical with

respect to the local meridian. The choice of one over the other was driven by local conditions such as the presence of RFIs;

- to test the fast-OTF scan technique and confirm that high-speed scans can be performed without affecting the data quality;
- to test the insertion of calibration scans within the survey schedules, in particular as concerns the time gap allowed to slew from the survey area to the flux calibrators.

We started with observations of the lowest Northern Declination belt, i.e. Dec = [0°,+15°]. Table 4.1 summarises the recursive scans parameters for this first section.

| | |
|---|---|
| Minimum Azimuth | 98.5° |
| Maximum Azimuth | 124.5° |
| Elevation | 30.0° |
| Scan azimuth speed | 15 °/min |
| Sampling interval | 40 ms |
| ΔLST – 1 step (interleave corresponding to 36 arcsec) | 3.36530 s |
| Gap (ramp-up + ramp-down for 1 scan) | 13.389769 s |
| $t_{scan}$ (cruise only) | 104.00000 s |
| $t_{bf}$ (back-and-forth scan including gaps) | 243.77954 s |
| $N_{bf}$ (number of back-and-forth scans per full sequence) | 376 |
| $N_{zz}$ (number of sequences – i.e. days – to fill the section) | 10 |

Table 4.1 – Main parameters for the horizontal scans executed in the very first test observations, performed pointing eastward to map the Declination section [0°,15°].

This section can be fully sampled in 10 days of observations, covering a total area of about 5500 square degrees. A huge amount of data was collected (~ 500 subscans/FITS files per day), which was useful to check the system stability. Our analysis follows in the next sections.

### 3.1. General system response: Software

The OTF component and the scheduling system worked correctly: no major faults occurred during the observing session. Minor bugs were identified and fixed.

### 3.2. General system response: Hardware

On the hardware side, sporadic problems originated from the subreflector, which happened to block in a few occasion, causing the antenna to point to a wrong position.

Unfortunately, the MF receiver showed some failures: channels 4 and 9, representing respectively the data streams recorded from Feed 4-LCP and Feed6-RCP (see Chapter 3 §3.1 for the complete channel-feed map), were flat. That was due to their Low-Noise Amplifiers (LNA) which were found to be out of order. This condition will persist until the MF receiver is removed from the Medicina antenna to be shipped to the Sardinia Radio Telescope, since no maintenance can be performed on the LNAs while the receiver is mounted on the antenna.

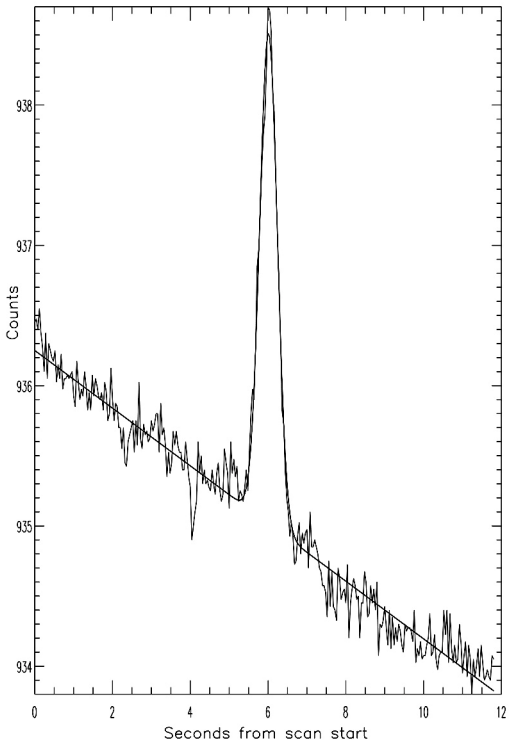


Figure 4.4 – Constant declination subscan over 3C286. Scan speed 3°/min. Gaussian fit is overplotted onto the data samples.

Scans on flux calibrators allowed to estimate the receiver sensitivity. Figure 4.4 shows a short RA subscan across 3C286, with a scan speed of 3°/min, in good weather conditions (clear sky, T = -2°C, RH = 62%, P = 1022,7 mbar), in the 20-22 GHz band. We measure an rms noise for a single sample integration time (40 ms) of one polarisation channel equal to 74 mJy rms. This translates, for one second of integration, into an rms value of 14.8 mJy.

These measured sensitivity closely matches the theoretical values computed in §2.3, such assessing the excellent system capabilities. The real sensitivity of the final map can thus be estimated as well. The strategy illustrated in Section 2.3 was a first order estimate. Precise numeric computations accounting for the setup configuration described in Table 4.1 give a scan spacing of 36 arcsec (as listed in the Table), which is shorter than ½*HPBW, thus increasing the number of scans and, in turn, the integration time per beam-sized pixel to $t_{px}$ = 0.96 s. Taking into account all these elements, the estimated sensitivity of the final map is:

$$\sigma_{px} \approx 10.7 \text{ mJy}$$

This confirms that the sensitivity requirements of a projects like KNoWS can be matched.

### 3.3. Tests for various frequency bands

We alternatively carried out observations in the 18-20 GHz, 20-22 GHz, 22-24 GHz and 24-26 GHz frequency bands – mostly the first two ones.

Tests confirmed that, as expected, the less weather-dependent sub-band is the lowest frequency one: 18-20 GHz. However, in case of thick clouds or precipitations, even at these frequencies the atmospheric emission increases dramatically. It was not possible to estimate the atmospheric opacity while the long survey schedules were running, since ESCS was not yet provided with tools to perform such measurements, but the water emission effects could be traced by means of a semi-qualitative analysis of the data. Bad weather – i.e. high values of the atmospheric opacity due to moisture, clouds or showers – affect the total power data causing the $T_{sys}$ to rise and the noise to increase. The cloud cover is never homogeneous along the subscan, so a plot showing signal amplitude against time exhibits a "bumpy" baseline (see Figure 4.5). In case of rain, the loss of sensitivity is so high that no significant information can be extracted from the data.

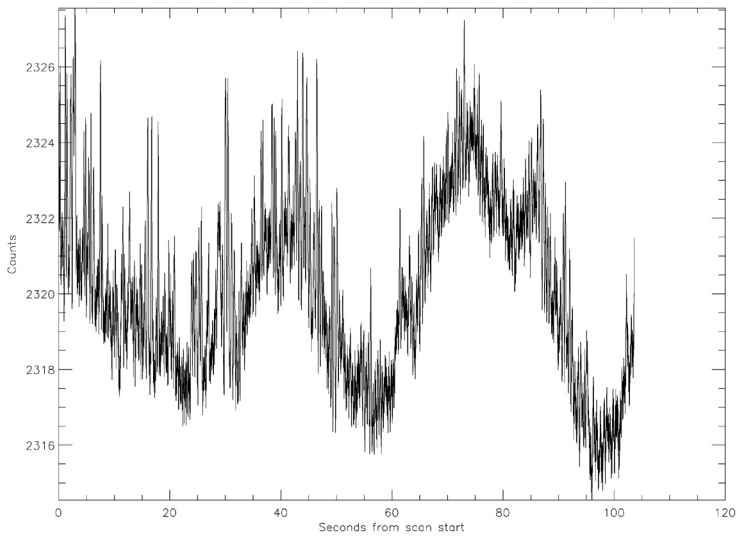


Figure 4.5 – Subscan performed in the 98.5°-124.5° range, 30° of elevation. X-axis: time (seconds from scan start), Y-axis: signal amplitude in arbitrary counts. The cloudy sky causes "bumpy" variations in the signal level. The higher noise present in the first 50 seconds cannot be explained in terms of weather-dependant effects.

Figure 4.5 also introduces one of the main features we encountered along the many test sessions: the presence of an apparently "spiky" noise, affecting one part of the subscan only. This phenomenon, and the chase for its explanation, is discussed in detail in §3.6 and §5.1, however during this session it appeared to be more frequent and evident in the lowest band (18-20 GHz).

Broad-band RFIs were detected in all bands at specific positions on the horizon. More details are given in the next section.

A peculiar feature (Figure 4.6) was found in a very restricted number of files. It consisted in regularly time-spaced pulses, whose origin is still unknown as the event, possibly due to some interference coming from nearby devices, was never noticed again.

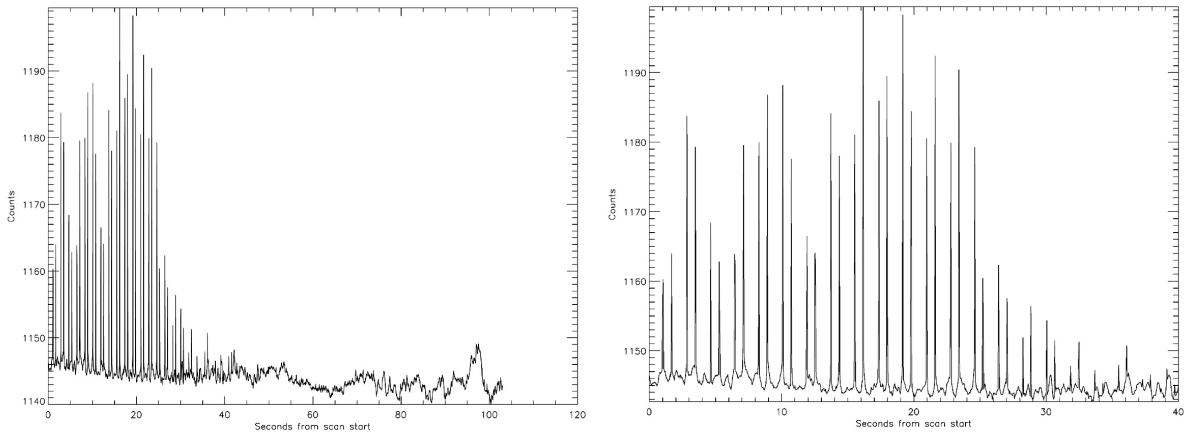


Figure 4.6 – Double-peaked pulsed signal very rarely present in the acquired data. The whole 104-s subscan is shown on the left, while the right plot zooms on the first 40 s. The distance between two consecutive pulses is 1.8 s, while the two peaks are separated by a 0.64 s gap. The origin of this signal is still unknown as this feature did not show up again.

### 3.4. Tests for different azimuth ranges

The first part of the session focused on the [98.5°,124.5°] and the [235.5°,261.5°] azimuth ranges – both of which, being symmetrical with respect to the local meridian, map the same Declination belt: Dec = [0°,15°].

Though sporadic weak interferences were present also in the eastward range, the worst scenario was offered by the westward region: we checked it along several days and at a different time (both daytime and night), and it was found almost constantly polluted by RFIs (Figure 4.7).

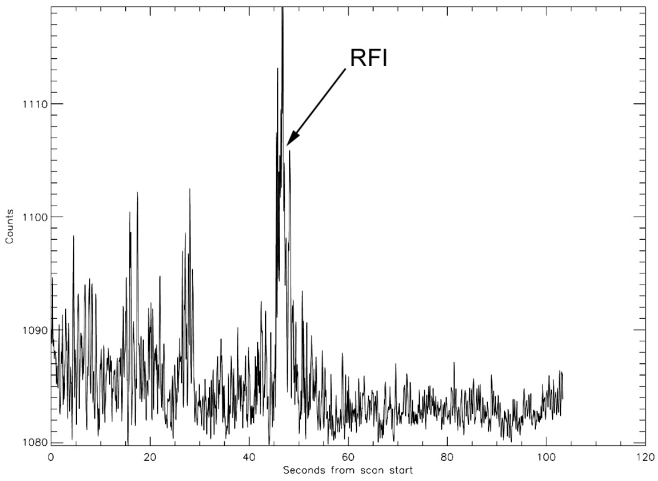


Figure 4.7 – Strong RFI observed during most of the acquisitions performed in the 235.5°-261.5° azimuth range. The peak corresponds to azimuth=249.8°

The signal was observed around the azimuth position of 249.8°, and was confirmed by independent measurements performed by the Medicina RFI mitigation staff.

After this detection, we carried out further observations to check other azimuth ranges. Ultimately, two 180°-wide scans were completed to identify the presence of RFIs along the entire horizon. The North and North-East regions turned out to be, at least at the time of the inspection, free from polluting signals.

### 3.5. Final setup selection: the "polar cap" at 20-22 GHz

On the basis of these information (§3.3 and §3.4), we decided to carry out all the subsequent test observations to cover the area for Dec > 72.3° ("polar cap") and in the 20-22 GHz band,– if no specific test needs required a temporary frequency change. The setup parameters of the recursive azimuth scans are listed in Table 4.2.

| | |
|---|---|
| Minimum Azimuth | 1.0° |
| Maximum Azimuth | 25.0° |
| Elevation | 44.52° |
| Scan azimuth speed | 15 °/min |
| Sampling interval | 40 ms |
| ΔLST – 1 step (interleave corresponding to 36 arcsec) | 7.8544399 s |
| Gap (ramp-up + ramp-down for 1 scan) | 13.623525 s |
| $t_{scan}$ (cruise only) | 96.000000 s |
| $t_{bf}$ (back-and-forth scan including gaps) | 219.24705 s |
| $N_{bf}$ (number of back-and-forth scans per full sequence) | 393 |
| $N_{zz}$ (number of sequences - days - to fill the section) | 4 |

Table 4.2 – Main parameters for the horizontal scans executed in the second phase of the test observations, performed pointing eastward to map the Declination section [72.3°, 89.3°].

This area covers about 1000 square degrees and can be fully sampled in only 4 days of observations, to reach the already mentioned rms sensitivity of 10 mJy.

The scans were performed at the elevation of the North Celestial Pole for the Medicina site (44.52°). This value, being appreciably higher than the 30° which is optimal for lower Declination sections, implies lower ground emission and atmospheric contribution, which further supported the selection of this Declination range for the next tests.

### 3.6. Tests changing the scanning speed

We had already assessed the reliability of the antenna pointing while performing scans at a speed up to 24 °/min through tests carried out after the implementation of the OTF component (see Chapter 3 §2.3), but no astronomical data had been acquired during those scans.

It was then necessary to investigate the effects of the speed on the recorded data, to identify any potential deterioration of the data quality. In particular, this verification was essential to try to correlate the scan setup parameters and the signal alteration already mentioned in Figure 4.5.

We produced a specific schedule listing subscans to map the polar cap with the same spatial setup, but at different scanning speeds: 2°/min, 5°/min, 7.5°/min, 10°/min, 15°/min. The sampling interval was 40 ms, as usual, for all the subscans.

No significant differences were found to exist in the acquired data, as all of the files showed the same characteristics, including – when it was present – the signal "jiggling" whose origin was at the time still unknown (details in §3.7).

Figures 4.8-4.10 show some examples extracted from the files acquired on March, 8$^{th}$ 2009 in excellent weather conditions.

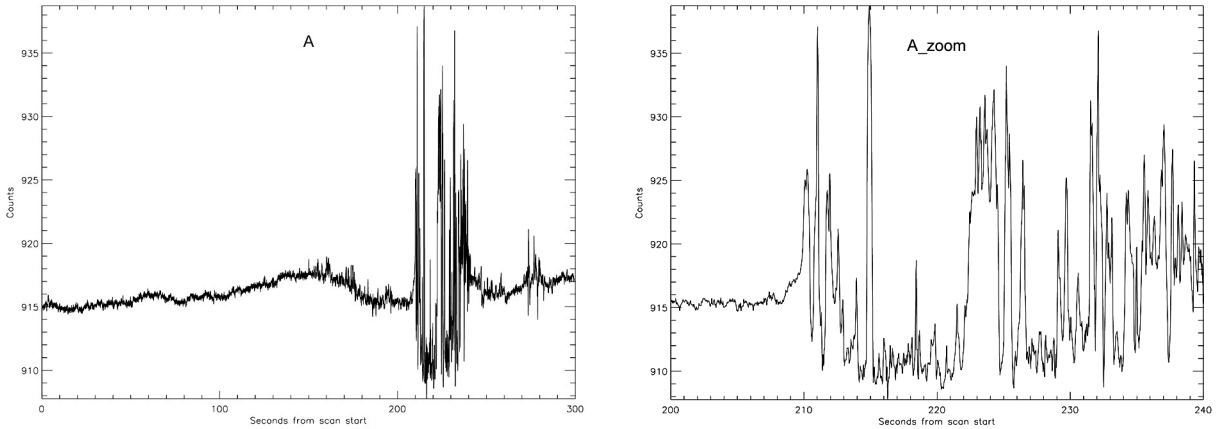


Figure 4.8 – One subscan performed at 5 °/min in the polar cap setup: Az=[1°,25°], El=44.62°. X-axis: seconds from subscan start, Y-axis: signal amplitude in arbitrary counts. The left plot shows the whole subscan, while the right box zooms on a section lasting 40 s, to better illustrate the "jiggling" effect.

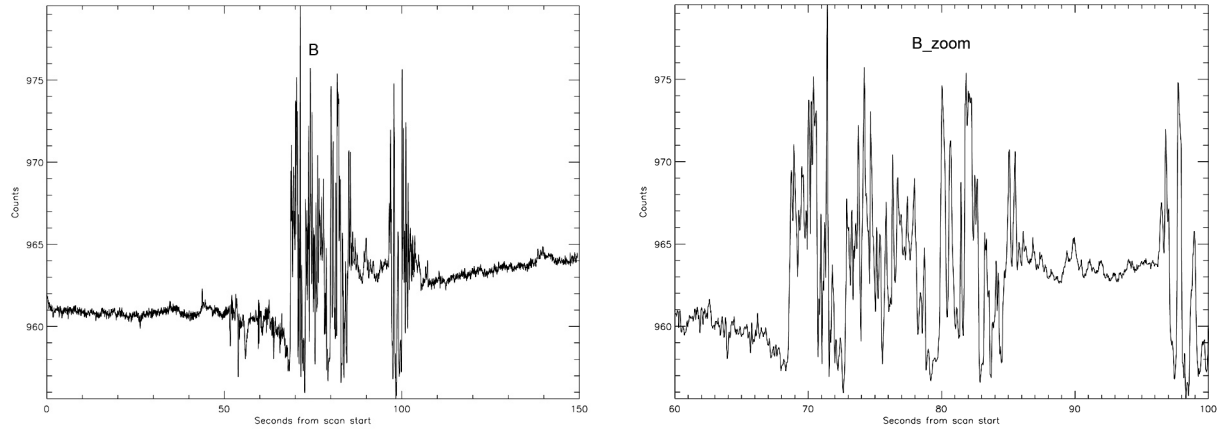


Figure 4.9 – Subscan at 10 °/min showing the same phenomenon.

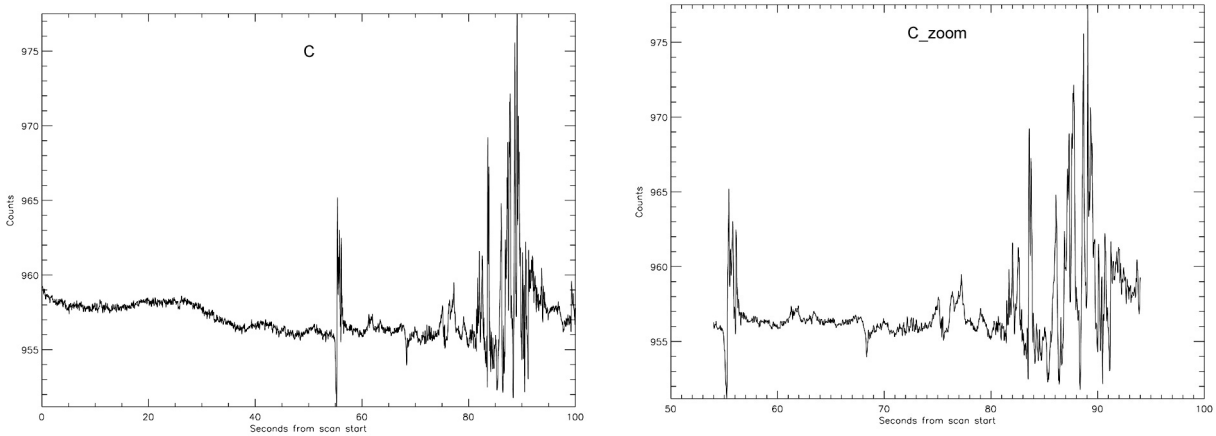


Figure 4.10 – As above, but speed is 15 °/min.

### 3.7. Peculiar data features

During the numerous days of observations in this first commissioning session, several peculiar features were identified inside the data. While many of them were rarely seen and/or could be explained almost straightforwardly – with the possibility to immediately act on their source – other features were caused by subtle hardware instabilities, which resulted hard and long to catch, and were so frequent to compromise the possibility to reach the expected sensitivity for continuum observations. The following paragraphs illustrate the main effects and their characteristics.

*Multiple peaks*

During the coldest days of February 2009, a strange phenomenon was observed.

This effect was evidenced only in the case of calibration scans, and consisted in the appearance of large peaks inside the signal, whose angular extension was not far from the receiver HPBW. For instance, it appeared in the evening of Feb. 19$^{th}$, when several RA and Dec subscans were performed on 3C 286 (Figure 4.11), but it was absent in the following sessions. Even though the phenomenon is still not fully understood, this was likely due to a thin ice layer on the cover of the secondary focus cabin causing a "deforming optical" effect.

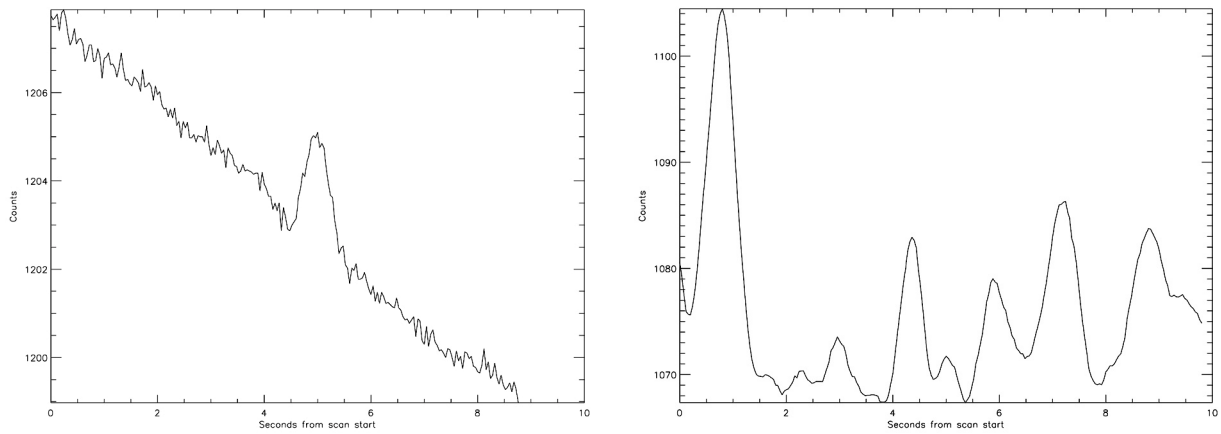


Figure 4.11 – Declination subscans performed at 3°/min across 3C286 on February 19$^{th}$ 2009. Left panel: 20:24 UT; weather conditions were good, the poor SNR is due to the low elevation of the source (16°) at the time of the acquisition. Right panel: 21:19 UT; the puzzling wavy baseline is present.

*Digital noise*

In March 2009 the acquisitions showed the presence of digital noise summed to the observed signal. In amplitude vs. time plots, this noise corresponds to samples whose amplitude value is offset (see Figure 4.12). The fraction of affected samples was not negligible, so even if in principle it would have been possible to remove the outliers using a median filter, applying such a technique would have affected the information embedded in the data.

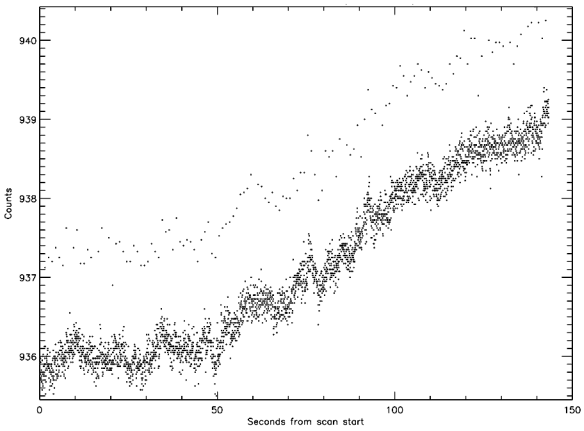


Figure 4.12 – Digital noise caused by cross-talk between the backend boards.

The source of this "signal pollution" was found to be a cross-talk between the backend boards, which were thus taken out and brought to the lab for maintenance. After this operation the digital noise disappeared, with the only exception of a residual effect observed for Channel 3 (Feed3 LCP).

*Signal level instability*

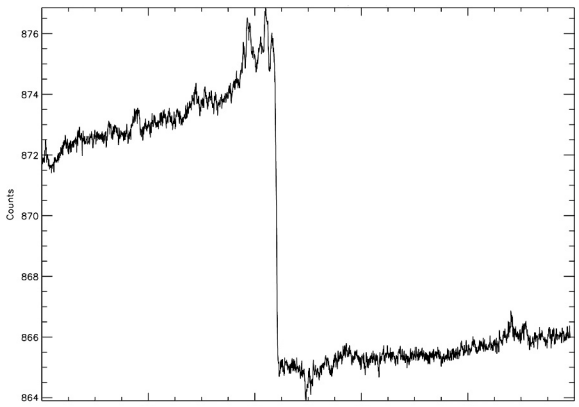


Figure 4.13 – Signal level jump

One of the most concerning faults we met was the occurrence of sudden jumps in the signal level (Figure 4.12). They afflicted a considerable amount of the acquired files (in some days the fraction of interested files reached 10%).

The source of the problem was surely internal to the hardware system, as it was observed also with a hot load in front of the feeds – which corresponds to blind out the receivers. It was suspected to be a power instability of the Local Oscillators (LO), as critical points in the distribution of the first

and second conversion LOs were already known to exist. Unfortunately, it had been impossible to modify the hardware before the installation of the MF on the antenna, as the required new pieces of equipment had not been delivered on time.

In addition, the level jumps were observed contemporarily in all the channels. This indicated that the problem must have resided in the parts which were common to all the channels – i.e. power supply or local oscillators.

Specific tests to ascertain the origin of this behaviour were carried out on May 4-5$^{th}$ 2009, exploiting the LO distribution lines. A first run of tests demonstrated that the HP synthesizer, responsible for the first conversion, was not the cause of the problem.

Attention then focused on the second conversion stage: the channels originally corresponding to the feeds with malfunctioning LNAs, Ch4 and Ch9, were connected to different oscillators at this stage, in order to directly monitor their signal while the subscans were performed.

In particular, Ch9 monitored the original Miteq oscillator – a commercial device, the one actually distributed to the other channels – which was known to suffer from instabilities. At the same time, Ch4 was connected to a Wiltron programmable synthesizer with the aim to check its stability and consider whether it could be a valid replacement for the Miteq oscillator.

During these tests it was also possible to modify the distributor, as the necessary components had finally arrived. The aim of this upgrade was to bring the LO output power levels within the ranges required by the mixer. The operation was expected to contribute to the stabilisation of the revealed signal level, but even if the jumps were reduced, they were still present and found to be caused by the Miteq oscillator. As a consequence, the device was uninstalled and shipped to the manufacturer for check-up and maintenance (or substitution), and was temporarily replaced by the Wiltron synthesizer.

The following observations have never shown considerable level jumps again, their manifestation being rare and of far smaller extent.

Two examples of the simultaneous occurrence of jumps in the Miteq signal and in the CH10 one (Feed0 LCP) are reported in the following figures.

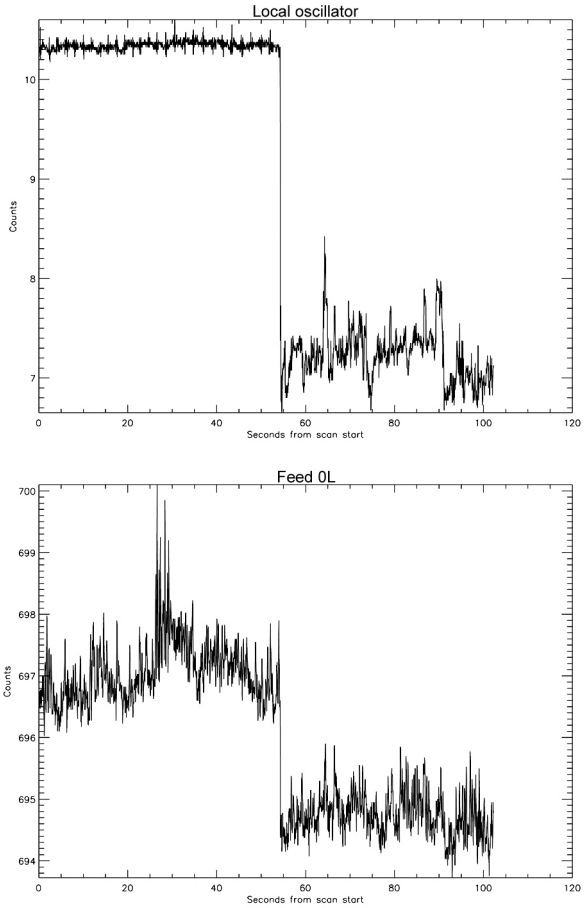


Figure 4.14 A – Top panel: output power of the second conversion LO (Miteq). Bottom panel: simultaneous acquisition performed through CH10 (Feed0 LCP).

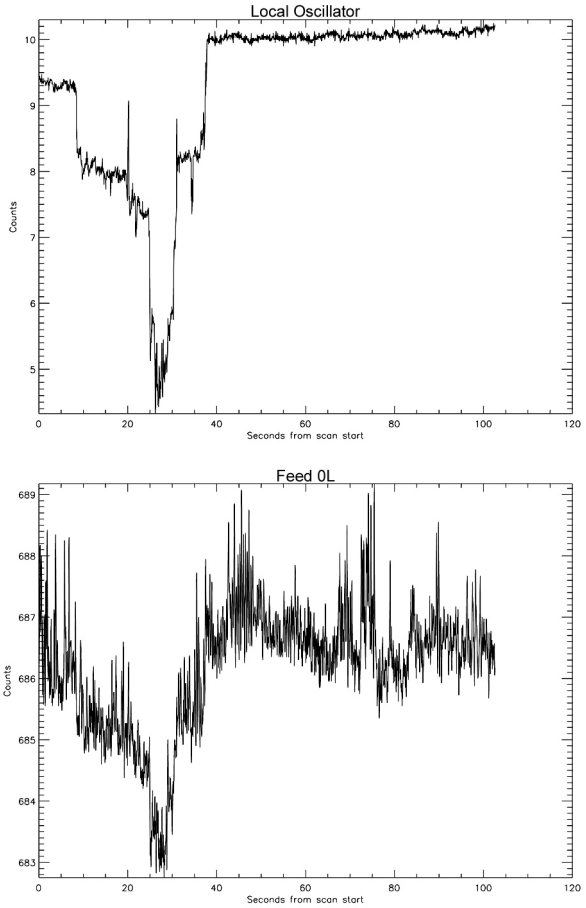


Figure 4.14 B – Top panel: output power of the second conversion LO (Miteq). Bottom panel: simultaneous acquisition performed through CH10 (Feed0 LCP).

*"Jiggling" signal*

Among all the features which were discovered in the acquired data, this deserves special consideration, as its incidence was extremely high – to the point of putting the chance to perform total power high-sensitivity observations at risk – and it was the most difficult to pinpoint and finally remove.

From the very beginning of the test observations, a significant fraction of the files was affected by sudden increases and decreases of the signal level. This "up and down" behaviour was later named "jiggling".

As Figure 4.15 shows, the peaks were not spike-like as they could seem at a quick inspection: the oscillations were traced by tens of samples (as usual the sampling interval was 40 ms, i.e.25 samples per second).

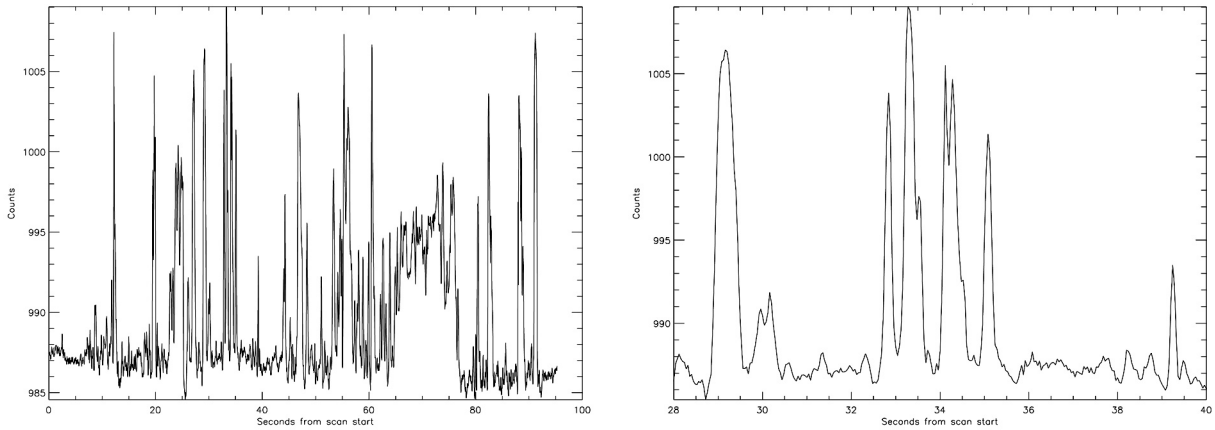


Figure 4.15 – A badly jiggling-affected file recorded on March 16th 2009. Left: the whole 96s subscan. Right: zoom on 12 seconds to show the shape of the signal level variation. Peaks have never shown to be equally spaced in time or to have the same duration (which is equivalent to width), but they also tended to seem quasi-periodic, as if induced by vibrations.

The jiggling peaks, reaching SNR values up to 100, have never shown to be truly regularly spaced in time, or to have the same duration, but they qualitatively seemed – during the inspection of the files – quasi-periodic, as if induced by some vibrations.

For this reason the first interpretation was in favour of a microphonic effect, possibly due to the vibrations caused by the fast and repetitive motions of the antenna during the recursive scans. To ascertain if this was a feasible explanation, several tests were performed varying the scanning speed (see §3.6) or even adding pauses between two consecutive subscans. This did not affect the jiggling occurrence. Indeed, the effect was observed even with the antenna pointing to a fixed position, or while it was stowed – i.e. parked in its rest position, pointing to the zenith.

During this first test session, the analysis of the large number of files was only visual, inspecting all the plots and then performing basic analysis on the data without any automatic “jiggling detection tool”.

Even if time consuming, this process was useful to analyse in detail the data behaviour and quality, and to keep track of the jiggling episodes. No correlation was found with either of these variables:

- *time* – no repetitive paths or preferred time intervals were found. Even the duration of the phenomenon inside the scans varied without an evident pattern;
- *antenna position* – the effect was present for any Azimuth or Elevation, even if in short time intervals it seemed to appear more frequently in the same azimuth range;
- *scan geometry and setup* – it was equally observed while performing horizontal or equatorial scans, in survey or calibration mode, and even in tracking mode;
- *weather conditions* – data was affected in all weather conditions, ranging from clear to rainy days. No correlation was evident with the ground-measured weather parameters which are recorded along with the data (temperature, pressure, relative humidity).

As the azimuth recursive scans technique was correctly working since the beginning, it was possible to produce the first maps. The mapmaking technique (described in Chapter 5 §2.6) is optimised for compact sources and removes the large scale structures from the subscans baselines. Nonetheless the jiggling effect was producing fairly fast oscillations in the signal level, not far from the spatial scales of the compact source, thus making impossible to clean it out.

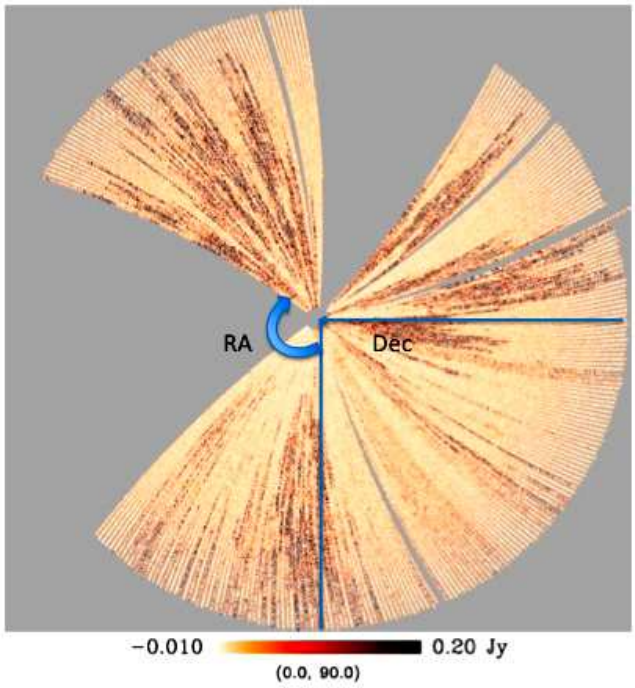


Figure 4.16 – Map of the polar cap obtained with 24 hours of observations (one sequence of subscans). Black-spotted stripes correspond to subscans affected by the "jiggling".

Figure 4.16 shows a map resulting from a single sequence of subscans, obtained along 24 hours of observations. Wide blank sectors correspond to data removed because of very bad weather, narrow gaps are due to the execution of calibration scans in the corresponding time intervals. Black-spotted stripes are the characteristic signature of

the jiggling effect, and completely mask any scientific information embedded in the data.

The threats posed by such instabilities to the scientific potential of the instrument seemed serious. The observing session ended without having found a solution to the problem.

## 4. TEST SESSION *II*: AUGUST-SEPTEMBER 2009

As the origin of the jiggling effect had not been identified, there were no certainties about which part of the system was responsible for it: telescope, receiver or backend.
For this reason, we thought of trying to separate the different parts of the chain, and carried out tests focusing on the backend only: it was used coupled to the 5 GHz receiver, which is located in the secondary focus like the MF and is an already tested device – though never employed with fast OTS scans. This way the summer period, which is unsuitable for high frequency observations, could be fruitfully exploited. The testing purposes were parallel to scientific goals, which are described in Chapter 5 together with the acquired data.
In the commissioning context, two elements highlighted during this session deserve to be stressed:

- the jiggling effect was not present, thus indicating that it was not a disturbance originating inside the backend;
- optical effects due to the antenna quadrupod were discovered, as the following section describes.

### 4.1. An intrusive signal

The 5 GHz observations were carried out exploiting the OTF strategy used for the K-band acquisitions, mapping the same region: the polar cap. The main setup parameters were coincident or similar to the 21 GHz scans: azimuth subscans were performed from 1° to 25°, at the constant elevation of 44.52°, and at a 15°/min speed. The 5 GHz receiver is a single beam with HPBW of 7.5 arcmin, which roughly corresponds to the overall size of the MF projection on the sky; this meant that the completion of the polar

cap area could take place in about the same time: the optimised coverage was obtained in 5 days (see Chapter 5, §2.2 for details).

Throughout these acquisitions, a strong signal (Figure 4.17) was detected in 4 distinct time intervals during each day. Table 4.3 lists, as an example, the intervals relative to August 9th.

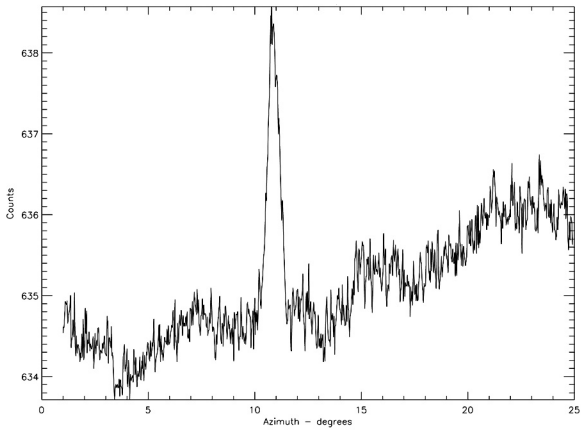


Figure 4.17 – An unknown signal detected in specific time intervals while mapping the usual polar cap at 5 GHz.

| UT interval | Duration | Time elapsed from the previous manifestation | Peak FWHM (measured as time) |
|---|---|---|---|
| 06:37 → 07:54 | 77’ | - | 1.14 s |
| 10:02 → 10:44 | 42’ | 126’ | 3.03 s |
| 12:35 → 13:15 | 40’ | 111’ | 2.19 s |
| 16:07 → 17:58 | 111’ | 172’ | 0.96 s |

Table 4.3 – summary of the signal manifestations for August 9th, 2009.

While the antenna was performing the back and forth subscans in the specified azimuth range, the signal changed position one subscan after the other, appearing like a drifting feature (Figure 4.18). This was an indication that its source was moving, but it could not be a celestial source directly pointed by the antenna and observed along the line of sight or captured via a secondary lobe, as the signal was present for long intervals (up to about 2 hours), during which the sky observed by the antenna changed completely. No large structures like the Galactic plane were crossed by the subscans in those time intervals.

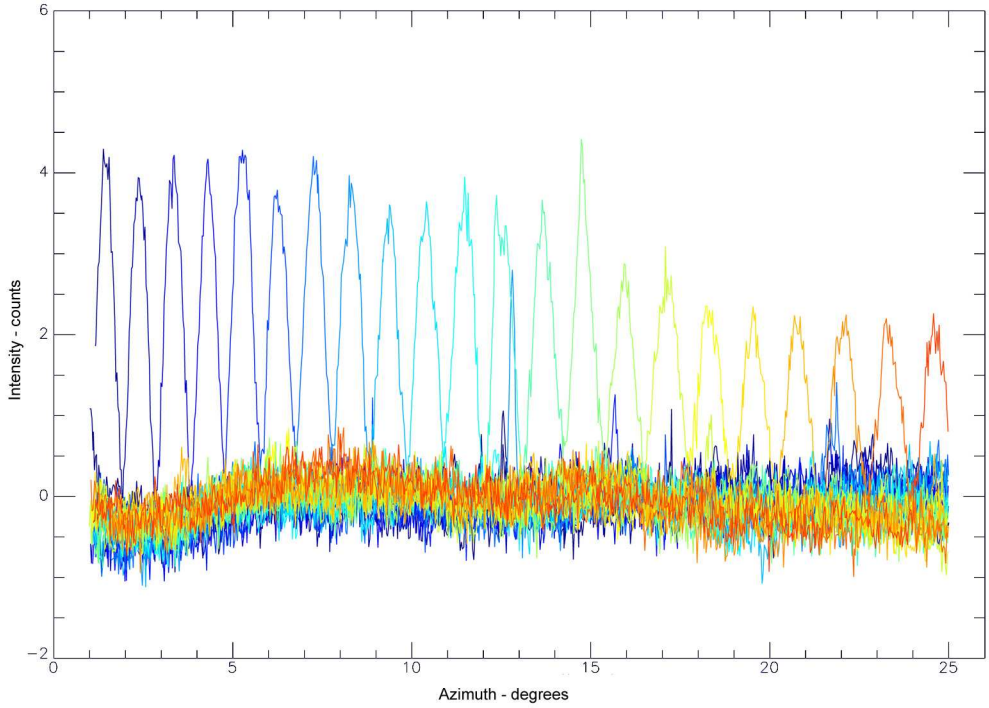


Figure 4.19 – Overplot of the different subscans achieved from 16:07 UT (blue) to 17:58 UT (red) on August 9th. Each subscan has undergone a linear baseline fit and removal.

Since the signal was observed only during daytime, the Sun was suspected to be implicated, even if it was not clear in which way its radiation was collected by the antenna. For this reason, the relative position of the Sun with respect to the antenna was checked for all the time intervals where the signal had appeared.

Figure 4.19 displays the Sun's diurnal arc for August 9th 2009 with respect to the antenna position, showing also the path of the recursive azimuth scans.

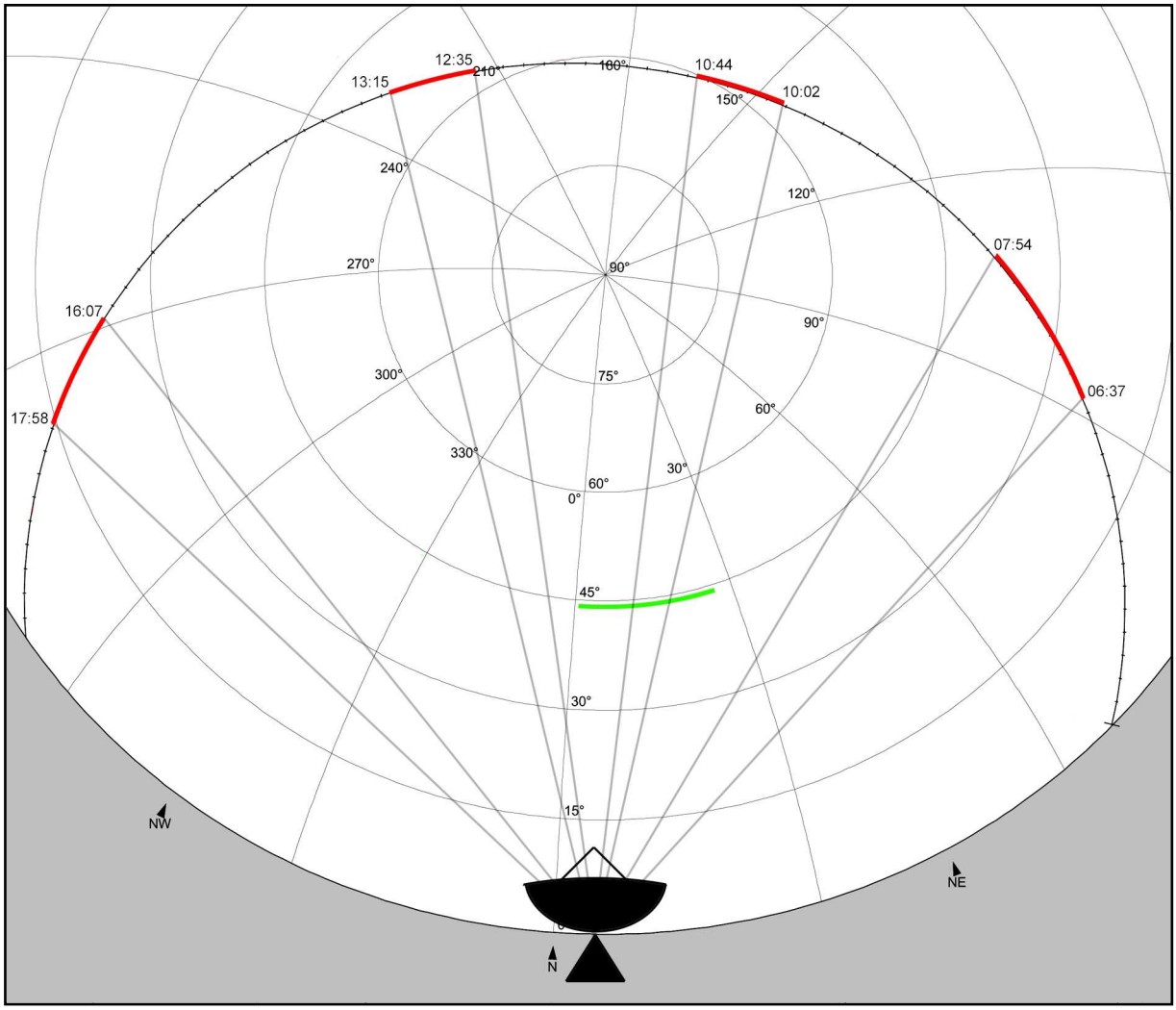


Figure 4.19 – The Sun diurnal arc for August 9th, 2009, against the horizontal frame grid. The sections in red correspond to the time intervals where the unknown signal was observed. The green stripe is the path run back and forth by the recursive scans.

The red sections correspond to the path covered by the Sun in the time intervals reported in Table 4.3. It is clear, though the scheme is only a rough approximation – as it depicts the antenna in a "frozen" situation – that the four sections were related to the positions the antenna was assuming while performing the scans.

The Sun distance from the pointed positions, computed when the signal was present in the middle of the subscan, ranged from 73° to 76°. At this distance from the main lobe, the gain drops by 50 dB. As the 5 GHz brightness temperature of the quiet Sun is ~ 17600 K (Zirin et al., 1991), the expected antenna temperature of the signal was ~ 175 mK. Once calibrated, the measured signal had an average amplitude of ~170 mK.

The observed intensity was therefore coincident with the expected one, yet it was necessary to explain why the signal was seen in the mentioned intervals only, in which the angular distance of the Sun from the antenna pointing direction was just slightly different from previous or following instants. In other words, why were there preferred times/directions for the phenomenon to happen?

A possible explanation can be found again considering Figure 4.19: the way in which the intervals are spaced matches with the displacement of the antenna quadrupod: the four "legs" form a cross which is rotated by 45° with respect to the North-South direction. The tentative interpretation of the phenomenon is then the following: in the given time ranges the quadrupod legs were positioned compared to the Sun so as to cause optical effects collimating its radiation into the feed.

On September 28$^{th}$ 2009 a simple test was carried out to check this hypothesis: the antenna was commanded to perform azimuth scans at the usual elevation of 44.52°, around the time when the Sun was reaching the same elevation it had on August 9$^{th}$ when the signal was present. The azimuth range in which to perform the scans had been computed in order to reproduce the same Sun-antenna geometry.

Table 4.4 lists the details about the Sun and antenna positions.

| | **August 9$^{th}$** | **September 28$^{th}$** |
|---|---|---|
| UT | 17:02 | 15:35 |
| Sun elevation | 13.9° | 13.9° |
| Sun azimuth | 278.5° | 252.5° |
| Antenna elevation | 44.52° | 44.52° |
| Antenna azimuth | 14.0° | 348° |

Table 4.4 – Sun position and antenna pointing for the central subscan in the 16-18 UT interval on August 9$^{th}$, from which the antenna position to be used on September 28$^{th}$ was extrapolated. The constraint was to reproduce the same Sun-antenna configuration, in the moment in which the Sun was at the same elevation.

The tests were then performed on September 28$^{th}$ by means of scans in the azimuth range [334°,358°], from 13:40 UT to 17:20 UT. The signal appeared from 14:40 UT to 16:14 UT (Figure 4.20), a longer interval than the original one, as the setting Sun was decreasing its elevation at a lower rate compared to September. This strongly supported our hypothesis. During the tests it was possible to observe that one leg of the quadrupod was casting its shadow on the dish passing through its centre – where the secondary

focus cabin lies – in the same time interval in which the signal was present, this being a further indication that the quadrupod legs alignments with the Sun originate this phenomenon.

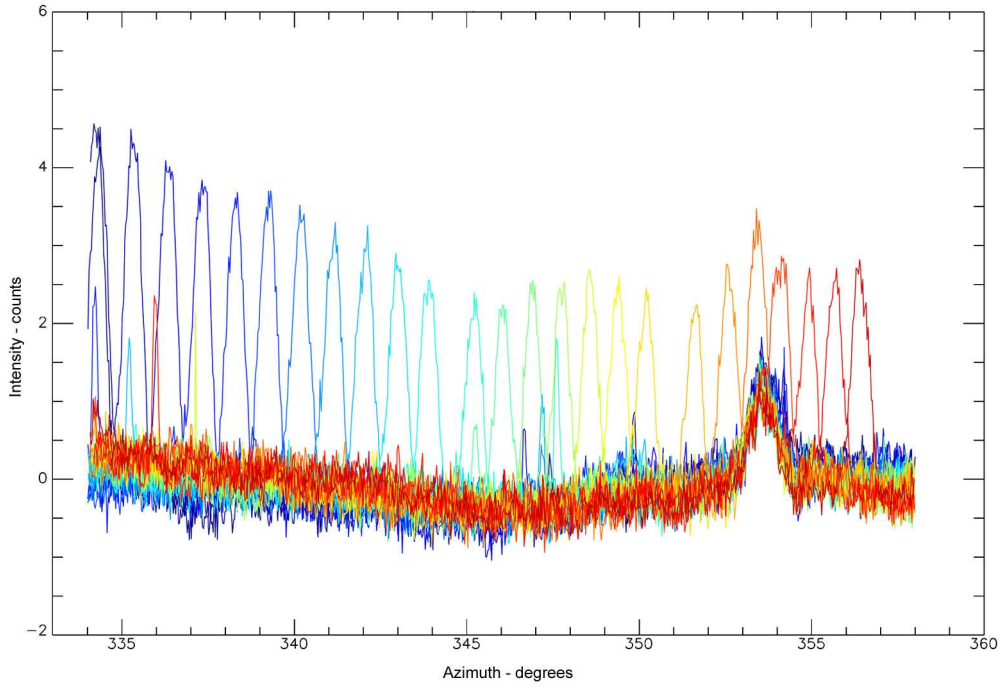


Figure 4.20 – The signal reappears in the expected time interval for the same Sun-antenna relative position. Notice the RFI for azimuth = 353.5°.

# 5. TEST SESSION *III*: DECEMBER 2009-MARCH 2010

Because of the still unfixed issues, more time was necessary to complete the commissioning. Observations at 21 GHz performed with the usual setup (see §3.5) were then carried out for the following purposes:

- to check if the modifications applied to the hardware system to solve some of the encountered problems (§3.7) had been effective;
- to pin down the origin of the "jiggling signal" phenomenon;
- to complete, once the instabilities were mitigated, the polar cap survey – which is the pilot survey for the KNoWS project – in order to confirm the scientific capabilities of the overall MF system.

It must be stressed that the whole session was plagued by an exceptional incidence of bad weather days. However, this did not affect the commissioning activities, as the necessary tests on the hardware components could be successfully carried out regardless of the weather conditions.

None of the instabilities or peculiar features registered during the first tests was encountered in this session, with the only exception of the jiggling, which was still present in a very conspicuous fraction of the acquisitions.

### 5.1. Focus on the "jiggling signal" effect

To try to identify the elusive origin of this phenomenon, different tests were performed. First of all, more quantitative statistics were obtained on its manifestation, carefully inspecting a sequence of 474 files achieved on December 26$^{th}$ 2009 between 00:00 UT and 14:30 UT. This work was carried out in cooperation with Marcella Massardi (INAF-OAPD). The number of affected files was determined:

- 22.2% of the acquisitions were affected for more than 25% of the subscan duration;
- 8.9% of the acquisitions were affected for more than 50% of the subscan duration.

The exact time intervals in which the jiggling was present were recorded, and a simple plot was produced to highlight a possible periodicity (Figure 4.21).

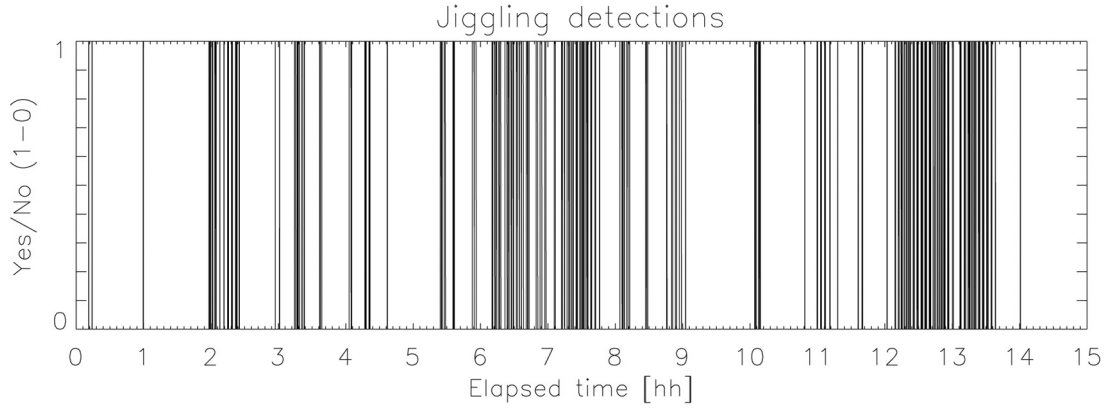


Figure 4.21 – Plot showing the presence of the signal (y=1) during the acquisitions performed on Dec. 26$^{th}$ 2009, from 00:00 UT to 14:30 UT. No periodicity is evident.

The analysis did not reveal any periodicity.

A correlation with the azimuth ranges in which the signal was observed was then investigated, but no relation was found even in this case (Figure 4.22).

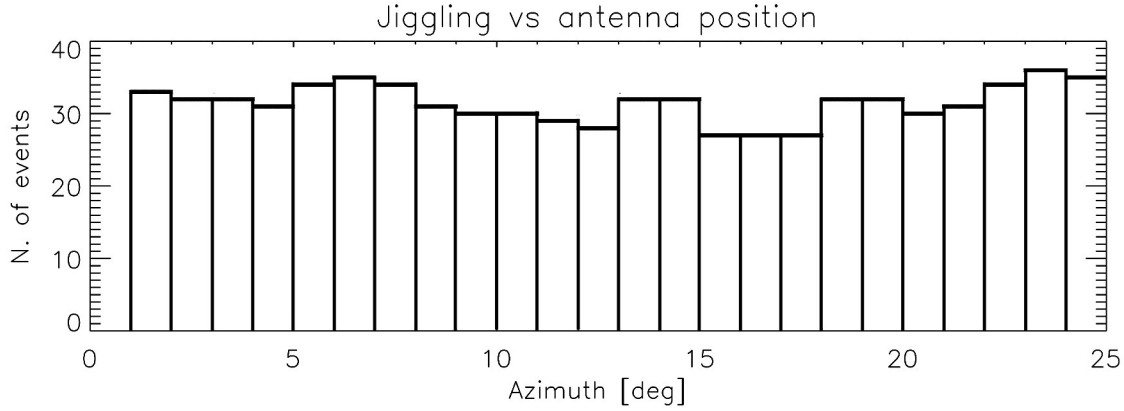


Figure 4.22 – Number of detections of the jiggling effect against the azimuth position of the antenna.

However, analysing more data taken on December 27$^{th}$ (84 files achieved from 00:00 UT to 02:30 UT) a possible relation with the azimuth position of the antenna was noticed (Figure 4.23) for this short time interval.

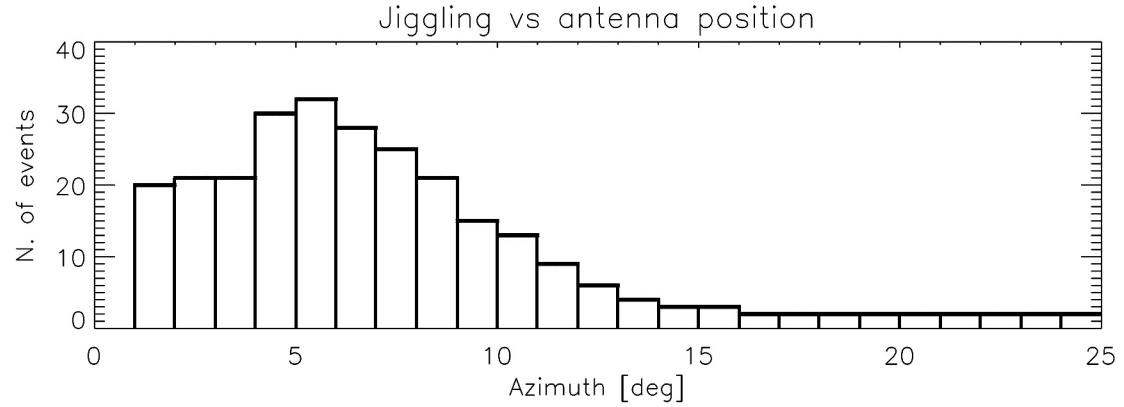


Figure 4.23 – In the 00:00-02:30 UT interval on Dec.27$^{th}$ the phenomenon seems to take place for preferred azimuth ranges.

This evidence suggested that the origin of the phenomenon could be external to the antenna, even if no correlation with the azimuth position had been previously ascertained.

To finally assess if the source of the problem was external to the telescope or was to be identified within the instrument, several experiments – involving the use of a hot load – were arranged.
The tests took place on January $4^{th}$ – $7^{th}$. This was the configuration of the hardware setup:

- Feed2 (channels Ch0 and Ch1) was covered with the hot load, so as to be completely blinded from the "outer world";
- Ch2 was connected to a noise source, to see if this internally generated signal was affected by the phenomenon;
- Ch4 was exploited to measure the current intensity of the alimentation that supplies all the chains, in search for possible instabilities related to the jiggling;
- Ch9 was used to monitor the first conversion Local Oscillator;
- Ch5 was connected to a spectrum analyser, to better analyse any possible radio frequency entering the system.

The observations were carried out with the usual scanning schedules, but also acquiring data with the antenna stopped in the stow position.
In all the cases, when the jiggling was present, it was absent in the hot load channels and could be seen only in the channels connected to the feeds actually observing the sky (Figure 4.24). No RFI was obviously detected by the spectrum analyser, however, and no instabilities due to the internal instrumentations were detected concurrently to the phenomenon.

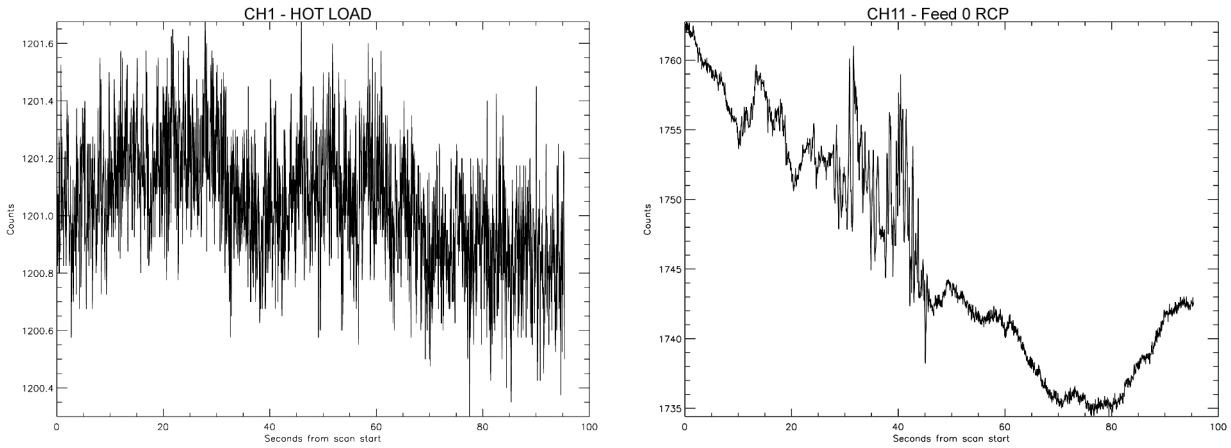


Figure 4.24 – Comparison between the signal observed through the hot-load covered feed (Feed2 RCP, Ch1, on the left) and the signal revealed by one feed observing the sky (Feed0 RCP, Ch11, on the right). Notice the very expanded y-scale for the hot load plot: the signal is flat. The feed observing the sky, instead, records the non homogeneous atmospheric opacity (bumpy baseline) and about 20 seconds of jiggling signal.

A further test was carried out in order to cancel any doubt about the possibility of a self-interference generated within the telescope: data was achieved switching off any unnecessary device inside the secondary focus cabin and in the primary focus cabin, and the jiggling effect was observed even so.

The inevitable conclusion was that the jiggling-shaped noise was originated by a subtle external radio frequency signal detected by the receiver.

The technicians involved in the commissioning activities, in the light of all the discarded theories, proposed to check if the phenomenon could be related to the plastic cover placed over the secondary focus cabin. The tarp is transparent to the incoming radiation, but a first hypothesis focused on the possibility that the humidity on top of it might affect the data, when the wind induced vibrations in the plastic cover. Another explanation, at present considered more feasible, involved the instauration of multiple reflections of the incoming signal due to the plastic cover vibrations, which remain the key point of the model.

This would explain the semi-regular behaviour of the jiggling peaks, which follow the quasi-periodic oscillations of the tarp, and the short-term relation between the manifestation of the jiggling and the antenna position: it is the interaction between the antenna orientation and the wind direction to originate the phenomenon. In addition,

since the wind direction is not one of the weather parameters to be recorded in the FITS files, it is explained why it had not been possible to discover a correlation between weather and jiggling earlier on.

To test this theory, an *ad hoc* polystyrene structure was arranged and mounted on the cabin, in order to tighten the plastic cover and suppress its vibrations

All the following observations turned out to be completely jiggling-free (Figure 4.25). With this ultimate effort, all the major sources of instabilities were removed, and the MF system could be used to finally acquire data exploiting its full potential.

Unfortunately, bad weather conditions have been plaguing ~ 50% of the observing runs available (data acquisitions are still going on at the time this thesis is being completed; the mapmaking and data analysis will follow soon afterwards).

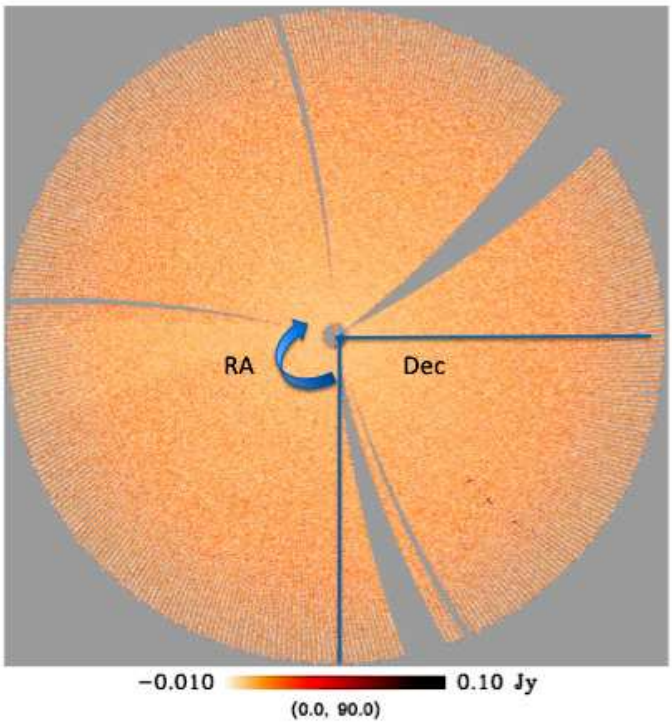


Figure 4.25 – 24h map which shows no trace of the jiggling.

As a final assessment of these commissioning sessions, we can state that the new observing system has proven to be reliable and stable, guaranteeing the possibility to fully exploit the MF system capabilities. The tests devoted to disentangle the various problems detected in the data allowed us to verify the hardware system functionality and to point out some features that are relevant for high-sensitivity continuum observations at high frequency. In addition, these findings will be of valuable help for the SRT.

# CHAPTER 5

# THE 6MS CATALOGUE: THE POLAR CAP AT 5GHZ

*See first, think later, then test. But always see first.*
*Otherwise you will only see what you were expecting.*
Douglas Adams

## 1. OVERVIEW

Observations at 5 GHz were performed, as introduced in Chapter 4 section §4, to test the new analogue backend independently of the MF receiver. This triggered the idea to lead the tests acquiring valuable and original scientific data. This chapter illustrates the scientific goals and the observational setup of the project, and discusses the preliminary results we have obtained.

## 2. 5 GHZ OBSERVATIONS

### 2.1. Scientific rationale of the 5 GHz survey

The experiment consisted in observing the same polar cap area already mapped at 21 GHz with the MF receiver. As mentioned in Chapter 4 §4, the identical setup (with the exception of the receiver) made this test capable to distinguish whether the instabilities were arising from the RF system (receiver) or the backend. In fact, all the elements relative to the antenna mechanics and motion (whose contribution to the observed instabilities was still partly not understood), and to the backend were identical.

The choice of this specific area was also driven by the aim to obtain valuable and original scientific data: mapping the polar cap would have led to the completion of the all-sky coverage at 5 GHz, as the previously available surveys – the Parkes-MIT-NRAO (PMN) and Green Bank 6cm (GB6) – globally cover the Declination range [-90°,+75°] (Gregory et al., 1994; Gregory et al., 1996).

The southern Declination limit of our area (73.2°) enabled a sizable overlap with the GB6 catalogue – Declination range [0°,+75°] – which was useful to cross check all our procedures to get to the source catalogue, from the map-making technique to the source extraction algorithm. Since the GB6 catalogue dates back to 1996, the flux densities

measured in our map could also be used to study the variability of the GB6 sources in the overlap area.

### 2.2. Observing setup

The 5 GHz receiver is a new single-feed system installed on the Medicina antenna in recent years. It is located in the secondary focus cabin, right next to the K-band MF receiver. Table 5.1 lists its main characteristics.

| | |
|---|---|
| **Type** | Cooled |
| **Channels** | 2 |
| **Polarisations** | LHCP – RHCP |
| **Noise temperature** | 12-14 K |
| **Central frequency** | 5.05 GHz |
| **RF band** | 4.30 – 5.80 GHz |
| **RF filter bandwidth** | 1500 MHz |
| **HPBW** | 7.5 arcmin |

Table 5.1 – Main characteristics of the 5 GHz receiver.

The receiver was connected to two channels of the new analogue backend (Ch0 and Ch1). Since this frequency band is highly polluted by RFI, it was not possible to use the entire bandwidth allowed by both receiver and backend. A spectroscopic survey of the azimuth range planned to be observed was carried out by the RFI-mitigation staff, who identified the sub-band 5.00 – 5.25 GHz as the one showing the best RFI conditions. This 250 MHz-wide band was then set for the observations, by means of proper IF filters.

The mapping strategy was the same employed for the K-band activities. Fast OTF scans were performed at the constant elevation of 44.52°, in the azimuth range [1°, 25°]. This receiver has a HPBW of 7.5 arcmin, which almost corresponds to the sky footprint of the entire set of the seven MF beams. As a consequence, the recursive scan setup parameters (Table 5.2) were mostly similar to those used for the 21 GHz observations, though the map optimisation led to 5 days of observing time rather than the 4 days required by the K-band case. A longer sampling interval (120 ms) was sufficient to map

one beamsize with 5.8 samples per subscan, and was still short enough to ensure system stability and low noise.

| | |
|---|---|
| Minimum Azimuth | 1.0° |
| Maximum Azimuth | 25.0° |
| Elevation | 44.52° |
| Scan azimuth speed | 15 °/min |
| Sampling interval | 120 ms |
| ΔLST – 1 step interleave (corresponding to 3.34182 arcmin) | 43.746835 s |
| Gap (ramp-up + ramp-down for 1 scan) | 13.068469 s |
| $t_{scan}$ (cruise only) | 96.000000 s |
| $t_{bf}$ (back-and-forth scan including gaps) | 218.13694 s |
| $N_{bf}$ (number of back-and-forth scans per full sequence) | 395 |
| $N_{zz}$ (number of sequences – i.e. days – to fill the section) | 5 |

Table 5.2 – Setup parameters for the azimuth recursive scans employed in 5GHz observations.

### 2.3. Expected sensitivity

The above setup implies a final integration of 2.8 s for an expected sensitivity of:

$$rms = \frac{k\ Tsys}{\sqrt{B\,t}} = 0.7\,\mathrm{mK} = 4.4\,\mathrm{mJy}$$

where k = $1/\sqrt{2}$, $T_{sys}$ = 26 K (for El=45°), B = 250 MHz, t = 2.8 s, and antenna gain at 5 GHz equal to 0.16 K/Jy.

The detection limit for sources at 5σ is then ~ 21 mJy. This value is comparable to the GB6 catalogue, which lists discrete sources with angular sizes < 10.5 arcmin and flux densities above S ~ 18 mJy.

### 2.4. General system response

The 5 GHz observations were carried out on August 6-10, 2009. A problem with the vacuum pump of the cooling system was discovered when many of the acquisitions had already been performed, and could not be fixed within the available session. Since the receiver was not properly cooled and the observed $T_{sys}$ was about 190 K during the entire run, the actual sensitivity of the final map worsened to a value of 32 mJy rms, such allowing detecting sources down to ~ 120 mJy at 4σ.

This limited the comparison to the GB6 catalogue bright sources, which however was sufficient to assess the correctness of our procedure as there are 130 GB6 sources in the Declination range [+72.3°,+75°] having flux densities brighter than 120 mJy.
Apart from this unexpected issue, the system worked correctly both on the hardware side and on the software side. As introduced in Chapter 4 §4.1, the only unwanted peculiar feature detected was the solar radiation pickup because of struts reflection in specific antenna-Sun configurations.

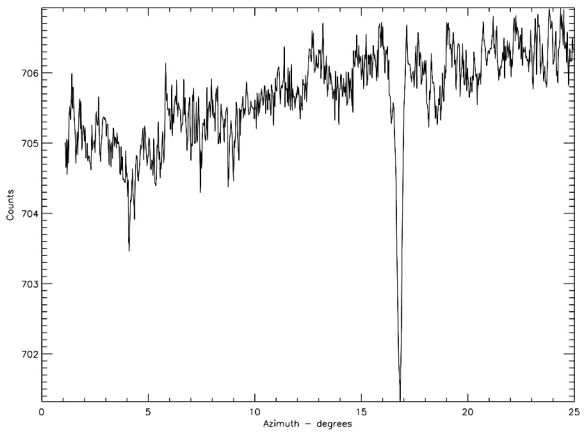


Figure 5.1 – A single subscan taken on Aug.10th. The intensity drop between 16° and 17° of azimuth is due to a strong RFI saturating the signal.

The RFI presence was mostly marginal, however a very strong signal regularly showed up during several time intervals – mostly on working days – and caused the signal to saturate and assume fake values below the average noise when the antenna crossed the 16.5° azimuth position, as Figure 5.1 illustrates.

In certain time intervals the signal showed some level instabilities (Figure 5.2), which at the time were not associated to the "jiggling" problem as the level oscillations were not comparable either in terms of duration or behaviour. The origin of this "longer ripple" is more likely to be related to the presence of strong RFI.

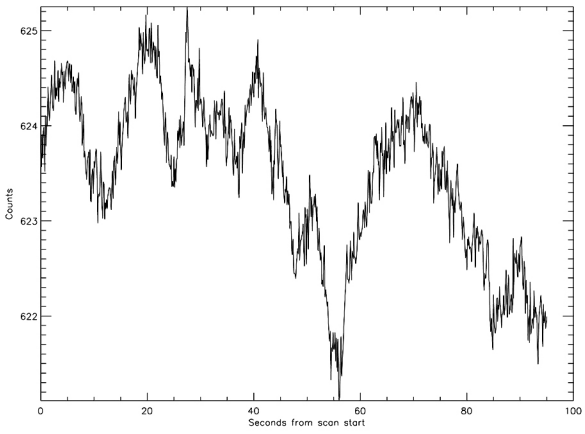


Figure 5.2 – A single subscan taken on Aug.11th. Here the signal shows oscillations, but they do not correspond to the behaviour of the "jiggling" detected at 21 GHz.

### 2.5. Data calibration

The calibration procedure involved the observation of flux calibrators at least 4 times along the 24 hours of each sequence. Calibrators were observed when they were at the same elevation of the survey scans (around 45°). A Gaussian fit on the OTF scans performed across the calibrators allowed the estimation of the calibration conversion factor. More refined procedures were not necessary, as the atmospheric contribution at this frequency is negligible even with overcast weather.

The flux calibration was performed within the SDFITS file generation procedure with one of the software tools developed, described in Chapter 3 §5.2.

### 2.6. Map-making

The map-making software was provided by E. Carretti and is based on that developed for the project S-PASS (Carretti et al. 2010, in prep.), but optimised for compact sources.

First, a high pass filter is applied to each scan to remove the large scale emission contribution. That way, the sky diffuse emission is removed making the job of source finding algorithms easier. In addition, this also cleans the long-term signal variations due to system instabilities like gain fluctuations, 1/f noise, and, for K-band observations, the atmospheric contribution.

A trade–off has been made ensuring that the signal on the beam-size scale was preserved leaving unaffected the flux from compact sources.

After that, the data from all the scans are binned in pixels the size of half a beamwidth to match Nyquist sampling criteria. The HEALPix (Hierarchical Equal Area isoLatitude Pixelization[1]) scheme is adopted. This has the big benefit to use equal area and isolatitude pixels, and is particularly suited for all-sky maps or maps around polar caps, where it is far superior to other schemes.

The HEALPix visualisation tool to generate gnomonic projection maps has been used for all the map images shown in this thesis.

[1] http://healpix.jpl.nasa.gov/index.shtml

Figures 5.3-5.5 report maps centred at the North Celestial Pole for the five days of the observing run, each corresponding to a single 24-h entire sequence of azimuth scans.

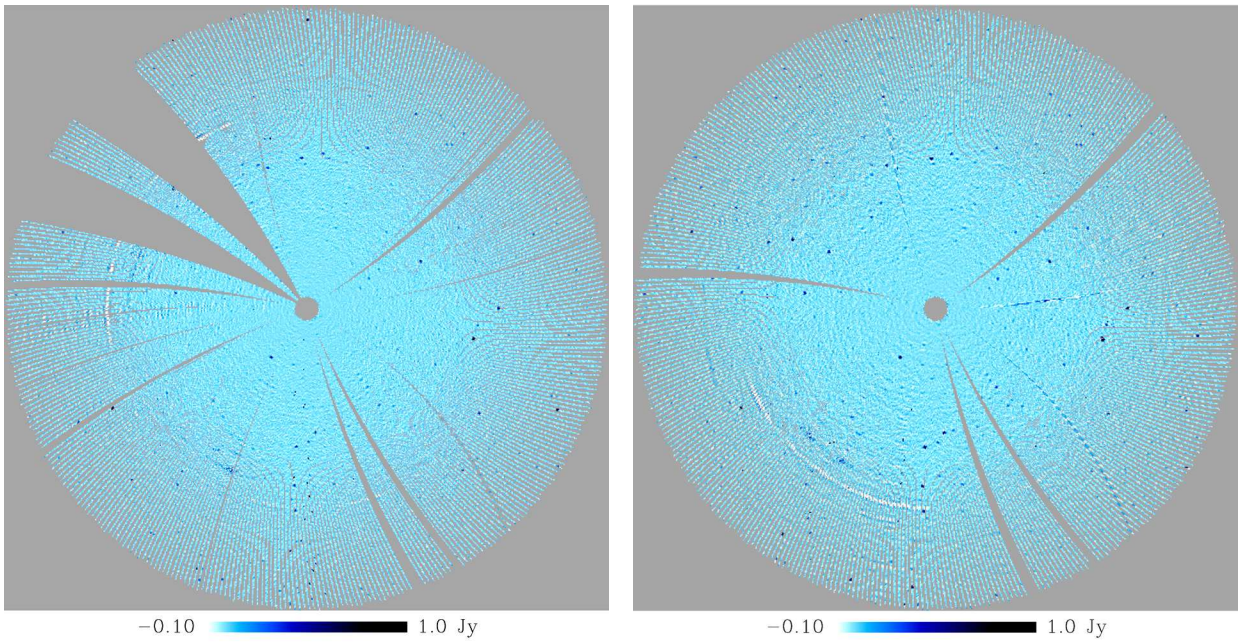


Figure 5.3 – Left: sequence 0, right: sequence 1. Gaps are due to the observation of flux calibrators.

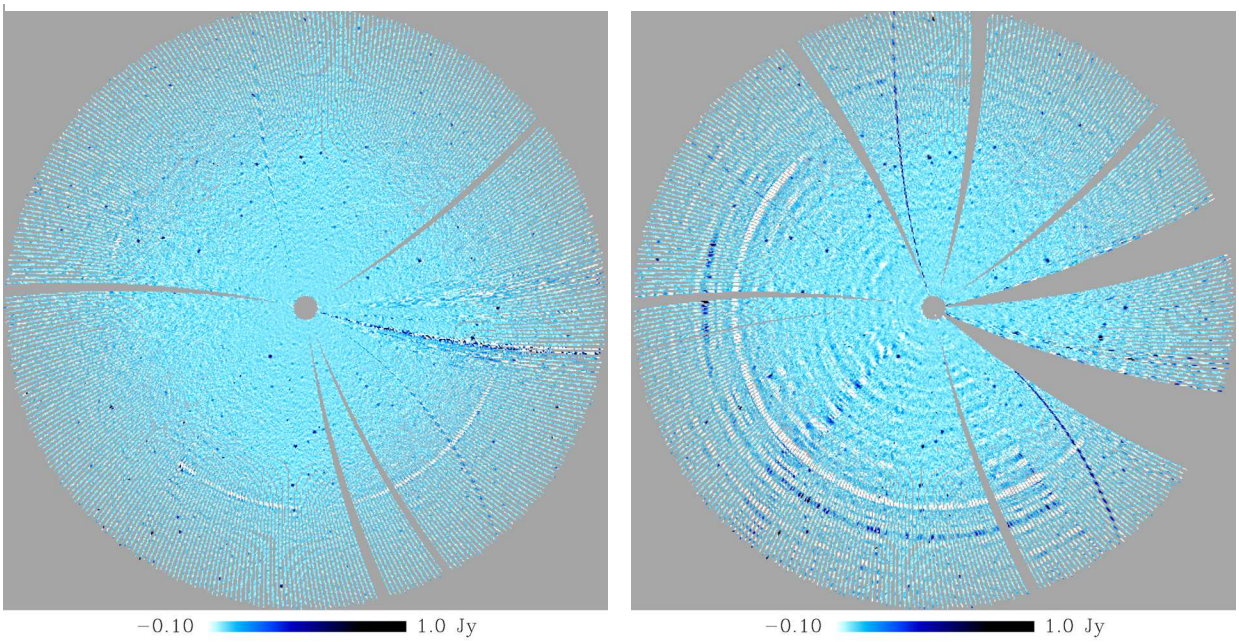


Figure 5.4 – Left: sequence 2, right: sequence 3. Gaps are due to the observation of flux calibrators. Sequence 3 faced more interruptions and suffered from more evident ripples in the signal (white concentric stripes correspond to the signal going under the noise average level for the same azimuth values, during the execution of the single subscans)

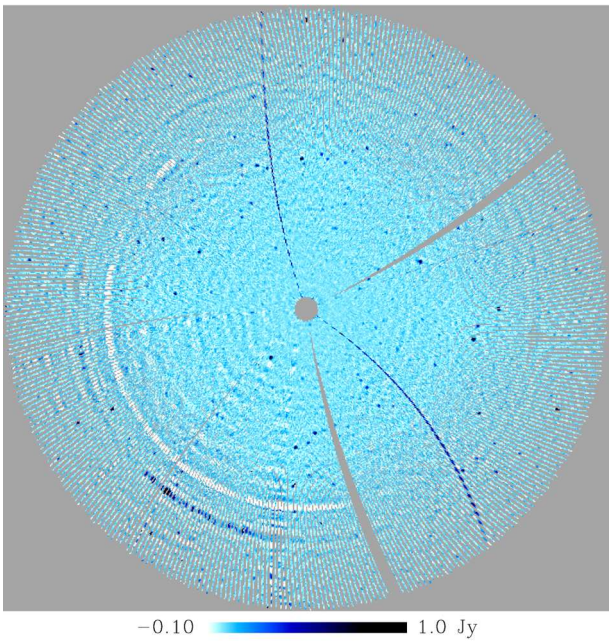


Left
Figure 5.5 – Sequence 4 data. The blue stripes, which are present in all the sequences but here are more evident, correspond to the signal coming from the Sun.

Below
Figure 5.6 – Zoomed area to highlight the map features.

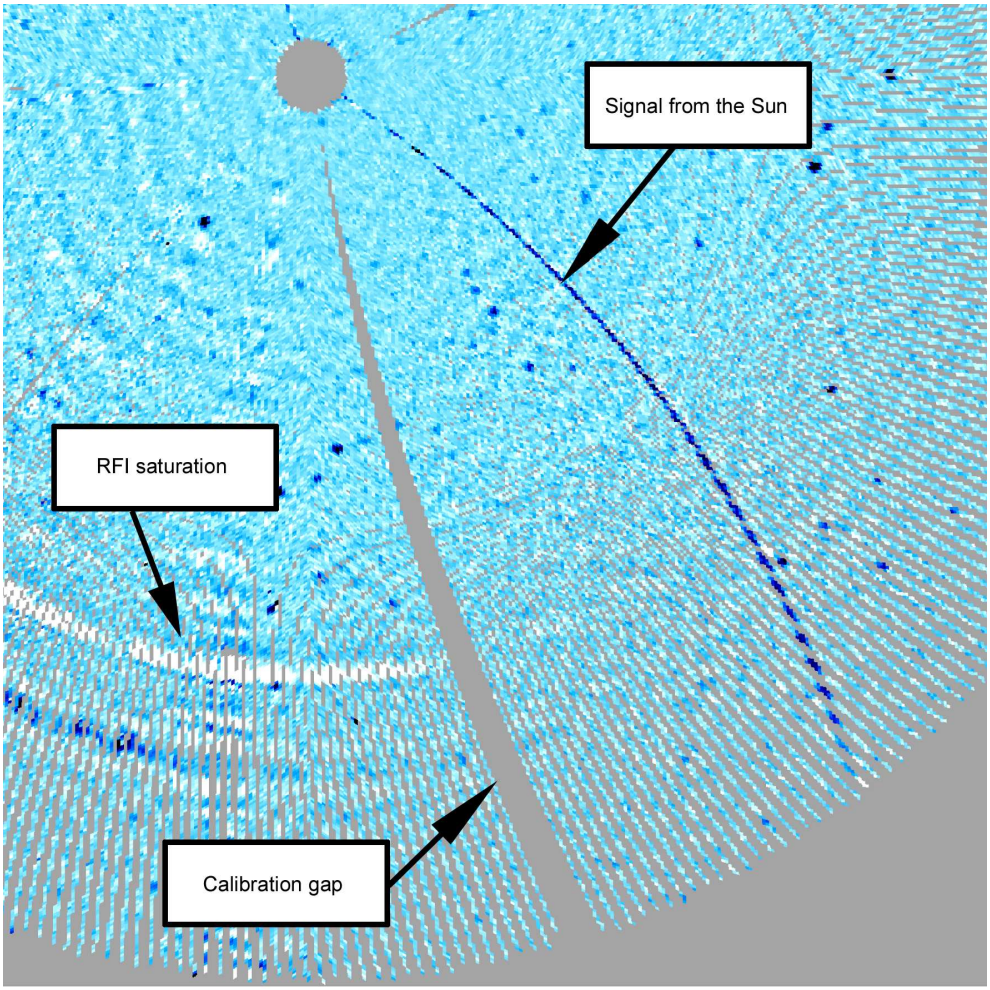

Figure 5.6 shows a zoomed section of the Sequence 4 map. It can be noticed how the subscans realise the map since their sky paths are evident at the outer edge, where all the sequences are needed to fill in the gaps (while the map is already fully sampled in the central region).

The final map, obtained binning all the 5 sequences, is reported in Figure 5.7, where the presence of several compact sources is noticeable.

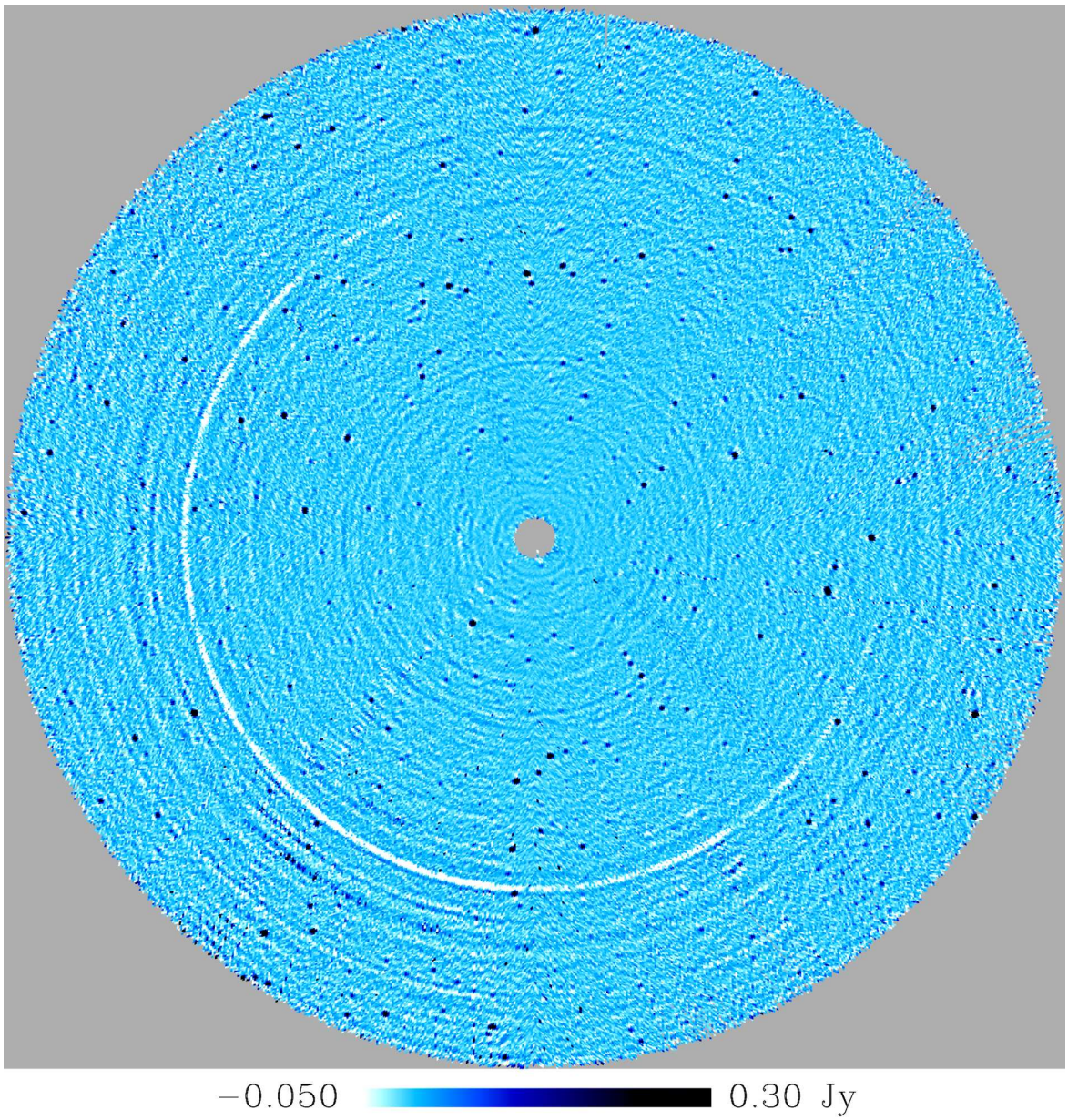


Figure 5.7 – The complete map obtained integrating all the 5 sequences of subscans. The white circle corresponding to the RFI-induced saturation could not be removed as it was a steady structure, present along most of the days of acquisitions. Traces from the Sun radiation are still visible – it can be noticed how they change position one day after the other.

### 2.7. Source extraction strategy

The software for the source extraction was kindly provided by Marcos Lòpez Caniego (Observational Cosmology and Instrumentation Group of the "Instituto de Fisica de Cantabria", Spain) under a collaboration between his and our group.

This code was developed in the light of the source extraction needs for maps obtained with the *Planck* satellite observations; it has demonstrated its reliability on WMAP 5-years maps (Massardi et al., 2009), but it had never been applied to low frequency single dish data.

As described in Massardi et al. (2009) , the software accepts FITS images as input, with data arrays formatted using the HEALPix scheme. It uses a filter called MHW2, which is the second member of the Mexican Hat Wavelet filter family (Gonz´alez-Nuevo et al. 2006). It analytically applies two times the Laplacian operator on the 2D Gaussian function. On the local scale, it simultaneously removes the large scale variations, for example the ones originated in the diffuse Galactic foregrounds, and the small scale noise.

It is possible to optimise the scale at which MHW2 operates in order to maximise the SNR of the sources. This is performed numerically, optimising the performance of the code for any specific patch of a globally larger map. The optimal scale is approximately equal to the HPBW±15%, reaching a variation up to a factor of 2 only for regions which are highly crowded. A comparison of the shapes in the Fourier domain of some matched filters with the corresponding MHW2 at the optimal scale can be found in Lopez-Caniego et al. (2006).

After filtering, in the simple blind approach the position of the maxima are identified, and the fluxes are then estimated at those positions. The search for sources, in this case, takes place over the whole map, identifying any maximum above a given SNR.

The code can also work in non-blind mode: providing a list of positions, patches of given extension are defined in order to be centred on the listed positions, then the SNR is measured.

A third approach, called "iterative blind", can be exploited. It works in two main phases. First, a blind detection is performed to identify the sources positions all over the map. Then, for every source a specific patch, centred on it, is produced, and a new estimation of the SNR is performed.

The end-to-end code provided for this work reads in an input parameter file containing the specific characteristics of the maps to be studied, reads in the input map in FITS format, extracts the patches to be analyzed using the tangential plane projection approximation, finds for each patch the optimal scale of the wavelet, filters each of them with the MHW2 code, produces a list of detections above a given SNR, converts the positions of the detected objects from the tangent plane to the sphere and, finally, combines the detections into a single output file.

In the blind approach, the user fills the input parameter file in order to command how the needed patches have to be produced. For our relatively small map, the code divides and projects the sky into a sufficient number of square patches such that the area of the original map is not only fully covered, but also there is a sufficient amount of overlap among the patches to allow cuts of the borders of the image. This is of critical importance in the regions at the boundary of the map, since blank pixels create problems in the determination of the filter optimal scale, and in the following estimation of the source flux. The size of the patches in the sky, the pixel size and the amount of overlap among patches are specified in the parameter file.

Once the patches have been determined, the code loops over each of them, finding the optimal scale, filtering the maps with the MHW2 at such optimal scale and detecting objects with SNR > 3. For each patch a temporary catalogue is obtained, and for each object, the flux at the position of the corresponding peak is estimated. Finally, the temporary catalogues are combined into a final one, removing duplications (in the case of multiple detections of the same source the one with the brightest flux is selected, as it normally corresponds to the most accurate position).

The rms of the map is obtained via a three step process. First, in order to avoid border effects after filtering, a 15 pixel border around the maps is flagged. Second, all the maxima in the image are identified and a histogram of their values is obtained. Then, the 5 per cent of the brightest maxima are masked, flagging the pixels within a 2 FWHM radius from the position of the maxima. Finally, the rms of the map is calculated excluding the flagged pixels.

In the non-blind approach, instead, the patches to be analyzed are centred on a given list of positions. The source position is known in advance, so the aim of the program is to

characterise noise rms level around it. The algorithm is the same as for the blind approach, with the following differences:

- we have an additional input file, containing the list of the coordinates of the sources;
- we search for maxima in a circle around the patch centre, within 1 FWHM radius;
- the rms fluctuation level is computed focusing on a corona around the patch centre, having inner radius of 1 FWHM and outer radius of 3 FWHM.

In practice, the amplitude of the central maximum (if any) gives an estimate of the source flux, the operations to compute the rms noise (flagging of pixels at the border, the search of maxima, and the flagging of the 5 per cent brightest) are performed only to the corona. In this way, a more accurate estimate of the noise in the vicinity of the object of interest can be achieved, avoiding the contamination by other bright nearby objects.

## 3. ON THE WAY TO THE 6MS CATALOGUE

We have chosen the iterative blind approach for the source extraction.

The input parameters for the initial blind detection were set to obtain flat projected patches of 7.3◦×7.3◦, each containing 256×256 pixels. The pixel area was 1.7′×1.7′, corresponding to the HEALPix resolution parameter Nside = 2048. The imposed overlap between patches was equal to 1.5°. This way the program extracted 61 flat patches which covered the whole map.

The combined catalogue produced by the program listed 509 detections for SNR>3σ, whose positions were then used to produce the same number of patches – centred on the detections and having dimensions 1.83°x1.83° to repeat the flux measurements on the original map obtained with the optimised resolution of 3.4’ (Nside=1024).

The resulting positions and flux density measurements are listed in Appendix B. This set represents the first stage of the 6-cm Medicina Survey catalogue (6MS ). Follow up will be conducted both to check for spurious detections and perform more accurate flux measurements.

### 3.1. Preliminary analysis of the detections

A first set of analysis and comparisons was carried out using the IDL software tools produced by Marcella Massardi. The detection list was correlated with the GB6 catalogue in the overlap Declination range [+72.3°,+75.0°] where we found 88 sources. We also compared our list to the NVSS catalogue at 1.4 GHz (Condon et al., 1998) in our entire area (Dec = [+72.3°,+89.0°]).

*Position*

The comparison with the GB6 catalogue led to 88 matches, which were found using a searching radius of 3.18 arcmin (corresponding to the Gaussian beam σ). The same procedure carried out against the NVSS catalogue identified 334 counterparts; in 115 cases there was a multiple matching and the brightest counterpart was chosen. Figure 5.8 illustrates the measured position errors.

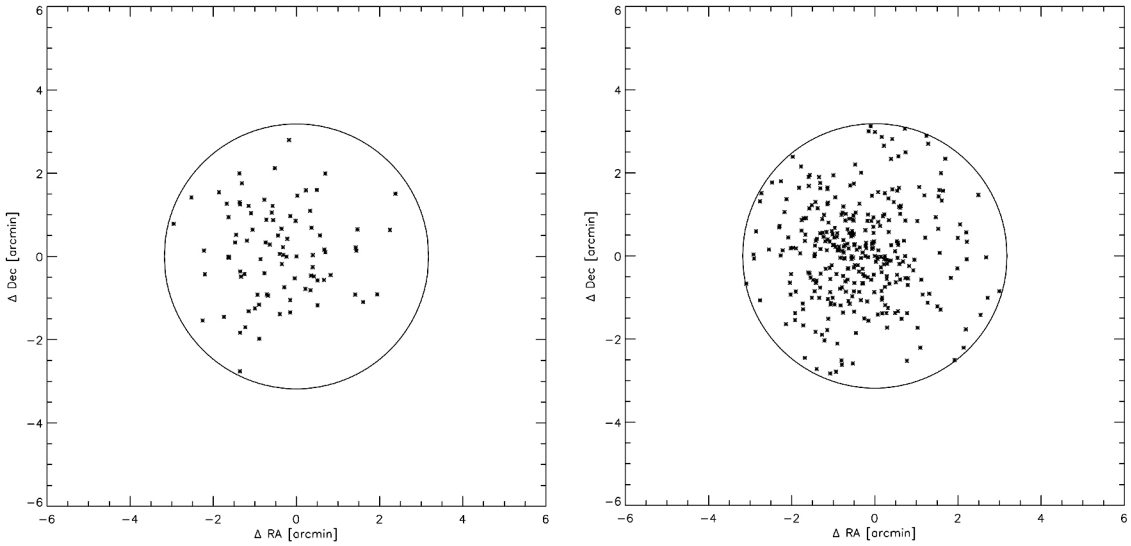


Figure 5.8 – Difference between the detected positions and the corresponding source coordinates in the GB6 catalogue (left) and in the NVSS catalogue (right). The circle indicates the size of the Gaussian beam.

The Medicina antenna pointing model, as described in Chapter 3 §2.3, has proven to be reliable even performing very fast OTF scans, with pointing errors < 10 arcsec.

The reason for the relatively significant position errors measured against the GB6 and NVSS catalogues could be due to the map/patches tangential projection

approximations, which get more critical for this very high Declination area. Further work will be carried out using a different reference frame for the map projection, in order to minimise this problem.

*Flux*

For the flux correlation, both the fluxes listed in the NVSS (1.4 GHz) and in the GB6 (4.85 GHz) catalogues have been extrapolated to 5.125 GHz, taking into account a steep spectrum population whose flux is proportional to $\nu^{\alpha}$ ($\alpha$ = -0.7). For every comparison, the brightest source found within one beamsize was considered, weighing its flux for the beam response function.

The comparisons show uncorrelated tails, confirming a flux limit of 100 mJy for our detections: for low fluxes the incidence of spurious detections/matches is higher, moreover the Eddington bias contributes to the observed effect. This bias is due to the fact that for low fluxes it is more probable to detect sources which:

- lie on a locally positive noise peak;
- are observed at the highest point of their variability.

Assuming that the flux spectral index of $\alpha$ = -0.7 is correct, the fluxes measured on our detections are obviously biased, as they are systematically underestimated with respect to the NVSS and GB6 catalogues (Figure 5.9).

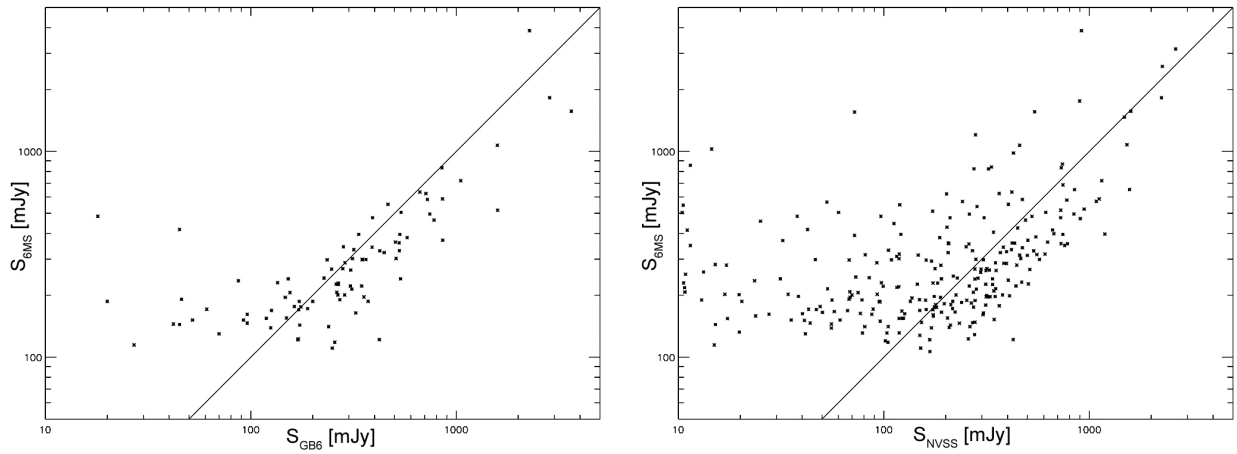


Figure 5.9 – Comparison between our measured flux densities (y-axis) and the extrapolated GB6 fluxes at 5.125 GHz (left). Right panel shows the analogous confrontation against the NVSS catalogue. The continuous line represents equal flux.

Further investigations are ongoing, but currently our guess is that the observed bias is due to the presence of blank (not observed) pixels in the outer regions of our map, mainly due to missing scans. Apart from the scans which were skipped in order to perform calibration observations, some acquisitions had to be flagged and removed from the binning because of the presence of RFI-related ripples (§2.4). A minor fraction of blank pixels is present also in the fully observed outer region. Their presence might not be negligible, and might affect the results produced by the photometry algorithm.

*Future work*

A possible approach could be to perform the interpolation for the null values, but the effectiveness of this technique using the specific photometry method employed is not known. Different software tools, such as MIRIAD/AIPS and SExtractor, will be exploited to perform the source extraction and flux estimation and compare the results with the values already achieved.

A more definitive plan is to fill in the missing gaps of the survey, or even to repeat the whole map using the properly cooled receiver and extending the map boundary to a lower southern limit, in order to obtain a larger intersection with the GB6 catalogue and match its sensitivity.

# CONCLUSIONS

The use of middle-sized radio telescopes, like the Medicina and Noto antennas, in single-dish mode is of great importance to conduct high efficiency wide sky surveys, or follow up and monitoring of large samples of sources in any of the typical single-dish observing modes like continuum, spectrometry and polarimetry observations.
One of the aims of this thesis work was to contribute to the design and development of ESCS, a new control system to be used specifically for optimised single-dish observations with all the Italian radio telescopes. The next phase focused on the verification of the system functioning and the assessment of the scientific potential of the observing techniques just made available.
At the same time, another goal was to carry out the commissioning of the new multi-feed receiver – the only K-band multi-feed available worldwide – together with a new total power analogue backend. Both devices have been built for the Sardinia Radio Telescope and were temporarily installed on the Medicina dish, to verify and improve their performance and estimate their scientific capabilities by means of the ESCS tools which have been developed.

On the software side, several software packages were implemented in ESCS – which was developed in the complex ALMA Common Software framework – in order to perform fast On-The-Fly scans and large maps, including tools for observation scheduling and for the production of FITS output files. External programs for quick-look and basic handling of the acquired data have been developed as well.

The receiver/backend commissioning was carried out along many observing sessions in winter 2009 and 2010, during which OTF scans were performed according to an innovative observing strategy to test the system stability and sensitivity. This allowed us not only to identify and correct major problems, such as the malfunctioning and consequent replacement of hardware components, but also to pinpoint subtle instabilities affecting the data and potentially hazarding the system capabilities. An exemplary case was the chase for the source of the puzzling “jiggling signal”, which

was found to afflict a substantial fraction of the acquisitions, and the successive development of an effective solution to the problem.
The test observations were mainly held on the "polar cap" region (Dec. > 72.3°, ~ 1000 square degrees) in the 20-22 GHz frequency band, following the OTF observing strategy of the KNoWS project (K-band Northern Wide Survey), for which these observations constituted a pilot survey. The very last portion of the data acquisition is still ongoing, and the full post-processing will be performed in the near future. Nonetheless the observations conducted so far have widely confirmed that the measured sensitivity very closely matches the theoretical expectations, such assessing the capabilities of both the software and hardware systems.

During the summer period, which is unsuitable for high frequency observations, tests were carried out on the total power backend only, coupling this device to a 5 GHz receiver. This offered the opportunity to further test the observing technique and the ESCS tools, and to simultaneously achieve original scientific data, as the observed polar cap had never been surveyed at this frequency. The acquired data will complement the Parkes-MIT-NRAO (PMN) and Green Bank 6cm (GB6) catalogues, providing an all-sky coverage at this frequency.
The data analysis is still underway, however preliminary results confirm that the observing strategy and the data reduction pipeline – comprising the map-making and source-extraction programs – effectively allow the production of maps and source catalogues. The detected sources constitute a preliminary version of the 6MS (6-cm Medicina Survey) polar cap catalogue.

*Future work*

The ESCS system is planned to be completed in the near future, with the implementation of tools for the observing modes which have been initially ranked as low-priority, the implementation of the MBFITS data format as the standard output and, in general, the fulfilment of all the originally designed system requirements.
Data reduction within both the KNoWS and 6MS projects is going on. It will lead, besides the achievement of original scientific results, to the optimisation of calibration,

map-making and source extraction procedures, refining the map quality and revealing more details about the data properties and the system performance.

# APPENDIX A

Preliminary list of the 6MS detections

| ID | RA h | DEC ° | Flux mJy | Flux Err mJy | ID | RA h | DEC ° | Flux mJy | Flux Err mJy |
|---|---|---|---|---|---|---|---|---|---|
| 1 | 0.0261 | 77.357 | 699.09 | 50.79 | 51 | 1.1122 | 76.860 | 214.21 | 38.13 |
| 2 | 0.0796 | 76.123 | 1552.82 | 83.01 | 52 | 1.1581 | 73.217 | 833.21 | 53.12 |
| 3 | 0.0930 | 84.796 | 111.67 | 21.11 | 53 | 1.1719 | 77.926 | 625.28 | 65.02 |
| 4 | 0.1273 | 83.962 | 358.30 | 28.52 | 54 | 1.1786 | 87.632 | 128.70 | 16.90 |
| 5 | 0.1273 | 73.459 | 312.28 | 47.80 | 55 | 1.2419 | 79.618 | 658.81 | 42.65 |
| 6 | 0.1583 | 76.061 | 316.99 | 39.06 | 56 | 1.2795 | 73.679 | 278.27 | 40.58 |
| 7 | 0.1714 | 86.268 | 139.55 | 18.78 | 57 | 1.2830 | 74.817 | 122.78 | 24.50 |
| 8 | 0.2045 | 85.706 | 188.39 | 19.21 | 58 | 1.3962 | 80.932 | 154.24 | 26.90 |
| 9 | 0.2079 | 77.825 | 652.12 | 71.48 | 59 | 1.4037 | 80.392 | 307.77 | 31.70 |
| 10 | 0.2160 | 72.497 | 359.38 | 42.10 | 60 | 1.4311 | 72.770 | 505.48 | 43.84 |
| 11 | 0.2390 | 79.427 | 835.49 | 56.01 | 61 | 1.4475 | 73.367 | 229.18 | 42.41 |
| 12 | 0.2509 | 72.258 | 212.58 | 41.21 | 62 | 1.4929 | 78.021 | 387.47 | 61.05 |
| 13 | 0.2588 | 75.491 | 471.66 | 40.21 | 63 | 1.5323 | 84.776 | 226.20 | 25.37 |
| 14 | 0.2803 | 81.590 | 1203.84 | 65.75 | 64 | 1.5434 | 74.084 | 175.50 | 35.16 |
| 15 | 0.2892 | 79.748 | 547.95 | 55.78 | 65 | 1.6591 | 79.159 | 343.75 | 35.28 |
| 16 | 0.3214 | 72.522 | 326.48 | 62.51 | 66 | 1.6591 | 79.159 | 343.75 | 35.28 |
| 17 | 0.3287 | 73.440 | 1070.90 | 72.96 | 67 | 1.7043 | 76.187 | 282.20 | 40.65 |
| 18 | 0.3570 | 73.211 | 476.07 | 67.15 | 68 | 1.7523 | 73.392 | 1091.29 | 66.03 |
| 19 | 0.3886 | 88.041 | 115.00 | 15.96 | 69 | 1.8409 | 76.230 | 381.68 | 46.52 |
| 20 | 0.4022 | 72.435 | 939.89 | 71.26 | 70 | 1.8654 | 75.842 | 240.34 | 44.24 |
| 21 | 0.4125 | 77.946 | 391.27 | 71.18 | 71 | 1.9153 | 79.688 | 657.30 | 49.15 |
| 22 | 0.4563 | 72.951 | 396.42 | 67.99 | 72 | 1.9269 | 77.980 | 616.33 | 63.64 |
| 23 | 0.4897 | 72.255 | 575.23 | 50.26 | 73 | 1.9499 | 76.148 | 270.76 | 47.80 |
| 24 | 0.5155 | 84.841 | 185.59 | 23.97 | 74 | 1.9544 | 74.680 | 518.03 | 40.65 |
| 25 | 0.5225 | 77.904 | 603.06 | 104.62 | 75 | 1.9656 | 72.952 | 240.34 | 43.37 |
| 26 | 0.5272 | 84.649 | 187.47 | 24.33 | 76 | 1.9801 | 73.380 | 211.17 | 37.36 |
| 27 | 0.5282 | 74.345 | 403.03 | 37.84 | 77 | 2.0459 | 78.085 | 265.67 | 53.61 |
| 28 | 0.6183 | 83.070 | 232.85 | 25.17 | 78 | 2.0539 | 72.570 | 287.60 | 38.88 |
| 29 | 0.6490 | 77.947 | 518.58 | 100.36 | 79 | 2.0560 | 81.096 | 243.22 | 32.36 |
| 30 | 0.6735 | 77.034 | 594.39 | 56.55 | 80 | 2.0876 | 75.375 | 302.02 | 36.01 |
| 31 | 0.7193 | 84.932 | 142.00 | 23.11 | 81 | 2.1004 | 75.723 | 559.74 | 47.70 |
| 32 | 0.7349 | 73.727 | 226.49 | 37.48 | 82 | 2.1165 | 84.192 | 162.62 | 23.84 |
| 33 | 0.7369 | 72.582 | 173.96 | 31.01 | 83 | 2.1221 | 79.908 | 384.02 | 38.93 |
| 34 | 0.7501 | 79.236 | 269.63 | 35.29 | 84 | 2.1613 | 72.490 | 329.32 | 44.76 |
| 35 | 0.7637 | 72.304 | 159.09 | 25.73 | 85 | 2.1899 | 76.190 | 434.04 | 48.13 |
| 36 | 0.7799 | 80.632 | 193.13 | 30.64 | 86 | 2.2379 | 87.288 | 150.99 | 19.21 |
| 37 | 0.8006 | 85.471 | 158.49 | 20.40 | 87 | 2.2379 | 72.286 | 1369.03 | 72.92 |
| 38 | 0.8417 | 86.448 | 197.50 | 18.90 | 88 | 2.2907 | 73.827 | 3860.44 | 200.05 |
| 39 | 0.8717 | 74.981 | 297.76 | 33.67 | 89 | 2.3805 | 86.312 | 1468.19 | 76.09 |
| 40 | 0.8808 | 83.704 | 174.24 | 25.75 | 90 | 2.4081 | 76.922 | 579.83 | 65.01 |
| 41 | 0.8989 | 75.260 | 673.02 | 43.35 | 91 | 2.4225 | 73.647 | 2991.20 | 191.61 |
| 42 | 0.9137 | 81.847 | 475.79 | 36.52 | 92 | 2.4678 | 74.386 | 225.30 | 45.23 |
| 43 | 0.9281 | 76.133 | 277.23 | 38.59 | 93 | 2.4815 | 77.728 | 571.58 | 86.14 |
| 44 | 0.9323 | 76.389 | 242.24 | 43.43 | 94 | 2.4830 | 79.875 | 1849.36 | 99.95 |
| 45 | 0.9663 | 72.295 | 191.90 | 26.85 | 95 | 2.4838 | 72.290 | 417.98 | 57.27 |
| 46 | 0.9911 | 76.205 | 278.92 | 40.39 | 96 | 2.4955 | 81.696 | 359.09 | 34.02 |
| 47 | 1.0575 | 78.743 | 354.07 | 36.37 | 97 | 2.5023 | 76.211 | 524.58 | 65.99 |
| 48 | 1.0585 | 78.171 | 596.14 | 80.10 | 98 | 2.5179 | 76.898 | 533.54 | 75.45 |
| 49 | 1.0622 | 76.251 | 317.64 | 43.01 | 99 | 2.5349 | 72.282 | 608.02 | 57.11 |
| 50 | 1.0727 | 81.492 | 531.54 | 39.74 | 100 | 2.5370 | 79.676 | 1477.33 | 82.94 |

| ID | RA<br>h | DEC<br>° | Flux<br>mJy | Flux Err<br>mJy | ID | RA<br>h | DEC<br>° | Flux<br>mJy | Flux Err<br>mJy |
|---|---|---|---|---|---|---|---|---|---|
| 101 | 2.5722 | 78.014 | 570.13 | 78.47 | 151 | 4.9723 | 76.238 | 202.24 | 31.14 |
| 102 | 2.5753 | 73.006 | 483.55 | 76.45 | 152 | 5.1241 | 79.216 | 188.94 | 27.63 |
| 103 | 2.6358 | 76.894 | 582.68 | 79.03 | 153 | 5.1451 | 72.422 | 152.34 | 27.10 |
| 104 | 2.6431 | 85.522 | 652.71 | 39.52 | 154 | 5.1685 | 84.542 | 131.23 | 22.59 |
| 105 | 2.6467 | 73.446 | 517.14 | 61.52 | 155 | 5.2235 | 72.334 | 117.67 | 23.82 |
| 106 | 2.6663 | 72.297 | 467.98 | 61.13 | 156 | 5.2355 | 72.617 | 199.42 | 32.92 |
| 107 | 2.6945 | 80.209 | 389.80 | 46.28 | 157 | 5.2634 | 73.466 | 291.13 | 38.48 |
| 108 | 2.7062 | 78.070 | 390.84 | 77.36 | 158 | 5.3047 | 74.599 | 150.02 | 29.27 |
| 109 | 2.7296 | 72.281 | 209.26 | 42.05 | 159 | 5.3659 | 76.854 | 229.58 | 40.80 |
| 110 | 2.7919 | 72.347 | 279.87 | 44.50 | 160 | 5.3846 | 78.030 | 431.94 | 48.20 |
| 111 | 2.8015 | 74.523 | 261.36 | 40.08 | 161 | 5.4833 | 77.967 | 262.09 | 46.91 |
| 112 | 2.8421 | 72.436 | 756.28 | 52.96 | 162 | 5.5473 | 72.527 | 133.94 | 26.82 |
| 113 | 2.8670 | 72.952 | 285.31 | 49.57 | 163 | 5.7098 | 78.126 | 360.11 | 60.00 |
| 114 | 2.9069 | 84.265 | 227.43 | 31.04 | 164 | 5.7248 | 81.293 | 154.24 | 29.72 |
| 115 | 3.0080 | 82.061 | 315.16 | 35.72 | 165 | 5.8227 | 78.011 | 448.85 | 61.71 |
| 116 | 3.0111 | 76.890 | 368.87 | 51.67 | 166 | 5.8981 | 72.284 | 223.54 | 26.01 |
| 117 | 3.0427 | 72.893 | 626.91 | 43.66 | 167 | 5.9375 | 77.963 | 381.53 | 58.86 |
| 118 | 3.0513 | 75.322 | 586.97 | 39.71 | 168 | 5.9548 | 72.301 | 281.64 | 28.49 |
| 119 | 3.0716 | 77.978 | 1530.91 | 124.43 | 169 | 6.0183 | 72.370 | 247.13 | 31.51 |
| 120 | 3.1004 | 79.913 | 905.05 | 60.31 | 170 | 6.0651 | 76.355 | 385.49 | 41.10 |
| 121 | 3.2077 | 80.628 | 431.95 | 35.42 | 171 | 6.1753 | 72.844 | 634.72 | 47.60 |
| 122 | 3.2712 | 72.352 | 267.98 | 27.05 | 172 | 6.1791 | 79.525 | 704.98 | 50.26 |
| 123 | 3.3207 | 77.552 | 459.51 | 88.87 | 173 | 6.1950 | 72.329 | 235.08 | 31.51 |
| 124 | 3.3394 | 72.409 | 151.45 | 23.38 | 174 | 6.2059 | 74.570 | 174.10 | 32.56 |
| 125 | 3.3539 | 74.261 | 187.98 | 28.49 | 175 | 6.2589 | 76.411 | 264.00 | 42.59 |
| 126 | 3.3545 | 74.556 | 138.89 | 27.91 | 176 | 6.3050 | 79.809 | 269.14 | 38.73 |
| 127 | 3.3893 | 85.549 | 133.06 | 22.29 | 177 | 6.3063 | 78.358 | 358.26 | 48.10 |
| 128 | 3.4885 | 77.958 | 399.65 | 52.43 | 178 | 6.3433 | 78.014 | 505.23 | 48.48 |
| 129 | 3.5711 | 76.877 | 1135.28 | 64.79 | 179 | 6.4289 | 82.031 | 823.28 | 51.18 |
| 130 | 3.5811 | 74.177 | 395.12 | 34.24 | 180 | 6.5050 | 76.569 | 268.89 | 37.55 |
| 131 | 3.9095 | 80.167 | 355.08 | 31.62 | 181 | 6.6245 | 84.186 | 279.89 | 27.99 |
| 132 | 3.9114 | 72.921 | 362.56 | 35.68 | 182 | 6.6531 | 73.436 | 624.31 | 46.53 |
| 133 | 3.9167 | 79.507 | 193.62 | 32.24 | 183 | 6.6733 | 78.207 | 268.30 | 40.11 |
| 134 | 4.0376 | 78.020 | 296.64 | 49.36 | 184 | 6.7836 | 75.043 | 242.61 | 31.08 |
| 135 | 4.0538 | 74.947 | 200.71 | 30.98 | 185 | 6.7961 | 76.216 | 416.79 | 40.77 |
| 136 | 4.0851 | 78.867 | 379.72 | 37.04 | 186 | 6.8628 | 78.070 | 507.52 | 48.52 |
| 137 | 4.1660 | 79.607 | 838.34 | 51.86 | 187 | 6.8924 | 73.281 | 343.94 | 38.46 |
| 138 | 4.1783 | 76.949 | 2588.89 | 135.37 | 188 | 7.0471 | 85.828 | 221.16 | 21.48 |
| 139 | 4.2207 | 74.857 | 720.49 | 44.91 | 189 | 7.0877 | 72.872 | 168.73 | 32.07 |
| 140 | 4.2711 | 72.995 | 209.25 | 38.40 | 190 | 7.1343 | 72.876 | 161.55 | 31.55 |
| 141 | 4.3917 | 77.957 | 512.15 | 64.06 | 191 | 7.1557 | 74.807 | 587.77 | 39.23 |
| 142 | 4.4533 | 77.980 | 504.08 | 67.80 | 192 | 7.1921 | 79.450 | 201.28 | 35.62 |
| 143 | 4.4749 | 84.174 | 240.33 | 26.11 | 193 | 7.2319 | 74.168 | 206.93 | 38.42 |
| 144 | 4.5167 | 85.460 | 321.01 | 24.32 | 194 | 7.2365 | 81.869 | 165.68 | 26.72 |
| 145 | 4.6798 | 73.375 | 240.27 | 34.97 | 195 | 7.2739 | 73.611 | 195.21 | 35.67 |
| 146 | 4.7123 | 77.970 | 324.79 | 55.73 | 196 | 7.3141 | 78.082 | 232.96 | 43.89 |
| 147 | 4.7867 | 73.353 | 214.14 | 42.51 | 197 | 7.3772 | 77.998 | 196.40 | 40.37 |
| 148 | 4.8124 | 82.541 | 220.00 | 25.15 | 198 | 7.4395 | 79.169 | 621.88 | 44.86 |
| 149 | 4.8223 | 77.995 | 233.71 | 41.49 | 199 | 7.5705 | 76.956 | 181.91 | 36.73 |
| 150 | 4.8581 | 72.779 | 2264.19 | 116.93 | 200 | 7.5891 | 72.920 | 171.05 | 33.91 |

| ID | RA h | DEC ° | Flux mJy | Flux Err mJy | ID | RA h | DEC ° | Flux mJy | Flux Err mJy |
|---|---|---|---|---|---|---|---|---|---|
| 201 | 7.6496 | 75.471 | 189.76 | 31.46 | 251 | 10.0504 | 72.984 | 259.43 | 30.24 |
| 202 | 7.6893 | 78.039 | 348.86 | 55.57 | 252 | 10.1069 | 72.319 | 136.17 | 20.90 |
| 203 | 7.7171 | 80.443 | 867.65 | 54.32 | 253 | 10.1311 | 81.535 | 152.36 | 31.15 |
| 204 | 7.7641 | 72.863 | 172.32 | 31.84 | 254 | 10.1716 | 82.837 | 428.25 | 33.46 |
| 205 | 7.7855 | 76.651 | 566.87 | 43.37 | 255 | 10.2274 | 72.385 | 701.28 | 41.75 |
| 206 | 7.8098 | 78.080 | 229.26 | 42.71 | 256 | 10.2363 | 74.616 | 496.42 | 36.38 |
| 207 | 7.8210 | 74.362 | 322.37 | 32.39 | 257 | 10.2404 | 85.897 | 279.43 | 24.68 |
| 208 | 7.8509 | 82.682 | 687.00 | 44.85 | 258 | 10.2946 | 81.087 | 340.53 | 34.31 |
| 209 | 7.8661 | 79.512 | 667.74 | 46.88 | 259 | 10.3828 | 78.070 | 238.23 | 32.40 |
| 210 | 8.0225 | 74.125 | 144.20 | 28.96 | 260 | 10.3961 | 80.537 | 356.63 | 33.84 |
| 211 | 8.1199 | 78.791 | 179.88 | 35.98 | 261 | 10.4911 | 78.877 | 424.52 | 35.51 |
| 212 | 8.1352 | 73.243 | 395.34 | 38.81 | 262 | 10.7422 | 80.900 | 839.89 | 50.61 |
| 213 | 8.2441 | 72.403 | 114.45 | 23.40 | 263 | 10.7665 | 73.360 | 298.82 | 34.43 |
| 214 | 8.2897 | 78.016 | 283.79 | 58.01 | 264 | 10.9769 | 81.241 | 483.38 | 43.13 |
| 215 | 8.3275 | 75.621 | 147.74 | 27.76 | 265 | 11.0312 | 72.419 | 370.36 | 29.95 |
| 216 | 8.3513 | 78.089 | 475.44 | 52.66 | 266 | 11.0715 | 76.974 | 524.27 | 40.96 |
| 217 | 8.4245 | 74.045 | 333.15 | 35.39 | 267 | 11.0715 | 79.554 | 356.32 | 34.23 |
| 218 | 8.4289 | 76.908 | 239.67 | 35.49 | 268 | 11.0780 | 75.688 | 134.43 | 26.93 |
| 219 | 8.4761 | 78.095 | 425.44 | 56.70 | 269 | 11.0929 | 73.317 | 177.13 | 33.41 |
| 220 | 8.4822 | 73.140 | 172.66 | 34.10 | 270 | 11.1203 | 72.516 | 190.32 | 31.21 |
| 221 | 8.5433 | 80.116 | 287.38 | 32.38 | 271 | 11.1888 | 79.579 | 458.15 | 39.09 |
| 222 | 8.5824 | 72.665 | 221.85 | 30.44 | 272 | 11.1989 | 72.323 | 181.69 | 28.48 |
| 223 | 8.7114 | 74.496 | 140.75 | 28.36 | 273 | 11.3940 | 73.823 | 242.12 | 32.42 |
| 224 | 8.7633 | 79.265 | 649.95 | 45.18 | 274 | 11.6557 | 76.919 | 245.35 | 34.07 |
| 225 | 8.8135 | 78.501 | 316.96 | 53.32 | 275 | 11.8064 | 79.381 | 199.20 | 28.04 |
| 226 | 8.8748 | 76.469 | 163.21 | 31.91 | 276 | 11.8847 | 80.964 | 1558.16 | 82.45 |
| 227 | 8.9083 | 80.576 | 208.00 | 32.34 | 277 | 11.8861 | 79.628 | 208.14 | 29.48 |
| 228 | 9.1249 | 73.374 | 154.40 | 30.17 | 278 | 11.9184 | 75.580 | 196.85 | 28.32 |
| 229 | 9.1392 | 73.125 | 134.95 | 27.64 | 279 | 11.9287 | 81.967 | 147.21 | 28.01 |
| 230 | 9.1394 | 83.762 | 174.79 | 27.19 | 280 | 11.9470 | 81.316 | 325.54 | 44.65 |
| 231 | 9.1536 | 83.453 | 140.66 | 27.68 | 281 | 12.0045 | 73.023 | 1824.20 | 96.74 |
| 232 | 9.1831 | 79.761 | 755.94 | 48.77 | 282 | 12.2595 | 73.414 | 202.24 | 35.13 |
| 233 | 9.1857 | 86.115 | 131.10 | 22.55 | 283 | 12.3901 | 80.663 | 539.79 | 38.77 |
| 234 | 9.1947 | 80.873 | 189.49 | 32.21 | 284 | 12.5216 | 74.039 | 2472.76 | 128.45 |
| 235 | 9.2784 | 72.380 | 96.62 | 19.69 | 285 | 12.5469 | 80.933 | 330.73 | 33.92 |
| 236 | 9.2798 | 73.730 | 230.09 | 29.96 | 286 | 12.5787 | 77.498 | 194.11 | 30.41 |
| 237 | 9.3379 | 78.409 | 296.34 | 35.89 | 287 | 12.6159 | 83.946 | 263.52 | 26.05 |
| 238 | 9.5011 | 86.204 | 166.76 | 23.04 | 288 | 12.7206 | 73.244 | 301.36 | 38.31 |
| 239 | 9.5373 | 79.103 | 471.57 | 37.67 | 289 | 12.7392 | 87.931 | 127.79 | 14.49 |
| 240 | 9.6621 | 83.277 | 396.44 | 33.52 | 290 | 12.7915 | 72.898 | 210.78 | 32.32 |
| 241 | 9.7335 | 82.910 | 258.67 | 35.90 | 291 | 12.9365 | 80.275 | 161.70 | 29.63 |
| 242 | 9.7619 | 83.952 | 200.29 | 28.18 | 292 | 12.9956 | 80.900 | 227.08 | 28.02 |
| 243 | 9.8183 | 73.214 | 553.26 | 43.19 | 293 | 13.0154 | 75.385 | 129.61 | 24.77 |
| 244 | 9.8190 | 79.755 | 598.32 | 42.21 | 294 | 13.0797 | 78.913 | 218.21 | 27.97 |
| 245 | 9.8456 | 78.130 | 439.63 | 41.76 | 295 | 13.0892 | 80.148 | 199.25 | 29.53 |
| 246 | 9.8646 | 72.342 | 103.04 | 19.41 | 296 | 13.1179 | 76.825 | 161.07 | 30.81 |
| 247 | 9.8861 | 79.975 | 153.93 | 30.49 | 297 | 13.1281 | 85.748 | 184.42 | 19.39 |
| 248 | 9.9031 | 78.026 | 410.96 | 41.07 | 298 | 13.2945 | 82.299 | 215.33 | 26.21 |
| 249 | 9.9094 | 74.564 | 463.82 | 35.42 | 299 | 13.3394 | 72.345 | 174.22 | 23.40 |
| 250 | 9.9939 | 81.447 | 197.21 | 30.80 | 300 | 13.3475 | 77.662 | 168.42 | 29.57 |

| ID | RA<br>h | DEC<br>° | Flux<br>mJy | Flux Err<br>mJy | ID | RA<br>h | DEC<br>° | Flux<br>mJy | Flux Err<br>mJy |
|---|---|---|---|---|---|---|---|---|---|
| 301 | 13.3479 | 84.822 | 197.33 | 21.17 | 351 | 17.1004 | 77.122 | 167.64 | 28.50 |
| 302 | 13.3641 | 83.264 | 242.42 | 24.04 | 352 | 17.2484 | 79.812 | 156.63 | 29.80 |
| 303 | 13.3909 | 79.705 | 570.59 | 38.92 | 353 | 17.2871 | 74.326 | 138.78 | 25.80 |
| 304 | 13.6057 | 72.593 | 117.33 | 24.17 | 354 | 17.3890 | 76.889 | 293.01 | 33.35 |
| 305 | 13.7722 | 73.340 | 342.41 | 34.12 | 355 | 17.3950 | 72.631 | 142.65 | 21.90 |
| 306 | 13.8847 | 75.577 | 214.97 | 25.59 | 356 | 17.4149 | 77.429 | 231.56 | 32.68 |
| 307 | 13.9105 | 72.707 | 129.86 | 26.13 | 357 | 17.4597 | 73.863 | 328.58 | 30.36 |
| 308 | 13.9555 | 83.675 | 120.00 | 21.63 | 358 | 17.4719 | 72.708 | 123.92 | 25.28 |
| 309 | 13.9611 | 76.725 | 495.75 | 37.38 | 359 | 17.5291 | 73.658 | 221.81 | 32.47 |
| 310 | 14.1811 | 72.532 | 145.75 | 20.76 | 360 | 17.5784 | 72.649 | 151.50 | 30.84 |
| 311 | 14.2744 | 79.726 | 152.31 | 28.65 | 361 | 17.6179 | 84.779 | 179.88 | 25.04 |
| 312 | 14.2823 | 80.998 | 247.72 | 26.47 | 362 | 17.6416 | 72.694 | 377.14 | 34.02 |
| 313 | 14.3303 | 76.035 | 285.20 | 29.92 | 363 | 17.6524 | 80.098 | 158.56 | 30.35 |
| 314 | 14.5188 | 73.203 | 143.25 | 28.69 | 364 | 17.6822 | 72.407 | 151.51 | 29.73 |
| 315 | 14.5864 | 79.560 | 245.72 | 28.87 | 365 | 17.6950 | 72.641 | 417.29 | 36.26 |
| 316 | 14.5917 | 76.095 | 483.27 | 39.20 | 366 | 17.8031 | 84.958 | 148.54 | 22.97 |
| 317 | 14.7135 | 77.124 | 349.33 | 38.28 | 367 | 17.8630 | 73.190 | 176.21 | 34.27 |
| 318 | 14.7409 | 74.765 | 117.73 | 22.73 | 368 | 17.9627 | 75.664 | 168.42 | 30.20 |
| 319 | 14.7627 | 85.225 | 131.11 | 20.69 | 369 | 18.0085 | 78.460 | 1758.41 | 92.31 |
| 320 | 14.7858 | 76.951 | 398.17 | 36.16 | 370 | 18.0229 | 72.584 | 141.48 | 29.11 |
| 321 | 14.8031 | 76.001 | 390.51 | 36.51 | 371 | 18.0573 | 74.217 | 189.69 | 36.15 |
| 322 | 14.9094 | 72.725 | 168.96 | 25.80 | 372 | 18.0671 | 74.419 | 188.68 | 29.83 |
| 323 | 15.0109 | 86.127 | 106.51 | 18.20 | 373 | 18.1713 | 73.866 | 298.50 | 36.17 |
| 324 | 15.0992 | 83.312 | 314.62 | 26.46 | 374 | 18.2977 | 79.646 | 316.09 | 33.92 |
| 325 | 15.1683 | 72.713 | 102.06 | 20.73 | 375 | 18.3597 | 82.958 | 202.29 | 25.03 |
| 326 | 15.2161 | 81.728 | 196.67 | 26.16 | 376 | 18.3792 | 79.650 | 550.38 | 69.88 |
| 327 | 15.3347 | 72.437 | 96.77 | 14.84 | 377 | 18.4019 | 74.346 | 584.22 | 39.40 |
| 328 | 15.3478 | 79.004 | 165.12 | 26.86 | 378 | 18.4613 | 73.443 | 313.24 | 42.60 |
| 329 | 15.4073 | 73.581 | 206.01 | 27.15 | 379 | 18.5388 | 72.529 | 440.57 | 44.74 |
| 330 | 15.4527 | 73.263 | 132.40 | 25.72 | 380 | 18.5422 | 72.729 | 308.64 | 51.29 |
| 331 | 15.6015 | 81.883 | 158.33 | 28.86 | 381 | 18.5687 | 73.466 | 620.27 | 50.61 |
| 332 | 15.7997 | 75.638 | 132.21 | 26.27 | 382 | 18.5726 | 73.666 | 436.79 | 54.04 |
| 333 | 15.8903 | 85.726 | 2494.11 | 127.17 | 383 | 18.6001 | 74.288 | 252.80 | 37.31 |
| 334 | 16.0253 | 80.284 | 198.70 | 29.34 | 384 | 18.6127 | 85.257 | 147.91 | 22.45 |
| 335 | 16.1149 | 85.029 | 313.36 | 39.96 | 385 | 18.6323 | 75.621 | 246.02 | 31.46 |
| 336 | 16.1549 | 79.680 | 312.45 | 30.83 | 386 | 18.6486 | 73.654 | 251.02 | 44.97 |
| 337 | 16.2159 | 78.198 | 497.95 | 36.06 | 387 | 18.7054 | 79.754 | 3143.91 | 160.75 |
| 338 | 16.3266 | 85.813 | 415.22 | 40.02 | 388 | 18.7117 | 77.726 | 529.44 | 39.81 |
| 339 | 16.4802 | 74.526 | 121.56 | 23.34 | 389 | 18.7621 | 81.817 | 171.30 | 27.08 |
| 340 | 16.5271 | 82.532 | 822.03 | 46.19 | 390 | 18.7913 | 80.841 | 319.17 | 32.43 |
| 341 | 16.5606 | 72.312 | 104.57 | 17.99 | 391 | 18.8189 | 73.044 | 284.19 | 37.19 |
| 342 | 16.5637 | 74.096 | 121.81 | 24.85 | 392 | 18.8472 | 72.572 | 212.09 | 29.54 |
| 343 | 16.6478 | 86.527 | 209.93 | 20.58 | 393 | 18.8785 | 73.412 | 186.72 | 35.82 |
| 344 | 16.7597 | 74.345 | 110.66 | 22.53 | 394 | 18.8889 | 83.584 | 226.10 | 26.42 |
| 345 | 16.8051 | 75.795 | 355.83 | 30.68 | 395 | 18.9073 | 84.145 | 149.27 | 24.15 |
| 346 | 16.9056 | 79.612 | 856.06 | 50.28 | 396 | 18.9141 | 83.949 | 240.40 | 27.06 |
| 347 | 16.9695 | 79.465 | 263.84 | 29.28 | 397 | 18.9152 | 84.546 | 217.72 | 26.49 |
| 348 | 17.0015 | 72.424 | 109.30 | 21.77 | 398 | 18.9181 | 73.855 | 381.29 | 37.53 |
| 349 | 17.0101 | 72.657 | 144.96 | 25.59 | 399 | 18.9834 | 77.785 | 298.17 | 33.56 |
| 350 | 17.0789 | 77.956 | 162.43 | 28.65 | 400 | 19.0540 | 85.599 | 177.73 | 23.63 |

| ID | RA h | DEC ° | Flux mJy | Flux Err mJy | ID | RA h | DEC ° | Flux mJy | Flux Err mJy |
|---|---|---|---|---|---|---|---|---|---|
| 401 | 19.0867 | 72.373 | 144.23 | 20.92 | 456 | 21.9247 | 77.964 | 1026.80 | 80.12 |
| 402 | 19.1151 | 73.034 | 164.19 | 28.92 | 457 | 21.9419 | 83.620 | 165.41 | 28.48 |
| 403 | 19.1359 | 81.018 | 149.48 | 28.17 | 458 | 21.9589 | 76.769 | 179.16 | 36.71 |
| 404 | 19.1446 | 74.010 | 160.64 | 28.63 | 459 | 22.0443 | 77.993 | 751.86 | 72.18 |
| 405 | 19.1708 | 74.813 | 284.17 | 27.92 | 460 | 22.1016 | 74.613 | 186.62 | 28.14 |
| 406 | 19.2745 | 77.867 | 242.30 | 30.21 | 461 | 22.1637 | 72.749 | 146.39 | 28.48 |
| 407 | 19.3219 | 74.549 | 196.21 | 36.79 | 462 | 22.1648 | 83.904 | 146.25 | 24.60 |
| 408 | 19.4695 | 73.947 | 1567.57 | 83.00 | 463 | 22.2999 | 72.295 | 114.73 | 22.60 |
| 409 | 19.5798 | 81.497 | 446.15 | 34.19 | 464 | 22.3967 | 73.185 | 163.51 | 33.19 |
| 410 | 19.6175 | 83.949 | 229.43 | 27.99 | 465 | 22.4497 | 76.854 | 212.41 | 38.10 |
| 411 | 19.6814 | 85.031 | 183.26 | 23.30 | 466 | 22.4567 | 75.539 | 140.68 | 26.99 |
| 412 | 19.7530 | 72.802 | 265.03 | 27.34 | 467 | 22.4671 | 78.020 | 414.15 | 48.57 |
| 413 | 19.8509 | 73.504 | 154.14 | 29.56 | 468 | 22.4693 | 73.443 | 167.38 | 32.73 |
| 414 | 20.0537 | 79.494 | 1067.26 | 60.05 | 469 | 22.5733 | 77.890 | 249.50 | 43.04 |
| 415 | 20.0833 | 77.894 | 981.87 | 58.03 | 470 | 22.6497 | 81.808 | 140.90 | 26.20 |
| 416 | 20.1162 | 74.870 | 118.10 | 24.27 | 471 | 22.6619 | 73.572 | 151.50 | 25.89 |
| 417 | 20.1537 | 72.466 | 593.76 | 37.97 | 472 | 22.7056 | 82.415 | 189.26 | 26.19 |
| 418 | 20.1725 | 72.266 | 114.99 | 23.40 | 473 | 22.7749 | 85.945 | 139.43 | 19.25 |
| 419 | 20.2255 | 84.621 | 154.90 | 24.81 | 474 | 22.7829 | 72.258 | 128.99 | 15.83 |
| 420 | 20.2827 | 74.663 | 240.31 | 26.07 | 475 | 22.8389 | 72.921 | 186.69 | 26.66 |
| 421 | 20.3007 | 73.457 | 269.24 | 31.80 | 476 | 22.9795 | 79.330 | 223.87 | 27.92 |
| 422 | 20.3707 | 76.200 | 512.27 | 37.28 | 477 | 23.1069 | 82.677 | 170.36 | 25.17 |
| 423 | 20.4062 | 87.398 | 4011.89 | 201.43 | 478 | 23.1182 | 74.438 | 155.01 | 26.49 |
| 424 | 20.4401 | 82.012 | 144.28 | 29.44 | 479 | 23.2004 | 72.710 | 297.31 | 29.85 |
| 425 | 20.4469 | 82.929 | 154.11 | 27.03 | 480 | 23.2576 | 86.511 | 195.51 | 19.42 |
| 426 | 20.4925 | 85.530 | 116.10 | 21.28 | 481 | 23.2700 | 73.125 | 206.70 | 30.30 |
| 427 | 20.5849 | 78.012 | 199.04 | 32.84 | 482 | 23.4143 | 74.314 | 125.41 | 24.58 |
| 428 | 20.7185 | 75.094 | 186.79 | 27.08 | 483 | 23.4184 | 79.283 | 313.38 | 29.85 |
| 429 | 20.7543 | 76.411 | 285.96 | 35.79 | 484 | 23.4367 | 80.228 | 138.56 | 25.72 |
| 430 | 20.9736 | 77.810 | 215.08 | 41.10 | 485 | 23.4399 | 82.542 | 236.68 | 42.88 |
| 431 | 20.9925 | 73.488 | 200.60 | 32.78 | 486 | 23.5165 | 72.221 | 201.41 | 21.64 |
| 432 | 20.9938 | 79.652 | 1095.11 | 62.52 | 487 | 23.5177 | 81.347 | 144.29 | 24.63 |
| 433 | 21.0627 | 76.567 | 652.86 | 49.15 | 488 | 23.5675 | 79.986 | 175.88 | 30.46 |
| 434 | 21.1396 | 72.981 | 193.85 | 35.82 | 489 | 23.5777 | 76.501 | 207.26 | 31.20 |
| 435 | 21.1549 | 80.356 | 170.54 | 27.44 | 490 | 23.6359 | 73.968 | 530.80 | 37.92 |
| 436 | 21.1631 | 74.584 | 159.01 | 30.51 | 491 | 23.6989 | 77.486 | 588.64 | 48.08 |
| 437 | 21.1741 | 73.581 | 176.47 | 32.97 | 492 | 23.7186 | 78.686 | 515.06 | 40.25 |
| 438 | 21.1903 | 72.578 | 191.13 | 30.34 | 493 | 23.7229 | 72.837 | 334.68 | 34.18 |
| 439 | 21.2037 | 74.151 | 156.83 | 31.76 | 494 | 23.7339 | 82.450 | 1077.17 | 60.42 |
| 440 | 21.2182 | 73.062 | 213.64 | 39.29 | 495 | 23.7405 | 77.131 | 228.20 | 34.23 |
| 441 | 21.2314 | 82.073 | 308.84 | 29.86 | 496 | 23.7442 | 73.060 | 360.40 | 35.50 |
| 442 | 21.2991 | 75.170 | 164.04 | 29.29 | 497 | 23.8185 | 75.300 | 170.07 | 28.78 |
| 443 | 21.3298 | 76.976 | 160.52 | 30.34 | 498 | 23.8735 | 75.121 | 163.05 | 30.87 |
| 444 | 21.4847 | 84.887 | 266.71 | 23.72 | 499 | 23.8739 | 83.561 | 200.18 | 25.43 |
| 445 | 21.5031 | 83.935 | 476.34 | 33.92 | 500 | 23.8917 | 77.782 | 511.97 | 45.27 |
| 446 | 21.5243 | 84.496 | 175.05 | 29.59 | 501 | 23.9135 | 74.432 | 201.10 | 30.30 |
| 447 | 21.5529 | 82.669 | 322.40 | 29.86 | 502 | 23.9225 | 72.807 | 220.70 | 30.76 |
| 448 | 21.6129 | 79.755 | 249.35 | 28.85 | 503 | 23.9235 | 79.931 | 405.26 | 35.61 |
| 449 | 21.7101 | 72.613 | 195.31 | 29.72 | 504 | 23.9324 | 81.874 | 475.86 | 49.82 |
| 450 | 21.7221 | 73.183 | 233.02 | 37.28 | 505 | 23.9416 | 78.701 | 1107.75 | 64.64 |
| 451 | 21.7280 | 72.969 | 205.76 | 35.33 | 506 | 23.9525 | 73.668 | 1077.71 | 60.49 |
| 452 | 21.7789 | 74.566 | 153.28 | 28.03 | 507 | 23.9637 | 80.934 | 470.93 | 35.82 |
| 453 | 21.8219 | 72.356 | 181.52 | 29.03 | 508 | 23.9787 | 79.447 | 371.32 | 38.73 |
| 454 | 21.8256 | 75.667 | 143.14 | 27.64 | 509 | 23.9853 | 74.900 | 186.11 | 28.78 |
| 455 | 21.9181 | 72.852 | 225.60 | 30.51 | | | | | |

# REFERENCES

*Calabretta M. R.,* Greisen E. W., 2002, A&A 395, 1077

*Calabretta M. R.,* Roukema B. F., 2007, MNRAS 381, 865

*Carretti E.,* Haverkorn M., McConnell D., Bernardi G., Cortiglioni S., McClure-Griffiths N. M., Poppi S., 2009, Revista Mexicana de Astronomia y Astrofisica Conf. Ser. 36, 9

*Carretti E.* et al., 2010 in preparation

*Chiozzi G.,* Sommer H., Schwarz J., 2009, ALMA Project documentation http://www.eso.org/~gchiozzi/AlmaAcs/OnlineDocs/ACSArchitecture.pdf

*Condon J. J.,* Cotton W. D., Greisen E. W., Yin Q. F., Perley R. A., Taylor G. B., Broderick J. J., 1998, AJ 115, 1693

*Garwood R. W.,* 2000, Astronomical Data Analysis Software and Systems IX, ASP Conf. Ser. 216, 243

*Gregory P. C.,* Vavasour J. D., Scott W. K., Condon J.J., 1994 ApJS, 90, 173

*Gregory, P. C.,* Scott W. K., Douglas K., Condon J. J., 1996 ApJS, 103, 427

*Greisen E. W.,* Calabretta M. R., 2002, A&A 395, 1061

*López-Caniego M.,* Herranz D., González-Nuevo J., Sanz J. L., Barreiro R. B., Vielva P., Argüeso F., Toffolatti L., 2006, MNRAS 370, 2047

*Mangum J. G.,* Emerson D. T., Greisen E. W., 2000, Imaging at Radio through Submillimeter Wavelengths, ASP Conf. Ser. 217, 179

*Mangum J. G.,* Emerson D. T., Greisen E. W., 2007, A&A 474, 679

*Massardi M.,* Ekers R. D., Murphy T., Ricci R., Sadler E. M., Burke S., De Zotti G., Edwards P. G., Hancock P. J., Jackson C. A., Kesteven M. J., Mahony E., Phillips C. J., Staveley-Smith L., Subrahmanyan R., Walker M. A., Wilson W. E., 2008, MNRAS 384, 775

*Massardi M.,* López-Caniego M., González-Nuevo. J., Herranz D., De Zotti G., Sanz J. L., 2009, MNRAS 392, 733

*Muders D.*, Polehampton E., Hatchell J., 2007, APEX Interface Control Document, http://www.apex-telescope.org/observing/APEX-MPI-ICD-0002.pdf

*Murphy T.*, Sadler E. M., Ekers R. D., Massardi M., Hancock P. J., Mahony E., Ricci R., Burke-Spolaor S., Calabretta M., Chhetri R., de Zotti G., Edwards P. G., Ekers J. A., Jackson C. A., Kesteven M. J., Lindley E., Newton-McGee K., Phillips C., Roberts P., Sault R. J., Staveley-Smith L., Subrahmanyan R., Walker M. A., Wilson W. E., 2010, MNRAS 402, 2403

*Orlati A.*, Righini S., 2008, INAF-IRA Technical Report 423/08 http://www.ira.inaf.it/Library/rapp-int/423-08.pdf

*Orlati A.*, Righini S., Maccaferri G., 2008, INAF-IRA Technical Report 424/08 http://www.ira.inaf.it/Library/rapp-int/424-08.pdf

*Ricci R.*, Sadler E. M., Ekers R. D., Staveley-Smith L., Wilson W. E., Kesteven M. J., Subrahmanyan R., Walker M. A., Jackson C. A., De Zotti G., 2004, MNRAS, 354, 305

*Righini S.*, 2008, INAF-IRA Technical Report 425/08 http://www.ira.inaf.it/Library/rapp-int/425-08.pdf

*Verma R.*, Maccaferri G., Orfei A., Prandoni I., Gregorini L., 2009, INAF-IRA Technical Report 430/09 - http://www.ira.inaf.it/Library/rapp-int/430-09.pdf

*Zirin H.*, Baumert B. M., Hurford G. J., 1991, ApJ 370, 779

*ALMA Common Software website* http://www.eso.org/~almamgr/AlmaAcs/index.html

*CORBA website* http://www.corba.org

*HEALPix website* http://healpix.jpl.nasa.gov/

*Medicina dish User Manual website* http://www.med.ira.inaf.it/parabola_page_EN.htm

# ACKNOWLEDGMENTS

I want to express my gratitude to Ettore Carretti, my scientific supervisor, for the patient support he was able to grant to me, even after he moved to Australia.
I express my thank also to Daniele Dallacasa, my tutor.
This work would not have been carried out without the on-site cooperation of many people at the Medicina station, who never cease to amaze me for the competence and passion they put in their job, and for their friedly attitude. Among them, I am particularly grateful to (in alphabetical order): Marco Bartolini, Claudio Bortolotti, Alessandro Cattani, Andrea Maccaferri, Giuseppe Maccaferri, Sergio Mariotti, Alessandro Orfei, Andrea Orlati, Mauro Roma, Alessandro Scalambra. Working in Medicina is just gorgeous, I hope I'll be around for some more time.
Several astronomers from the Bologna headquarters joined the group. Among them, to Karl-Heinz Mack, Alessandra Zanichelli and Loretta Gregorini goes a special "thank you", as their help and advice always accompanied me.

To Andrea Orlati, who to me is a colleague, a friend and… *the* "husband-to-be", I have so much to say "thank you" for. I still don't understand how he manages to bear me almost 24/7 after eight years, let alone why he wants to marry me… Yet, I'm *so* glad he does.